流星質量計算についてのメモ (単体理論による)

1979-X-12
2 長沢 工

2nd MSS

1) 力学質量 (その1)

m_d (Dynamic Mass)

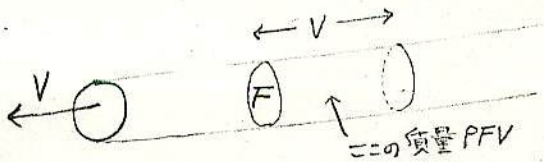

$$m_d \dot{V} = -\Gamma F \rho V^2 \quad \cdots\cdots (1)$$

質量 × 加速度 = 力

$V, \dot{V}$: 流星速度, 加速度
F : 断面積
ρ : 大気密度
Γ : 抵抗係数 … 1前後の単位のない数値 { 流星 ~ 1, 球 ~ 0.46
ρ_m : 流星体密度

$\dot{V}, V, \rho$ は既知. Γ は仮定 残るは m_d と F

断面積 F は体積の $\frac{2}{3}$ 乗に比例

体積は $\frac{m_d}{\rho_m}$ だから

$$F = A\left(\frac{m_d}{\rho_m}\right)^{\frac{2}{3}} \quad \cdots\cdots (2)$$

A : 形状因数 … 1前後の単位のない数

球 $A = (9\pi/16)^{\frac{1}{3}} = 1.20899$

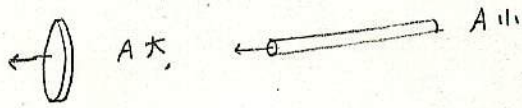

(2)を(1)に代入して

$$m_d^{\frac{1}{3}} = -\Gamma A \rho_m^{-\frac{2}{3}} \rho V^2 / \dot{V} \quad \cdots (3)$$

$A = 1.2$, $\rho_m \sim 0.3\ g/cm^3$ ぐらいを仮定して m_d が求められる

{ 正の加速度のところでは, 地球引力による加速をさし引かないと正しい値が求められない

2) 力学質量 (その2)

$$\underbrace{\varsigma \dot{m}_d}_{\text{気化に必要なエネルギー}} = -\frac{1}{2}\Lambda F \rho V^3 \quad \cdots\cdots (4)$$

運動エネルギー $\frac{1}{2}[F\rho V]V^2$

$\dot{m}_d = \frac{dm_d}{dt}$: 単位時間の質量減少

ς : 単位質量の流星体を気化するのに必要な熱エネルギー (エルグ/g) (気化熱) ~ 8×10^{10} エルグ/g

Λ : 大気が供給する運動エネルギーのうち流星体の気化に使われる割合 (熱輸送係数) ~ 0.02

(4) ÷ (1) を変形して

$$\frac{\dot{m}_d}{m_d} = \frac{\Lambda}{2\Gamma\varsigma} V\dot{V} \quad \cdots\cdots (5)$$

$\frac{\Lambda}{2\Gamma\varsigma} = \sigma$ とおいて σ : 摩耗係数 大きくは変化しない

$\sigma \sim 1.25 \times 10^{-11}\ (s^2/cm^2)$

積分して (積分定数 C)

$$\log m_d = \frac{\sigma}{2} V^2 + C \quad \cdots\cdots (6)$$

ある点で 質量 m_0, 速度 V_0 であるとすると

$$m_d = m_0 e^{\frac{\sigma}{2}(V^2 - V_0^2)} \quad \cdots (7)$$

σ をうまくきめると, このような形で質量変化があらわせる

3) 測光質量

m_p (Photometric Mass)

($\log I = 9.72 - 0.4M$, M: 流星の絶対等級)

光のエネルギー … 気化して減少した質量に比例すると一般に考えられている (エルグ/秒)

気化した質量 $-\dot{m}_p$ は そのとき $-\frac{1}{2}\dot{m}_p V^2$ の運動エネルギーを持っている

そのうち τ の割合が写真域に対する光エネルギー I に変換されるとして

$$I = -\frac{\tau}{2}\dot{m}_p V^2 \quad \cdots\cdots (8)$$

τ : 光力係数 (単位なし)

(8)式から

$$\dot{m}_p = -\frac{2}{\tau}\frac{I}{V^2} \quad \cdots\cdots (9)$$

積分して

$$m_p(t) = \frac{2}{\tau}\int_t^{t_e} \frac{I(t)}{\{V(t)\}^2}\,dt \quad \cdots\cdots (10)$$

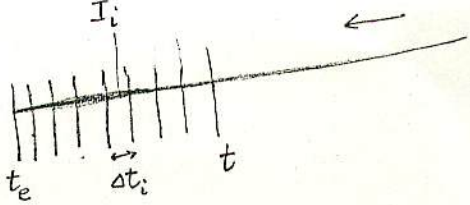

実際の計算は光跡の末端で m_p は 0 になるものとして 径路をたくさんに分割し、それぞれの区域で

$\frac{I_i}{V_i^2}\Delta t_i$ を計算し、末端から合計していく。 Δt_i はその部分の時間の間隔。

この計算は フィルム上で光が飽和していない、あまり明るくない流星を使う。

τ の値の例　　写真に対して $\tau_p = 5.248\times10^{-10}\cdot V$　(V：はcm単位)

τ にはヤッキアの表示法といわれる全く別の表示法がある。これは光の量の単位として 0等星の光量を単位として示すもので ある。この場合 τ は単位 ($sec^3\cdot cm^2 g^{-1}\cdot 0mag$) をもつ量となる。 ヤッキアの表示による数値を τ_J とすると

$$\tau_J \times 5.248\times10^9 = \tau$$

であらわすことができる。

4) 力学質量と測光質量の調和

m_d と m_p はなかなかうまく一致しない　　理由 { Γ, A, ρ_m などの推定値が誤っている / $\dot{V}$ の決定精度が不十分 / τ の値が悪い / 測光精度が悪い }

これをうまく合わせる方法。

$m_d = m_p = m$ として

(10)式 m_p を (5)式の m_d に代入
(9)式 $\dot{m}_p$ を (5)式の $\dot{m}_d$ に代入　} 整理

$$\sigma(t) = \frac{\Lambda}{2\Gamma S} = \frac{I}{-V^3\dot{V}\int_t^{t_e}\frac{I}{V^2}\,dt} \quad \cdots\cdots (11)$$

観測できる量だけで σ を求めることができる。 この $\sigma(t)$ を使って (5)式を積分

$$\log m = \int \sigma V\dot{V}\,dt + C \quad \cdots\cdots (12)$$ 矛盾ない質量関係の式

また (10)式の m_p を (3)式の $\dot{m}_d$ に代入

$$K = \Gamma A \rho_m^{-\frac{2}{3}} = -\frac{\dot{V}}{\rho V^2}\left(\frac{2}{\tau}\right)^{\frac{1}{3}}\left(\int_t^{t_e}\frac{I}{V^2}\,dt\right)^{\frac{1}{3}} \quad \cdots\cdots (13)$$

τ の他は観測される量だけで $K = \Gamma A \rho_m^{-\frac{2}{3}}$ を求めることができる。 この K を使って (3)式の計算をすれば 測光と力学とが矛盾ない形で質量が求められる。

◎ σ、K には Γ, Λ, S, A, ρ_m の 5つの未知量が入っている。これを分離して求めることはできないが、 Γ, A を仮定するなどで ρ_m を知るといったように 流星体についての情報の手がかりを得ることができる。

高匹の流星は径路途中で爆発的に増光をくりかえす場合が多く、このような流星には単体理論は適用できない。

h	ρ	V_{obs}	V	$\dot{V}$	m
55.85 km	5.066 $\times 10^{-7}$ g/cm^3	14.25 km/s	13.89 km/s	-1.437 km/s^2	544 g
55.58	5.232	13.44	13.82	-1.492	519
55.26	5.435	14.26	13.74	-1.546	505
54.99	5.612	13.28	13.66	-1.600	484
54.68	5.823	14.00	13.58	-1.655	472
		13.23			
54.41	6.013	13.95	13.50	-1.709	456
54.11	6.232	12.96	13.41	-1.763	444
53.82	6.499	13.50	13.32	-1.818	431
53.53	6.672	13.02	13.23	-1.872	420
53.25	6.897	13.35	13.13	-1.927	406
52.97	7.129	12.80	13.03	-1.981	394
52.70	7.363	13.01	12.93	-2.035	382
52.40	7.632	12.55	12.83	-2.090	375
52.15	7.866	12.90	12.72	-2.144	361
51.87	8.139	13.14	12.62	-2.199	354
51.58	8.435	12.10	12.50	-2.253	346
51.34	8.689	12.39	12.39	-2.307	334
51.06	8.997	12.08	12.27	-2.362	325
50.79	9.304	11.75	12.15	-2.416	317
50.56	9.575	11.76	12.03	-2.471	305
50.30	9.891	12.24	11.91	-2.525	296
50.04	10.218	11.63	11.78	-2.579	287
49.79	10.536		11.65	-2.634	277

In the calculation,

$\Gamma = 1$,

$A = 1.2$

and $\rho_m = 1$ g/cm^3

are assumed.

6th-MSS Nov. 11 '79

Asteroidal Meteors : Density and Interrelation between Comets and Asteroids

小笠原 雅弘 (日本天文学会)

最近、彗星・小惑星・隕石といったものをバラバラに研究するのではなく、これらを太陽系生成史を秘めるものとして位置づけ、その関連を調べる研究がふえてきた。Delsemme 論文の題名「Comets - Asteroids - Meteorites」はその典型であろう。

Wetherill らによる 死んだ彗星核 = アポロ・アモール型小惑星論議はこの研究に一つの大きな問題を投じたものといえよう。

流星で数多くのサンプルから その密度を調べる方法についてはいろいろな研究が発表されている。(Verniani 1969, Ceplecha 1977 小笠原 他 1979)

力学的質量と測光質量の一致という観点に立って流星の密度を調べて その起源をさぐる一助としたい。

$$\begin{cases} \text{力学的質量} & m d^{\frac{1}{3}} = -\Gamma A \rho_m^{-\frac{2}{3}} \rho V^2 \dot{V}^{-1} \quad \cdots (1) \\ \text{測光質量} & m_p = \frac{2}{\tau} \int_{t=0}^{t=End} I(t) \cdot V(t)^{-2} \cdot dt \quad \cdots (2) \end{cases}$$

(1), (2) を比較する場合、それぞれの係数を考えてみると、

Γ : 抵抗係数 — 普通の流星では ~1. 火球では圧縮されたガスキャップができるので ~0.46 になるといわれるが、細かな論拠はほとんどない。

A : 形状因子 — 手にとって見るわけにはいかないので 球形 ~1.2 とする。

τ : 光力係数 — 人によって表記法に差があるが、

$$\tau = \tau_0 \cdot V \qquad \tau_0 = 10^{-19}$$

これは純鉄の人工流星で求めた結論なので 鉄の組成比 28% = 0.28 をかけて

$$\tau_0 = 0.28 \times 10^{-19}$$

Sodium の強い発光を含んでいないので

$$\log \tau_{pan} = \log \tau - 0.2 \quad \cdots (3)$$

パンクロフィルム

パンクロのフィルム（TriX, SSS）ではこの値を用いる必要がある。（Ayers etal., 1970）

ρ：大気密度 — U.S. Standard Atmosphere (1962)

V, $\dot{V}$, $I(h)$は観測値を求めて、それを使用する。

(1)式で、ρ_m：流星体密度 がパラメータとなる。これを0.2～3.7g/cm³まで変化させながら測光質量と最も良くフィットするところをさがす。

ρ_mの分類（Ceplecha, 1977）

ρ_m	性質
0.2g/cm³	軽い彗星物質（ジャコビニ）
0.6	普通の彗星物質（流星群）
1.0	密な彗星物質（ふたご）
2.1	炭素質コンドライト
3.7	普通コンドライト

このようにして、KPM 7711の検討をした結果、この流星は3.7g/cm³とするときに良い一致が得られることがわかった。

普通コンドライトに近い密度をもっている。

小惑星のメインベルトには、炭素質コンドライトが多い（Gaffey, McCord, 1977）、ところが普通コンドライトはほとんどみつからない。地球上の隕石では、普通コンドライトが最も多い（85%）それでは、これらの普通コンドライトはどこからやってきたのか。

(433) Eros, (1685) Toro は、その反射スペクトルが普通コンドライトと似ていることが指適されており、これらのアポロ・アモール型小惑星がその起源と考えられる。彗星核から分離するものは密度が1以下であるから、それがもし、死んでアポロ・アモール型小惑星になるとすると、1g/cm³以下のガサガサしたものを、密度の大きい岩状のものにするメカニズムが必要だが、はたしてそれはありえるのだろうか。→効力不可能

詳しくまとめたものは「天文と気象」誌 1980年2月号に「同時観測から流星の起源をさぐる－II」として掲載予定。

6th MSS

Space Sci. Reviews 10 (1969)
p. 230 – 261

STRUCTURE AND FRAGMENTATION OF METEOROIDS

構造　分裂

FRANCO VERNIANI

Istituto di Fisica dell'Atmosfera del Consiglio Nazionale delle Ricerche, Roma, Italy

(Received 27 May, 1969)

Abstract. This paper is a review of the present knowledge on the structure of meteoroids.

A summary of the evidence concerning the common occurrence of fragmentation among both photographic and radio meteors is given first. Then, an attempt is made to examine all the present observational, theoretical and laboratory data on the luminous and ionizing efficiencies of meteors, with the aim of establishing a mass scale. This allows the computation of the bulk density of meteoroids, which, on the average, turns out to be about 0.3 g/cm³.

かさ比重（すきまの体積も含めた）

The paramount importance of progressive fragmentation, the behavior of abrupt-beginning meteors and the low density of nearly all meteoroids (even of those of relatively large sizes) support a porous and fragile structure for most of these particles. In turn, the crumbly structure and the cometary origin confirm Whipple's theory of comets and meteor production. A critical analysis of recent papers proposing different conclusions shows that the new theories always arrive at results which do not agree with well-established observational data.

4. Densities

Once the mass scale has been established by determining the luminous efficiency, one can evaluate the densities of the original meteoroids. I shall first summarize my latest results (Verniani, 1967a). I computed the density ϱ_m of 220 sporadic and 104 shower meteors selected from Harvard precisely-reduced material. A selection was necessary to discard all meteors showing either an abrupt beginning or a very short, flare-like light curve or other clear irregularities: the mean of $\log \varrho_m$ for the sporadic meteors was -0.558 ± 0.025 corresponding to a logarithmic mean density of 0.28 g/cm³, with a standard deviation of 6%.

The meteor density depends on the orbital characteristics as can be shown by regarding it as a function of the aphelion distance Q: the average density of a meteor with $Q = 2$ AU turns out to be about 50% larger than the average density of a meteor with $Q = 4$ AU. The mean logarithmic density as a function of the aphelion distance is shown in Figure 1: for short-period meteors, the density increases as the aphelion distance decreases. This remarkable dependence, as well as other systematic differences in some physical characteristics between meteors in short-period and long-period orbits, has been tentatively ascribed by Jacchia *et al.* (1967b) to the different conditions in which the meteoroids were formed and to the different resistance to destroying agents. Most of the meteors in short orbits may have originated in short-

period comets that by now are completely evaporated; those that came from the inner core of Whipple's icy conglomerate should be denser because of the greater pressure to which they were subjected. Meteoroids with a loose structure are probably destroyed faster by collisions, erosion, and thermal effects.

The logarithmic spread in $\log \varrho_m$ due to the orbital dependence is of the order of

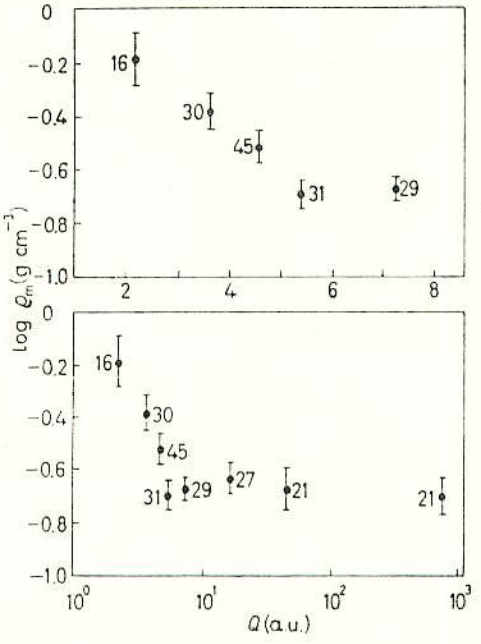

Fig. 1. The mean logarithmic density of 220 sporadic Super-Schmidt meteors, as function of the aphelion distance Q (Verniani, 1967a).

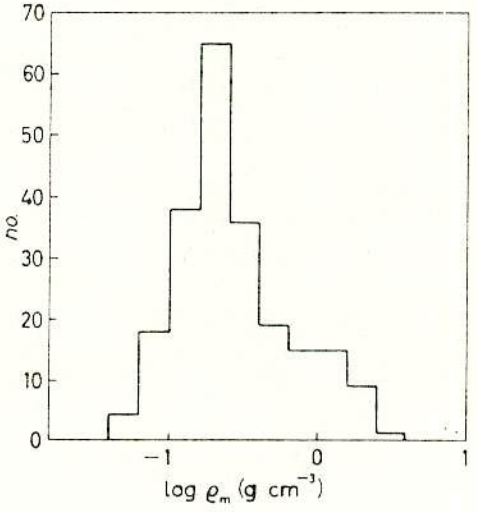

Fig. 2. The density distribution for 220 sporadic Super-Schmidt meteors (Verniani, 1967a).

only 0.1, very small in comparison with the observed standard deviation of ± 0.8 for one observation. Since the errors due to atmospheric variability, changes of shape and observational inaccuracies are random, we would expect a Gaussian distribution for $\log \varrho_m$ centered around the logarithmic mean. Figure 2 shows, on the contrary, that the $\log \varrho_m$ distribution extends itself much more on the high-densities side. In Figure 3 the same meteors have been divided according to their aphelion distance, and the density distribution is shown separately for meteors with $Q < 5.4$ AU and $Q > 5.4$ AU. It is immediately apparent that the density distribution of the long-period meteors is Gaussian. A χ-square test confirmed that the distribution obtained is fully compatible with a Gaussian curve centered around the logarithmic mean and with the dispersion fixed by the observed standard deviation. The mean logarithmic density for these long-period sporadic meteors is 0.21 g/cm^3, with a standard deviation of 7%.

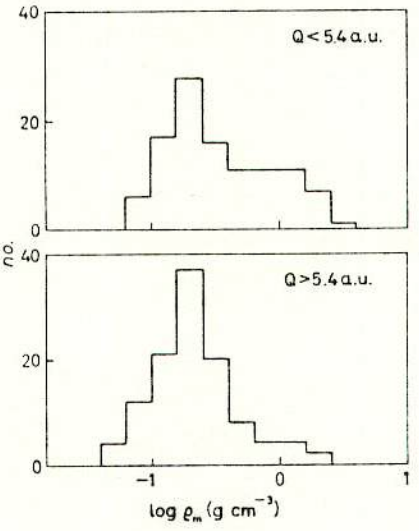

Fig. 3. The density distribution for two groups of sporadic Super-Schmidt meteors, respectively in short- and long-period orbits (Verniani, 1967a).

The median is also 0.21 g/cm^3. The distribution of the short-period meteors is different. The low- and middle-density regions are quite similar to the corresponding ones in the distribution of long-period meteors. Conversely, on the high-densities side it extends considerably, and it looks as though there is an overlapping of two Gaussian distributions, one centered around $\log \varrho_m = -0.7$, as for the long-period meteors, and the other centered around $\log \varrho_m = 0.1$. I was thus led to the conclusion that a small group of short-period meteors may have densities of the order of 1 g/cm^3. Among the 108 meteors with an aphelion distance smaller than 5.4 AU, about 30 meteors are in the high-density group. However, the true consistence of this group cannot be estimated simply by these figures. In fact, this sample of meteors is far from being random. In selecting the meteors to be reduced, Jacchia used the basic criterion that they should yield excellent decelerations, a fact that strongly favored the inclusion

of long-period meteors, and thus enhanced the probability of the inclusion of high-density meteors. It is nevertheless important to have established the probable existence of a small percentage of meteors in very short orbits having much higher densities than the great majority of all cometary meteors.

Among the original sample of 413 meteors, 123 belonged to well-established showers. Nineteen of these meteors were discarded for various reasons. Table IV gives the results about the average density of each individual shower, as well as the density of two groups of sporadic meteors. For most showers, although the data are very

TABLE IV

Average densities ϱ_m for Super-Schmidt meteors. Q is the aphelion distance (Verniani, 1967a)

Group or shower	Mean $\log \varrho_m \pm$s.d. (g cm^{-3})	ϱ_m (g cm^{-3})	Median ϱ_m (g cm^{-3})	Mean $Q \pm$s.d. (AU)	No. Obs.
Sporadic, all	-0.56 ± 0.02	0.28	0.23	–	220
Sporadic ($Q > 5.4$ AU)	-0.68 ± 0.03	0.21	0.21	–	112
Geminids	0.03 ± 0.09	1.06	1.14	2.6 ± 0.0	20
Southern Taurids	-0.56 ± 0.04	0.28	0.25	3.4 ± 0.2	18
α Capricornids	-0.85 ± 0.07	0.14	0.16	5.5 ± 0.7	12
Quadrantids	-0.70 ± 0.14	0.20	0.17	5.0 ± 0.2	9
Perseids	-0.54 ± 0.07	0.29	0.32	59 ± 11	8
δ Aquarids	-0.57 ± 0.07	0.27	0.27	5.3 ± 0.3	7
Southern ι Aquarids	-0.52 ± 0.10	0.30	0.32	4.7 ± 0.6	5
Orionids	-0.60 ± 0.08	0.25	0.23	66 ± 19	4
κ Cygnids	-0.78 ± 0.08	0.17	0.17	5.3 ± 0.4	4
Northern Taurids	-0.58 ± 0.04	0.26	0.27	4.7 ± 0.7	4
σ Hydrids	-0.40 ± 0.18	0.40	0.58	56 ± 31	3
Lyrids	-0.41 ± 0.13	0.39	0.30	51 ± 19	3
Northern ι Aquarids	-0.20 ± 0.45	0.63	0.63	3.6 ± 0.6	2
Draconids	–	< 0.01	–	5.6 ± 0.1	2
Virginids	-0.13	~ 0.7	–	4.4	1
Leonids	-0.21	~ 0.6	–	24	1
η Aquarids	-0.25	~ 0.6	–	26	1

scanty, the average density is near the average density of sporadic meteors. The most important exception, as is already well known (Jacchia, 1952; Verniani, 1965; JVB, 1967) are the Geminids. On the average, they are about four times more dense than the sporadic meteors and they have a distribution strongly resembling that of the high-density group of meteors in very short orbits. It is worth noting though, that they crumble just as easily as any ordinary meteor. At the other extreme of values, the Draconids have an extremely small density. On the average however, there is no difference between sporadic and shower meteors. The mean density for all sporadic meteors (0.28 g/cm^3) agrees very well with the density found with a different method by the author (Verniani, 1964) for 284 faint Super-Schmidt meteors, 0.30 g/cm^3, when we correct for the shape factor, which was then assumed to be 1.21 instead of 1.5.

McCrosky (1967) has published provisional values of the density of 28 fireballs ($-5 \geq M_p > -18$) recorded under the Prairie Network Project. Though the sizes of

 6th MSS

the original meteoroids must have been very large, the average density turned out to be 0.4 g/cm^3, essentially the same as that determined by the writer for Super-Schmidt meteors. It is worth mentioning that, out of over 100 density determinations for his 28 fireballs, McCrosky did not find any individual value in excess of 1.2 g/cm^3. These figures indicate that the structure of large meteoroids with a typical mass between 1 and 10 kg does not differ significantly from the structure of meteors observed with the Super-Schmidt cameras (mean mass of the order of 1 g). At the other extreme (very small particles), preliminary results are available for meteors detected by radar methods (average mass of the order of 10^{-4} g). For those small bodies a somewhat larger density, such as 0.8 g/cm^3, appears to be in order (Verniani and Hawkins, 1965; Verniani, 1966).

Russian observations due to Babadzhanov and Kramer, as quoted by Babadzhanov (1966), suggested an average density of the order of 0.1 g/cm^3. Ceplecha (1967, 1968b) finds, on the contrary, average meteor densities one order of magnitude larger than the values presented above. A detailed discussion on Ceplecha's procedure, leading to the conclusion that his high-density values are wrong, has already been published by this writer (Verniani, 1967b and 1967c).

I wish to conclude this section by recalling the importance of knowing the density of meteoroids in space for the correct design of spacecraft, which must be protected against the meteoric hazard.

5. Origin and Structure

Evidence summarized in section 2 proves that meteor fragmentation is definitely a common occurrence, as is shown beyond any reasonable doubt by the deceleration anomalies and by the blending of the exposed segments: a simple look at the photographic image of most Super-Schmidt meteors is enough to convince anybody of its existence and extent. Meteor densities have been discussed in the preceding section and we have seen that the average value, directly computed by decelerations, is about 0.3 g/cm^3.

A century ago the orbits of several major showers were clearly connected with those of some comets. Recently, orbital data obtained from precise photographic material (both from small cameras and from Super-Schmidt cameras) indicates that most meteors have their origin in comets (Whipple, 1954; Jacchia and Whipple, 1961; Babadzhanov and Kramer, 1967); I do not deem it necessary to summarize here the evidence pointing to this well-known fact. In Öpik's (1966b) words: "There is no doubt that meteor streams as well as their remnants, the sporadic meteors, are the remains of disintegrating comets." Another proof of the cometary origin of the overwhelming majority of the photographic meteors is the fact that heights, decelerations and other physical characteristics of sporadic and shower meteors not related to known comets, taken in their totality, do not show any systematic differences from those of the shower meteors connected with comets (JVB, 1967). Writes Whipple (1968b): "We now know that almost all the smaller particles in near-earth space are of cometary origin". Among over 400 precisely reduced meteors *only one* has all

the expected characteristics of an asteroidal meteor (JVB, 1967): this in spite of the fact that especially long trails were selected, thus favoring the inclusion of asteroidal meteors.

All these facts clearly point to the conclusion that most meteors are of cometary origin and are porous, crumbly objects made of loosely conglomerate, spongelike material. This conclusion fits well into the frame provided by Whipple's theory of comets and meteor production.

6. A Discussion of the Objections to the Concept of Porous and Fragmenting Meteors

Kramer (1966) writes that meteors whose origin is connected with comets "are now universally regarded as possessing a loose structure". This may well represent the viewpoint of most Russian scientists; however, several authors have recently challenged this conclusion as well as other aspects of the picture presented in the preceding sections. Let us now examine their arguments.

Allen *et al.* (1965) have studied the effect of radiation cooling on meteor flight. As a conclusion, they suggested surface radiation as a possible explanation, instead of fragmentation, for the anomalous behavior of the light curves of faint meteors. Though radiation cooling may indeed affect meteor beginnings, their explanation is certainly at variance with the results of the observations. As a matter of fact, surface radiation becomes more and more important as the meteor mass decreases during the atmospheric flight and therefore the deceleration should increase more slowly than predicted by classical theory: this is just the opposite of what we observe. Moreover, radiation cooling alone cannot explain the other anomalies shown by faint meteors, e.g. blending. Terminal blending is clearly caused by the meteoroid comminution into smaller fragments widely ranging in size.

The effects of radiation cooling on meteor phenomena have been studied also by Jones and Kaiser (1966). They have generalized the classical theory of meteoric ablation to include the effects of thermal radiation, thermal conduction and the heat capacity of meteoroids which are assumed to be solid stony particles. These authors show that, in the magnitude range $+3 < M < +10$, thermal radiation may be neglected while the finite heat capacity of the meteoroids delays appreciably the onset of ablation. In this connection, it is interesting to recall here that the height analysis of the 413 precisely reduced meteors (JVB, 1967) showed that meteors begin about 6 km lower than expected to, according to the classical theory. Jones and Kaiser find that "evaporation profiles are significantly shorter than predicted by the classical theory" and this is, of course, in agreement with the observational results. Moreover, the effect of the thermal diffusivity of the meteoric substance would set up a system of stresses *within* the meteoroid which, in the opinion of Jones and Kaiser, could be sufficient to produce the fragmentation of the meteoroid itself. They find that "particles with radii greater than about 0.1 cm are expected to fracture before the onset of ablation and as a result fragments are likely to be released suddenly into an abnormal environment

7th MSS

Fragmentation of the Meteor (流星がくだけちる現象)

V_0 30 km sec^{-1}

$\cos z = 1$ $(z = 0°)$

1 sec. Duration

Mass loss rate 0.1 Mo/0.1 sec.

US-standard Atmosphere

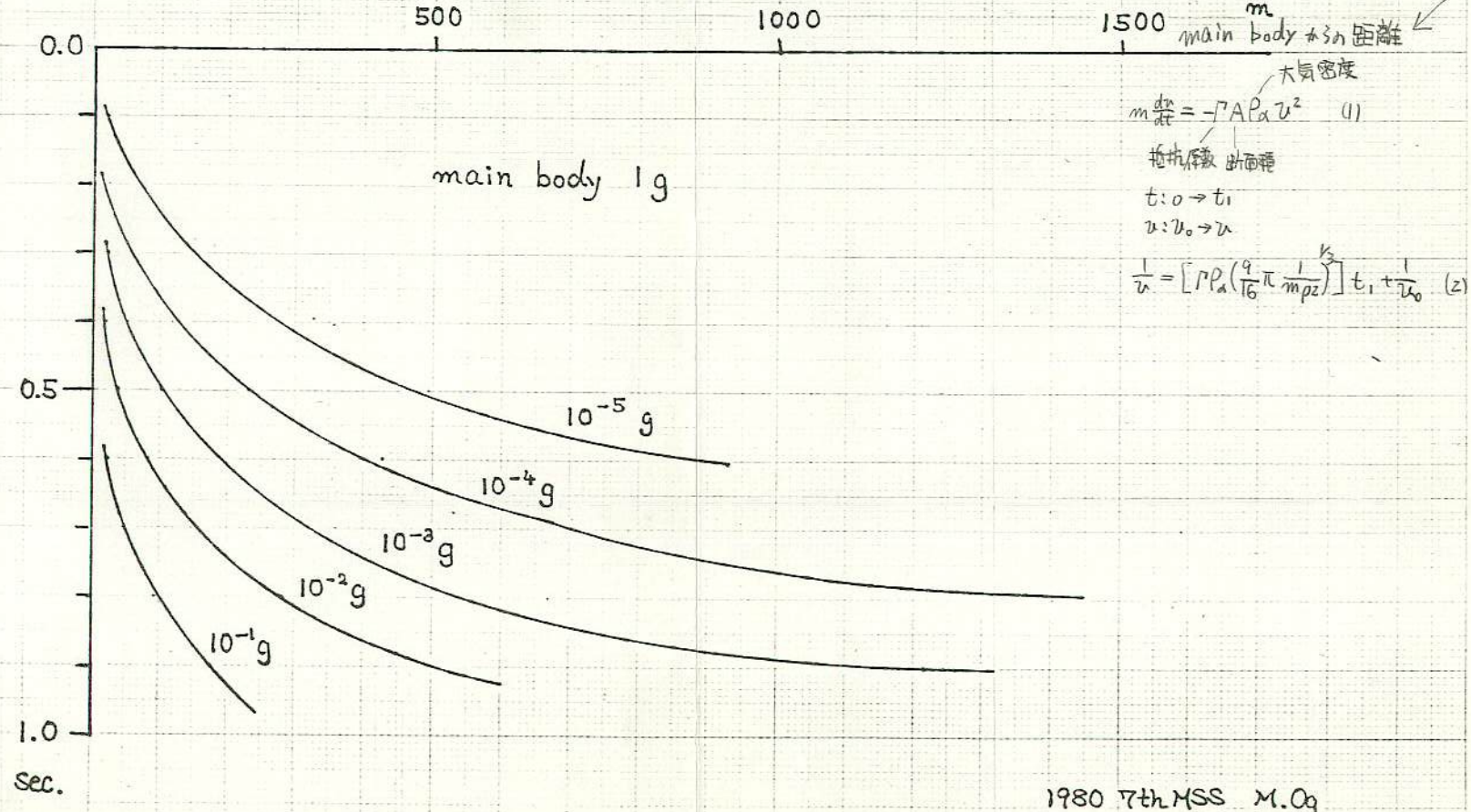

大気密度

$m\frac{dv}{dt} = -\Gamma A \rho_a v^2$ (1)

抵抗係数 断面積

$t: 0 \to t_1$

$v: v_0 \to v$

$\frac{1}{v} = \left[\Gamma \rho_a \left(\frac{9}{16}\pi \frac{1}{m\rho z}\right)^{1/3}\right] t_1 + \frac{1}{v_0}$ (2)

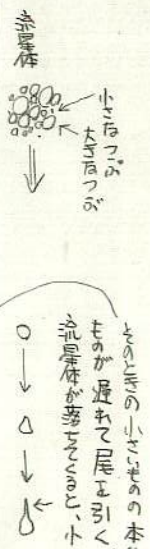

1980 7th MSS M.Og

MSS-007

MSS-008

NEDERLAND 5 VOOR HET KIND SYMPOSIUM
惑星間固体物質／7

流星観測の立場からみた隕石落下

長沢　工（ながさわ　こう）
東京大学地震研究所 助手

隕石は大気中で摩耗し，はじめの大きさより小さくなって地表に到達する．それでは，どのぐらい小さくなるのであろうか．流星観測の手法で計算してみると，大気中の摩耗は一般に想像されるよりはるかに大きく，隕石となって地表に落下するのは非常に稀な，どちらかといえば例外的な場合であることが推測される．

1. はじめに

1980年11月，埼玉県越生で開かれた“太陽系内小天体シンポジウム”の討論で，隕石落下について，大きな意見の相違のあることがわかった．その問題点を煎じつめれば，次のように要約することができる．

隕石研究者などの考え：大気中での隕石の摩耗，減量はそれほど大きなものではなく，初めの質量のかなりの部分（たとえば50％程度）が地表まで到達する．

筆者などの考え：大気中で隕石は大きくその質量を減らし，地表に到達するのは初期質量のせいぜい数％にすぎない．

ここで議論の対象となっているのは，地上に発見されるごくあたりまえの大きさ（数100 g～数10kg程度）の普通コンドライト質の隕石と考えていただきたい．

その後わかったことは，流星研究者は，流星，火球などの大気中の発光強度と質量減少の関係などを基にして大気中の隕石のふるまいを調べているのに対し，隕石を直接に研究している方がたは，太陽系空間での宇宙線照射が隕石にどのぐらい貫徹するかといったことを基礎にして，大気圏に突入する前の隕石の大きさを推定しているということであった．そして，この方法の違いが，前記のような意見の相違を生じる根本の原因であった．

しかし，異なった2つの意見が両方とも真実であるはずはない．少なくとも一方が，場合によっては両者がともに誤っているに違いない．ここで筆者は，流星観測の立場から，どのようにして先に述べた結論に達したのか，その概略を述べて多くの方の御批判を乞うこととし，真実はどうであるか，2つの考えにどの程度歩み寄りの余地があるかなどを皆さんに考えていただきたいと思うのである．

MSS-008

2. 問題提起

話をわかりやすくするために，ここで，具体的な問題を考えてみよう．

問題．1トンの隕石が地球大気に突入してきたものとする．そのうち地上に落下するのはどのくらいであるか．ただし，隕石は密度 3.7 g cm^{-3} の普通コンドライトであるとして（球形なら半径約 40 cm），大気突入前の地球に対する速さが 20km s^{-1}，地表と45°の角度で進行してきたものとする．

この答はどのぐらいと皆さんお考えになるだろうか．これに対する計算結果はあとから示すことにして，参考資料をいくつかあげてみよう．

1 エネルギー収支

ここで，隕石の運動エネルギーが徐々に熱に変化し，その熱によって，隕石が表面から少しずつ融解，気化していくというモデルを考えてみる．この場合のエネルギー収支はどのぐらいになるか．

コンドライトや岩石などのケイ酸塩の気化熱を測定したデータはほとんどないので，ここでは鉄について考えてみる．鉄の気化温度は，3,135°Kであり，0°Kから1 gの鉄を気化するまでに必要なエネルギーは，

0°K～3,135°Kまで	2.0×10^3 J
融解熱	0.3×10^3 J
気化熱	6.3×10^3 J
計	8.6×10^3 J

である．このほかに相転移などにともなうエネルギーも必要であるが省略した．この計算に使用した比熱の値などは常温，常圧に対するものであり，隕石が気化する場合には温度，圧力条件が違うので，ここに示した値はごく概算である．

一方1 gの鉄がもっている運動エネルギーは正確に計算できる．20km s^{-1} の速さではこれは 2×10^5 Jとなる．したがって，はじめにもっている運動エネルギーの5％が加温，気化にふりむけられれば，その鉄を完全に気化することができる．コンドライトは鉄よりも気化しやすいと考えられているので，このように隕石が融解，気化をしていく過程を考えるかぎり，エネルギー的には，隕石全部を気化することが十分可能であろう．

第1表 プレーリー・ネットワークの結果（McCrosky *et al.* 1977）の一部（普通コンドライト）

初期質量	大気外での対地速度	最終質量
kg	km s^{-1}	kg
270	31.0	0.45
100	17.9	3.9
490	14.2	(20)……（ロスト・シティ隕石 発見は17kg
76	13.2	0.02

2 プレーリー・ネットワークの結果

1963年から1975年にかけて，アメリカでは，写真を利用して大規模な火球観測が行なわれた．これがプレーリー・ネットワークと呼ばれるものである．これは落下直後の隕石を発見することを目的のひとつにしていたが，隕石が発見できたのはロスト・シティ隕石の1回だけであった．

この観測結果を McCrosky ら（1977）がまとめているが，そこから，物質が普通コンドライトであろうと推定されるものいくつかについて，はじめの質量，大気を通過したあとの最終質量をぬき書きしてみると，第1表のようになる．

この表を見て，最終質量が非常に小さいとお感じになる方が多いだろう．ロスト・シティ隕石の場合で約4％であるにすぎない．

大気外の質量は直接に測定することはできない．隕石が発見できない場合の最約質量にしても同様である．それでは，第1表の値はどのようにして求めたのだろうか．まず，これについて，次章以降で述べることにしよう．

3. 流星，火球の観測法

流星，火球の位置，速度，あるいは質量，密度というようなことを研究するには，通常，その流星の写真を基にする．

この目的のためには，第1図に示したように，カメラの前に，回転シャッターという一種のプロペラのようなものを装着し，それを定速度で回転しながら撮影をする．するとカメラはシャッターでおおわれたり露光したりを繰り返すことになる．その結果，流星は第2図に示したように，シャッターでおおわれるたびに露光が中断され，破線状に撮影される．シャッターの

MSS-008

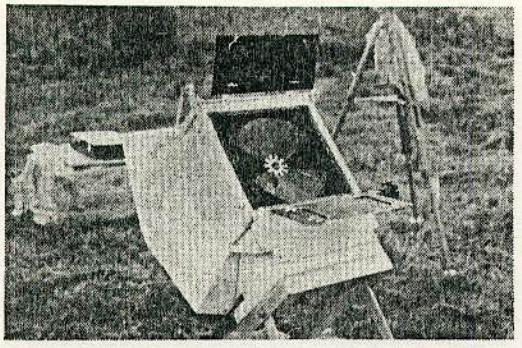

第1図　回転シャッターを備えた流星カメラ

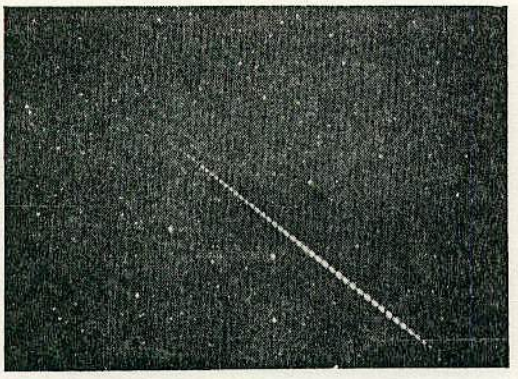

第2図　破線状の流星写真

回転数からその時間間隔は正確にわかるので，フィルム上で流星の切断点の位置を測定することにより，この流星の見かけの角速度が計算できる．さらに，同じ流星を地上の別の地点で写真撮影していれば，三角測量の原理でこの流星の空間位置が定まり，ひとつひとつの切断点の位置を正確に求めることができる．そこから，各切断点に対しての速度，加速度も計算できる．

一方，それぞれのフィルムには露光基準となるもの，たとえば光学ウェッジの焼き込みを行ない．写真測光によって，経路各点での流星の明るさを測定できるようにしておく．

4. 流星，火球の質量計算法

以下に述べるのは単体理論といわれるもので，流星となる物質（流星体）が表面から少しずつ摩耗し，だんだんに小さくなっていくというモデルに対して成立つものである．

流星経路の各点での流星体の質量を決める方法は，大きく分けて2つある．力学的に決める方法と測光学的に決める方法である．前者によって決めたものを力学質量，後者によるものを測光質量という．

1　力学質量

地球引力の影響を無視し，大気抵抗だけを考慮すると，流体力学でよく知られているように，流星体の運動方程式はつぎのようになる．

$$m\dot{v}=-\frac{C_D}{2}S\rho v^2 \qquad \text{（基本式Ⅰ）}$$

ここで，

m：流星体の質量

C_D：抵抗係数

S：進行断面積

ρ：大気密度

v：流星体の速度

また，ドットは時間による微分をあらわすものとする．

流星体の密度を ρ_m とすると，その体積は m/ρ_m である．進行断面積（S）はその2/3乗に比例すると考えられるので，

$$S=A(m/\rho_m)^{2/3} \qquad (1)$$

と書き直すことができる．A は形状因数と呼ばれる比例係数である．これは形により，また進行方向によってその値が異なるが，塊状のものでは概略1前後の値をとり（球では1.209）極端に大きい値や小さい値をとることはない．通常はこれを定数とする．(1) を基本式Ⅰに代入することで，

$$m^{1/3}=-\frac{C_DA\rho v^2}{2\dot{v}\,\rho_m^{2/3}} \qquad (2)$$

の関係が導かれる．これが流星体の質量を与える式である．

(2)式の右辺で，v，$\dot{v}$ は観測から求められる量，大気密度（ρ）も推定できる量である．したがって，抵抗係数（C_D），形状因数（A）および流星体の密度（ρ_m）を与えれば経路各点で流星体の質量を知ることができる．この関係から求めたものが力学質量である．

仮定しなければならないものでは，A はさきに述べたように1ぐらい（1.2をよく使う），C_D は一定値ではないが，隕石落下の際はその前面に圧縮された大気

MSS008

層ができるため，C_Dは0.5ぐらいであると考えられ，一定値として扱かうことが多い．また普通コンドライトでは ρ_m は 3.75g cm^{-3} 程度である．

以上に述べてきたことからわかるように，流星体の力学質量は C_D, A などの仮定のしかたによって，ある範囲で系統誤差が生じる．また，発光初期には加速度 ($\dot{v}$) がほとんど0であり，精度よく決めるのが困難なので，質量の決定精度が非常に悪い．発光の末端では決定精度が急激によくなってくる．第1表の最終質量は主としてこの方法で決めた発光経路末端の力学質量である．

2 測光質量

流星の光のエネルギーは，流星体の失っていく運動エネルギーに比例する．このように考える積極的な理由があるわけではないが，流星研究者は通常そのように考えている．

この比例係数を光力係数といい，これを τ で表わすことにすると，上記の関係は，

$$I=-\frac{\tau}{2}\dot{m}v^2 \tag{3}$$

と書ける．I は単位時間当りの流星の光のエネルギーである．この関係を書き直すと，

$$dm=-\frac{2I}{\tau v^2}dt$$

$$m=-\int\frac{2I}{\tau v^2}dt+m_E \tag{4}$$

となる．m_E は発光経路末端での残存質量である．流星写真の測定によって，経路に沿っての流星の明るさ (I) および速度(v) を求めることができるから，τの値さえわかれば，(4) 式にしたがって，経路末端から順次に積分していくことで，各点の流星体質量を求めることができる．こうして得られた質量を流星の測光質量という．経路全体にわたって積分すれば大気突入前の初期質量が得られる．残存質量 (m_E) は0と考えて計算する場合が多い．第1表の初期質量の値はこうして求めたものである．

ここで問題となるのは光力係数 (τ) の値である．この値の決定に関しては多くの話題があり，研究者によって，非常にバラツキのあるさまざまの値が提唱されていた．これは，ロケットから，形，成分のわかっている物体を人工流星として発射し，これを測定するという研究 (Ayers 1970) が行なわれて，かなり正確な値が求められ，結着がついた．それによると，τ は速度に比例して，

$$\tau=\tau_0 v \tag{5}$$

の形に書ける．明るさの単位に絶対等級0等の明るさをとり，その他の単位ＳＩ系で示すと，τ_0 は，

$$\tau_0=10^{-10}(\text{0等の明るさ・，kg}^{-1}\text{m}^{-3}\text{s}^4), \tag{6}$$

ぐらいの値になる．これによると，仮に流星が 20kms^{-1} の速さで，絶対等級0等の明るさで，1秒間光り続けたとするなら，その流星体の初期質量は 2.5g ぐらいになる．現在では，τ_0を定数とせず，多少の速度依存性を考えて，より正確な質量の値を求める努力も行なわれている．

5. 力学，測光質量の比較と流星体密度の推定

前章に述べた方法で，同一流星から，力学質量，測光質量の両方を求めることができる．当然のことながらこれは一致するはずのものである．力学質量の決定精度のよくなる発光経路の後半で，両者の比較をすることができる．

前のところでは詳しく述べなかったが，力学質量の計算には，流星体の密度 ρ_m を与えなければならないが，観測の段階ではこれを知ることはできない．そこで，力学質量と測光質量が一致しているかどうかをチェックするのではなく，ρ_m をフリー・パラメータとして，力学，測光質量がなるべく一致するような ρ_m を探し出すという立場で考えてみることにする．経路上のすべての点で完全な一致を期待するのは無理であるが，かなり両者の一致がよいように ρ_m を決めることは可能である．この方法で流星体の密度を求めることができる．こうして決めた密度はそんなに悪いものではなく，ごく普通の流星で 0.2～0.3g cm^{-3} ぐらいになる．この値が 3～4 g cm^{-3} 程度であれば，この本体はコンドライト質のものであろうと推定できる．ブレーリー・ネットワークで発見したロスト・シティ隕石でも，C_D, A の当初の推定値に多少の修正を加えただけで，写真観測から求めた密度と，隕石の実測密度の一致がみられた．

MSS-008

6. 隕石質量減少の理論的見積り

今まで述べたように，流星，火球の観測から，経路に沿ってどのように質量が減少していくかを知ることができる．これをもう少し理論的な形でまとめると，質量減少の基礎方程式はつぎのような形になる．

$$\zeta\dot{m}=-\frac{\Lambda}{2}S\rho v^3 \qquad \text{(基本式Ⅱ)}$$

ここで，

ζ ：流星体単位質量の気化熱

Λ ：熱輸達係数（流星体の失なう運動エネルギーのうち気化に使われる割合）

がある．

この式の右辺は次のように理解すればよい．まず，単位時間内に流星体が掃過する大気質量 m_a は，

$$m_a=S\rho v,$$

である．流星体はこの大気に v の速度を与える形になるから，大気の得る（したがって流星の失なう）運動エネルギーは，

$$\frac{1}{2}m_a v^2=\frac{1}{2}S\rho v^3$$

となる．そのうち Λ の割合が気化に使われるので，その形が基本式Ⅱの右辺である．

ここで，S に対して，(1) 式を適用して書き直しをすると，

$$\dot{m}=-\frac{\Lambda}{2\zeta}A\left(\frac{m}{\rho_m}\right)^{2/3}\rho v^3 \qquad (7)$$

となる．

ここで適当な地心直交座標系をとって，2次元で，流星の運動方程式を書いてみる．基本式Ⅰは x, y の2方向に分割し，地球引力の項も加える．質量減少の関係式(7)も加えて，これは，

$$\begin{aligned}\ddot{x}&=-Cm^{-1/3}\rho v\dot{x}-\mu\frac{x}{r^3}\\ \ddot{y}&=-Cm^{-1/3}\rho v\dot{y}-\mu\frac{y}{r^3}\\ \dot{m}&=-\sigma Cm^{2/3}\rho v^3,\end{aligned} \qquad (8)$$

と書くことができる．ここで μ は地心引力定数，また

$$\begin{aligned}r^2&=x^2+y^2\\ C&=\frac{C_D}{2}A\rho_m^{-2/3}\\ \sigma&=\frac{\Lambda}{C_D\zeta}\quad：摩耗係数\end{aligned} \qquad (9)$$

である．μ を含む項は地球引力の影響をあらわすが，隕石の質量減少を考える限り，この項の効果はごく小さい（隕石の落下地点を推定するような場合には，コリオリ力をはじめその他の細かい影響の考慮がさらに必要となる）．第2章で提出した問題のように，与えられた初期条件に対して隕石の質量減少を計算するには，その初期条件によって，微分方程式 (8) を数値的に解いていけばよい．

ここで一番問題になるのは，摩耗係数 (σ) の値をどのようにとるかということである．

σ には，ζ, Λ など決定精度のよくないものが含まれているので，精度のよい値を決定するのが困難であるように思われる．しかし，意外にも，まとめて σ の値を決めるのにはあまり問題がない．4章に述べた方法で，質量減少の様子は観測から求められる．その結果をなるべく忠実に再現することのできる σ を求めてみると，σ は案外によい精度で決まってくる．たとえば，普通コンドライトを考えられる流星体に対して，

$$\sigma\fallingdotseq 3\times10^{-2}\text{s}^2\ \text{km}^{-2} \qquad (10)$$

ぐらいの値が求められる．この値の誤差は，大きめにみても2割以内であろうと思われる．

ここまで説明してきて，やっと第2章で提起した問題に解答をする準備ができた．与えられた初期条件で，微分方程式(8)の数値解を求めればよいのである．

計算結果をひとつ示そう．隕石の発光，摩耗は，ほとんどすべて 100km 以下の大気層で起こるので，計算は高さ 100km からスタートし，地表まで行なった．その他のパラメータの値は，ロスト・シテイ隕石落下の例を参考にして，次のようにとった．

$\sigma=3\times10^{-2}\text{s}^2\ \text{km}^{-2}$

$A=2.0$

$C_D=1.2$

この計算に基づく実経路と，横軸を同じにとって質量減少の様子を示したものが第3図である．この図だけからもいろいろのことがわかるが，これは次のようにまとめられる．

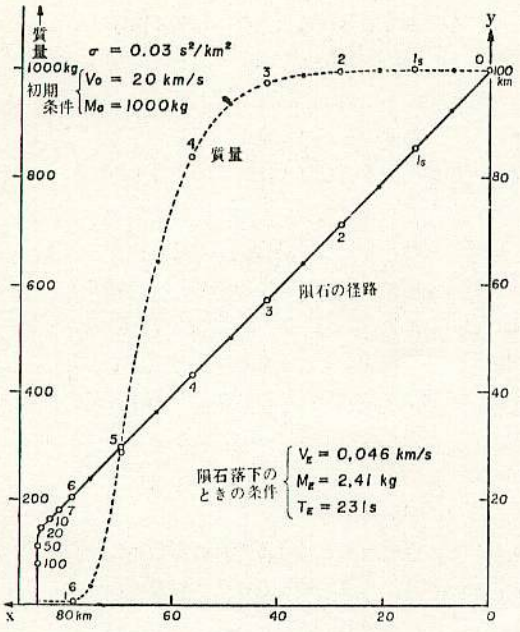

第3図　隕石落下の経路と質量減少曲線

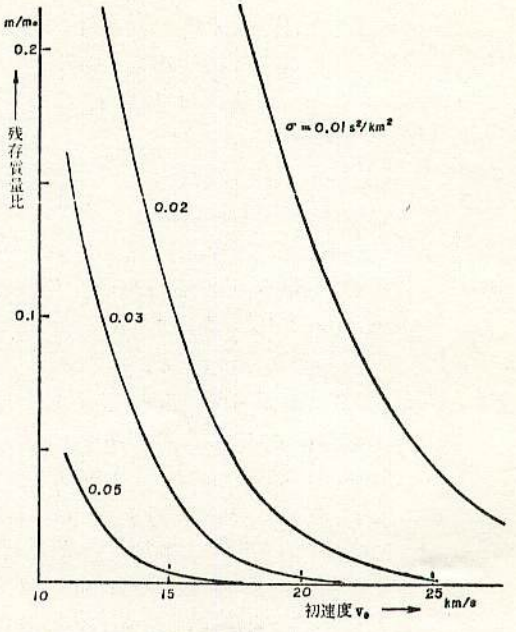

第4図　初速度に対する隕石の残存質量比

1）隕石は高さ30kmぐらいまではほとんど減速せずに落下し，それ以後急激に速度が落ちる．

2）高さ15km以下のところはほぼ自由落下の形となり，隕石はおおむね鉛直に落下する．

3）質量減少は高さ50～20kmの間で非常に激しく，ここで初期質量の大部分を失なう．最後の自由落下のところでは質量はほとんど減少しない．

そして，この計算によると，落下した最終質量はわずかに2.4kgである．これは，初期質量の0.24%にすぎない．これが，第2章で提起した問題の答である．

この計算では，摩耗係数をはじめ，パラメータの値に必らずしも正確ではない数値を使ったり，定数といえないものを定数と考えたりしているので，得られた結果がそのまま正確なものといえないのは当然である．こういう数値のうちで質量減少にもっとも敏感に影響を与えるものは摩耗係数（σ）である．しかし，仮にσが2割小さいと考えても，隕石の落下質量は8.0kgにしか増加せず，摩耗が非常に大きいという結果に変わりはない．

7. 落下質量比の略算法

前章では，隕石の最終落下質量を，微分方程式（8）の数値解を求めるという手段で計算したが，ここで，もう少し簡単に概算する方法を述べよう．

前にあげた基本式Ⅰ，Ⅱは，

$$\dot{m} = -\frac{\Lambda}{2\zeta} S\rho v^3 \qquad \text{（基本式Ⅱから）}$$

$$m = -\frac{C_D}{2\dot{v}} S\rho v^2 \qquad \text{（基本式Ⅰから）}$$

と書き直すことができる．この2式を辺々割り算して，

$$\frac{\dot{m}}{m} = \frac{\Lambda}{C_D\zeta} v\dot{v}$$

$$= \sigma v\dot{v} \qquad (11)$$

となる．この関係式は直ちに積分することができ，

$$\log m = \frac{\sigma}{2} v^2 + \text{const}$$

あるいは，

$$\frac{m}{m_0} = \exp\left\{\frac{\sigma}{2}(v^2 - v_0^2)\right\} \qquad (12)$$

という形になる．ここでm_0は初期質量，v_0は初速度と考えてよい．

この式は，隕石の初期質量に対する残存質量の割合

を，隕石の速度の関数として表現した形になっている．ここでvを最終速度とすればmは最終の落下質量になる．考えている隕石の質量範囲では，v_0^2 に対して v^2 は無視してもよいぐらいの値である．v^2を無視すると，(12)式は，

$$\frac{m}{m_0} = \exp\left(-\frac{\sigma}{2} v_0^2\right), \tag{13}$$

となる．ここから，隕石の残存質量比が概算できる．つまり，残存質量比は，隕石の大気突入前の速度だけで決まり，突入の角度には影響を受けない．

ここで述べているのは，あくまでも概略の話であるが，(13)式から，残存質量比が初速度によってどのように変わるかを，σをパラメータとして第4図に示した．

第4図をみると，地球に対する初速度が 20km s^{-1} を超すと，残存質量比が急激に小さくなることがわかる．第2章での問題で隕石の初速度を20km s^{-1} としたのは，この限界値のところだったわけで，速度がもう少し小さければ，隕石落下量はかなり大きくなるであろうことがこの図から想定できる．一般的にいって，隕石が落下するためには，

1）はじめの質量がきわめて大きい，か

2）対地速度が 20km s^{-1} 以下であること

が，必要条件であろうと思われる．

8. 炭素質コンドライト

今までは普通コンドライトについて考えてきたが，ここで話を少し変えて，炭素質コンドライトのことを考えてみる．

彗星起源と考えられる流星を別とすると，観測される流星，火球はほとんどすべてがコンドライト質のものであろう．こうしたものが大気中で消滅し隕石を生じない場合に，それが普通コンドライトであるか炭素質コンドライトであるかを，発光の様子から区別することができるであろうか．

観測する立場からいうと，このような火球の発光には，明らかに，つぎのような典型的な2つのタイプがある．

タイプⅠ：発光の様子が穏やかで光度変化がゆるやかであり，相当低空まで発光が継続するもの，この火球の密度は3～4 g cm^{-3} のものが多い．

タイプⅡ：やや高空から光りはじめて光度変化が激しく，ある点で爆発的に増光し，高空で消滅するもの．密度は2 g cm^{-3} 前後である．

この2つのタイプを比べると，光りはじめの様子がほぼ同じであっても，タイプⅠの火球が発光して通過する大気層の実効的な厚さは，タイプⅡの場合の100倍に達することさえある．

流星，火球が発光する場合，その速度，進入角度，質量などは実にさまざまであるから，その発光の様子はいろいろに異なってくる．したがって，観測した火球を上記2つのタイプのどちらかに分類することは，実はそう簡単ではない．しかし，努力の末，だいたいの分類は可能になってきた (Ceplecha and McCrosky 1976)．

大ざっぱにいえば，タイプⅡの火球はよく光り，質量減少が大きいのである．そのため隕石にはなりにくい．以前には，火球の明るさはその質量の反映であり，明るいものほど質量が大きく，隕石になりやすいと想像されていた．しかし，それは誤った考えであることがわかってきた．たとえば，プレーリー・ネットワークで観測したもっとも明るい火球（40503と番号がつけられている）はタイプⅡに属するものであって，最大絶対光度が−20等，大気突入前の質量460トンという見積りもあるが，力学的に求めた最終質量はほとんど0で，隕石も発見できなかった．

タイプⅡの火球は，タイプⅠの火球に比べてはるかに光りやすく，これに対しての摩耗係数は，ほぼ，

$$\sigma = 0.05 \text{ s}^2 \text{ km}^{-2} \tag{14}$$

程度と見積られている．しかし，この摩耗係数でも，経路途中の爆発的な増光を説明することはできない．この急激な増光は，隕石が表面から摩耗していくというより，全体が破砕して実効的な断面積が急激に増すためと考えた方がよいように思われる．

では，どのぐらいの力で破砕が起こるのであろうか．ここでは，一例として，20 km s^{-1} の速度の火球が，高さ55kmで破砕増光した場合を考えてみよう．基本式Ⅰを変形して流星体に対する圧力の式に直すと，

$$\frac{m\dot{v}}{S} = -\frac{C_D}{2}\rho v^2, \tag{15}$$

となる．高さ55kmでの大気密度ρを5.7×10^{-4}kg m^{-3},

MSS-008

抵抗係数 C_D を1として(15)式の右辺を計算すると，圧力として 1.1×10^5Pa が求まる．つまり，この場合，一方向から 10^5Pa 程度の圧力を受けて流星体が破砕したと考えられるわけで，通常指先でつぶせる程度といわれる炭素質コンドライトの強度と，ほぼ見合っているということができる．

以上に述べた結果を総合して考え，

タイプⅠの火球←→普通コンドライト

タイプⅡの火球←→炭素質コンドライト

という対応をつけるのが一応妥当であろうかと思われる．

ところで，今まで述べてきたように，タイプⅡの火球あるいは炭素質コンドライトは，普通コンドライトに比べてずっと摩耗しやすく破砕しやすい．したがって，同じ質量のものが同じ条件で地球大気に突入したとしても，普通コンドライトの方だけが隕石となるといった場合が当然考えられる．つまり，炭素質コンドライトの隕石は地球近傍の太陽系空間に存在するであろう割合よりずっと少なくなる．太陽系空間では，炭素質コンドライトの存在比は，地球上の隕石の場合よりもっと多いはずである．

Ceplecha と McCrosky(1976) は，プレーリー・ネットワークで観測した火球のうち232個を解析した．この火球は，明るさ，発光継続時間などを基準にして選び出したものであって，母集団からの無作為抽出とはいえず，統計的資料とするのに問題はあるが，その分類結果は，

タイプⅠ	94個（うち隕石1個）
タイプⅡ	90個
彗星起源のもの	40個
判断できないもの	8個
計	232個

となっている．このことは，地球近傍の空間では，普通コンドライトと炭素質コンドライトの存在個数が，概略同じオーダーにあることを想像させる．

9. 結論

今までの内容を，つぎのようにまとめて結論とする．

1）石質隕石の場合，地表に落下する部分は，大気突入前の質量のほんの一部だけである．対地速度が20 km s^{-1} 以上になると経路途中の摩耗によって，隕石落下の可能性が非常に小さくなる．隕石として落下するためには，初期質量が大きく，対地速度が小さいことが必要である．

2）対地速度が小さいという条件を満たすために，落下した隕石の軌道は，特別な条件をもったものに偏っていると思われ，地球と交叉する軌道をもつ一般的な天体の代表とは考えにくい．たとえば，逆行軌道，あるいは長周期彗星のような軌道のコンドライトがあったとしても，それらが隕石として落下する可能性はごく小さい．

3）炭素質コンドライトは落下条件がさらにきびしい．これは主としてその構造的なもろさに原因があると思われる．隕石として落下した炭素質コンドライトは，もともと非常に大きく，対地速度がごく小さい（11～13km s^{-1} ぐらい）ものであったと推測される．地球近くの太陽系空間では，普通コンドライトと炭素質コンドライトの存在数は，概略同じ程度である可能性が大きい．

10. おわりに

はじめに，隕石の摩耗についての意見のくいちがいが大きいと述べたのであるが，今回の特集号を見れば，その違いはそう大きくはないように思われる．たとえば，今村氏から教示をいただいた資料（Bhandari *et al*. 1980）によると，速度のよくわかっている隕石3例について，宇宙線照射などをもとに推定した摩耗の割合は第2表のようである．

最後の欄に(13)式による計算値を付記した．この結果は必ずしも一致しているとはいえないにしても，初期質量の大部分が大気中で失なわれるという点で，流星研究の延長としてみちびいてきたわれわれの結果と，そう大きなへだたりがあるとは思われない．

なお，この他の点でも，筆者の内容に対して数多くのコメントがあった．そのひとつは重要なものと思われるので，以下に簡単に説明する．それは，

"4章の，基本式Ⅰの左辺は $m\dot{v}$ となっているが，これは $\frac{d}{dt}(mv)=m\dot{v}+\dot{m}v$ とするべきではないか．質量減少が小さくない場合に $\dot{m}v$ の項を省略するのは適当と思われない" というものであった．

MSS-008

第2表．宇宙線照射から求めた摩耗率

隕石	速度	摩耗率	(13)式による摩耗率
プリブラム隕石	20.9km s^{-1}	96%	99.9%
ロスト・シティ隕石	14.2	85	95
イニスフリー隕石	14.5	>99	96

運動量の時間変化が力となるのであるから，この指摘は正しい．質量の減少の激しいところで $\dot{m}v$ の項を無視することは，結果に系統的な誤差を生じさせることになるであろう．

この点について考慮してみたところ意外なことがわかった．まず，基本式Ⅰの形は次のように変わる．

$$m\dot{v}=-\frac{C_D}{2}S\rho v^2-\dot{m}v. \tag{16}$$

ここへ，基本式Ⅱから得られる関係，

$$\dot{m}=-\sigma\frac{C_D}{2}S\rho v^3 \tag{17}$$

を代入すると，

$$\dot{m}v=-\frac{C_D}{2}S\rho v^2(1-\sigma v^2) \tag{18}$$

となる．式の形からみて明らかに，

$$\sigma v^2<1 \tag{19}$$

でなければならない．これは，今まで考えていた摩耗係数 σ の値が大きすぎることを意味する．そして，この結果は，今まで述べてきたこと全体に，かなり大きな影響を与える可能性がある．

それでは，どのように考えればよいか．この点についての検討はまだ不十分であり，今後時間をかけて考えてみたいと思っている．

参考文献

[1] Ayers, W.G., R.E. McCrosky and C.-Y. Shao: Smithsonian Astrophysical Observatory Special Report, 317(1970).
[2] Bhandari, N., D. Lal, R. S. Rajan, J. R. Arnold, K. Marti and C. B. Moore: Nucl. Tracks, 4, 213~262(1980).
[3] Ceplecha, Z. and R. E. McCrosky: Center for Astrophysics Preprint Series, No. 442(1976).
[4] McCrosky, R. E., C.-Y. Shao and A. Posen: Center for Astrophysics Preprint Series, No. 721(1977).

SYMPOSIUM

惑星間固体物質／8

固体惑星探査のすすめ

長谷川　博　一（はせがわ　ひろいち）
京都大学理学部 教授

流星の大気中の運動について

寺田 充

流星は、単体モデルとして扱うときには、以下の方程式に従うことが知られている。

$$\frac{dv}{dt} = -\Gamma A m^{-\frac{1}{3}} \rho_m^{-\frac{2}{3}} \rho_a v^2 \quad \sim (1)$$

（$\frac{dv}{dt}$：観測量、ρ_a：観測量、v^2：観測量）

$$\frac{dm}{dt} = -\frac{\Lambda}{2\xi} A m^{\frac{2}{3}} \rho_m^{-\frac{2}{3}} \rho_a v^3 \quad \sim (2)$$

ここで　v；対地速度　　m；流星の質量

Γ；抵抗係数　　A；形状因数

ρ_m；流星体の密度　　ρ_a；大気密度

Λ；熱輸送係数

球の場合　$A = 1.209$

一般的には、$\Gamma = \begin{cases} 0.46 & \text{for five balls} \\ 1 & \text{for faint meteor} \end{cases}$

$\xi = (0.2 \sim 1.0) \times 10^{11}\ erg/g$

$\Lambda = 0.1 \sim 0.6$

(1)(2)を解くことにより、流星体の運動を単体モデルとして知ることができる。(1),(2)の方程式中、特に興味ある量は、流星体の密度である。

方程式中、観測可能なものは、v（速度）、$\frac{dv}{dt}$、さらにρ_a（大気密度）は、知られている。これだけでは、全く情報不足なので、流星の光量は、次式で与えられるものとする。

$$I\,dt = -\tau\,dE \quad \sim (3)$$

I；流星の光量

E；流星体のもつ運動エネルギー

$E = \frac{1}{2} m v^2$，$dE \simeq \frac{v^2}{2} dm$

さらに

$$\tau = \tau_0 v \quad \sim (4)$$

τ_0；const.

Iを用いて流星の絶対等級Mは

$$M = 24.30 - 2.5 \log I \quad \sim (5)$$

MSS-009

今回は次のようなモデルも仮定した。

流星の密度 $\rho_m = 0.3\ g/cm^3$　　輻射点の天頂角 30°

速度の初期値 $v = 60\ km/s$　　$P=1$, $A=1.209$

$\tau_0 = 1\times10^{-5}\ sec/km$

ρ_a は、US 標準大気を用いた。

○ $\left[\frac{\Lambda}{\varepsilon}\right]$ の値による 大気減速 (Fig 2)、光度変化 (Fig 1) の差異

A ; $\frac{\Lambda}{\varepsilon} = 1.0\times10^{-12}\ [g/erg]$　　B ; $\frac{\Lambda}{\varepsilon} = 2.0\times10^{-12}\ [g/erg]$

C ; $\frac{\Lambda}{\varepsilon} = 4.0\times10^{-12}\ [g/erg]$　　D ; $\frac{\Lambda}{\varepsilon} = 8.0\times10^{-12}\ [g/erg]$

E ; $\frac{\Lambda}{\varepsilon} = 1.6\times10^{-11}\ [g/erg]$　　F ; $\frac{\Lambda}{\varepsilon} = 3.0\times10^{-11}\ [g/erg]$

以上の 6 つについて計算を行なった。質量の初期値は 1g

Fig 1 を見るとそれぞれのモデルにより、光度が最大となる高度がかなり違うことがわかるが、最大の光度は、あまり変わらない。

Fig 2 では、減速の様子は、それぞれのモデルで似ており、速度変化から $\left[\frac{\Lambda}{\varepsilon}\right]$ を推定することは、不可能と思われる。

○ 初期の質量の差による光度変化の差 (Fig 3)、速度変化 (Fig 4)

初期の質量を 0.1g, 1g, 2g, 5g 10g として、計算を行なった。

$\left[\frac{\Lambda}{\varepsilon}\right] = 8.0\times10^{-12}\ [g/erg]$ とした。

○ 流星密度 ρ_m を知る手がかりとして、光度変化は、あまり直接的な手掛りにはなりそうもない。なぜならば、$\left[\frac{\Lambda}{\varepsilon}\right]$ の値の巾が、かなり大きいからである。

ρ_m の値をいろいろ変えて、速度変化を調べるつもりであったが、時間の都合で、できなかった。

MSS-009

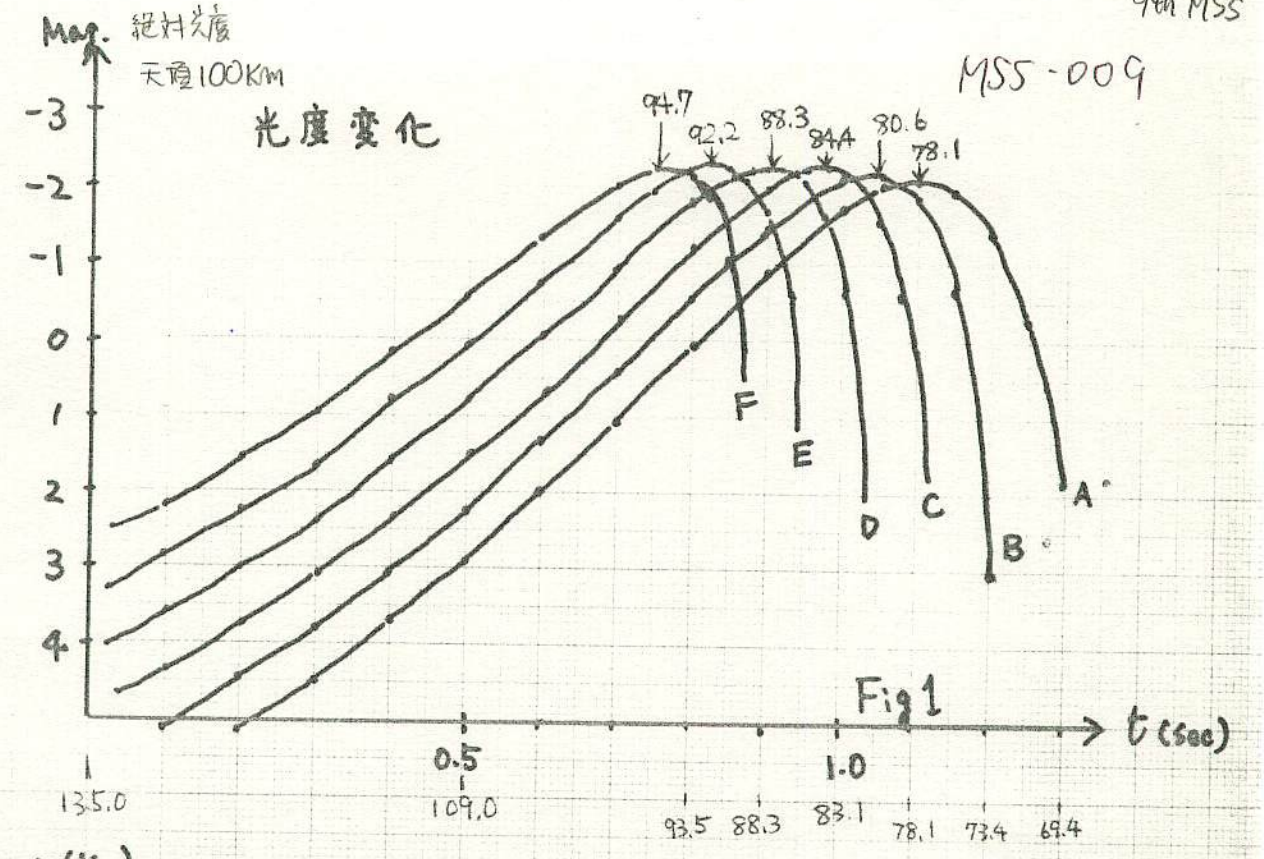

Fig 1

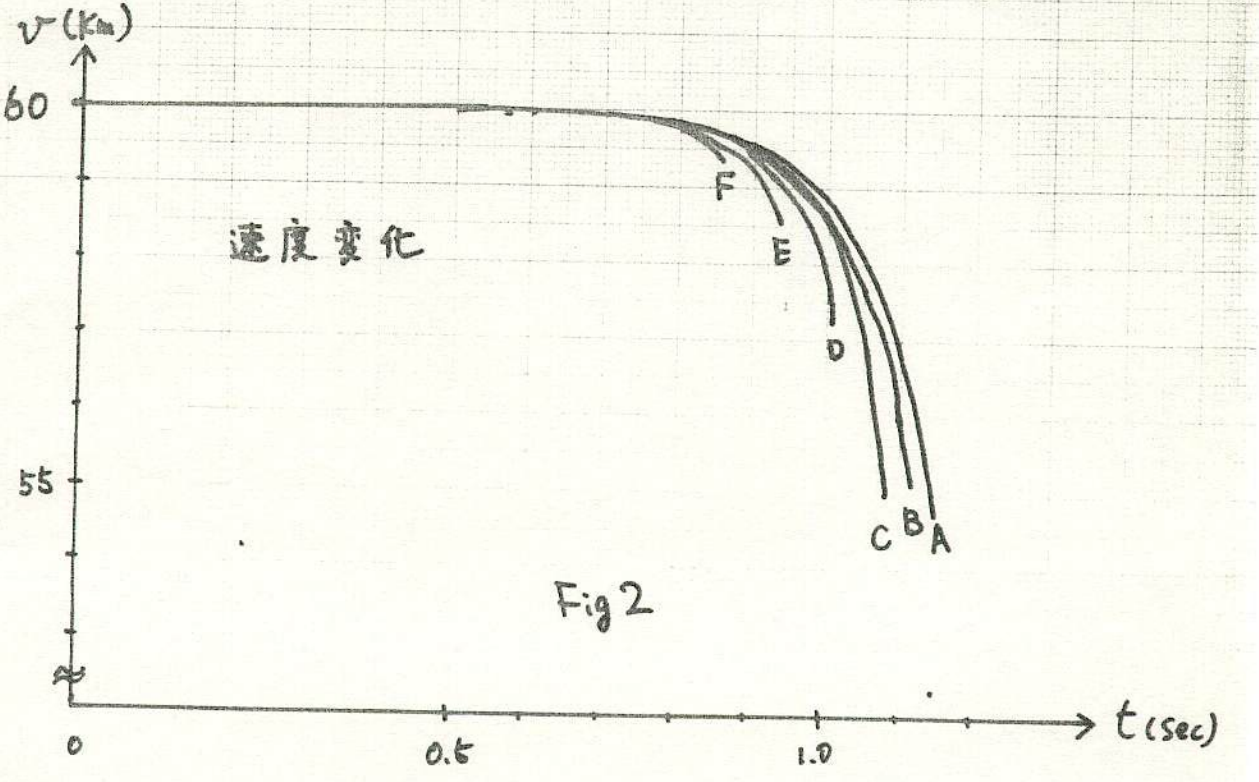

Fig 2

M55-009

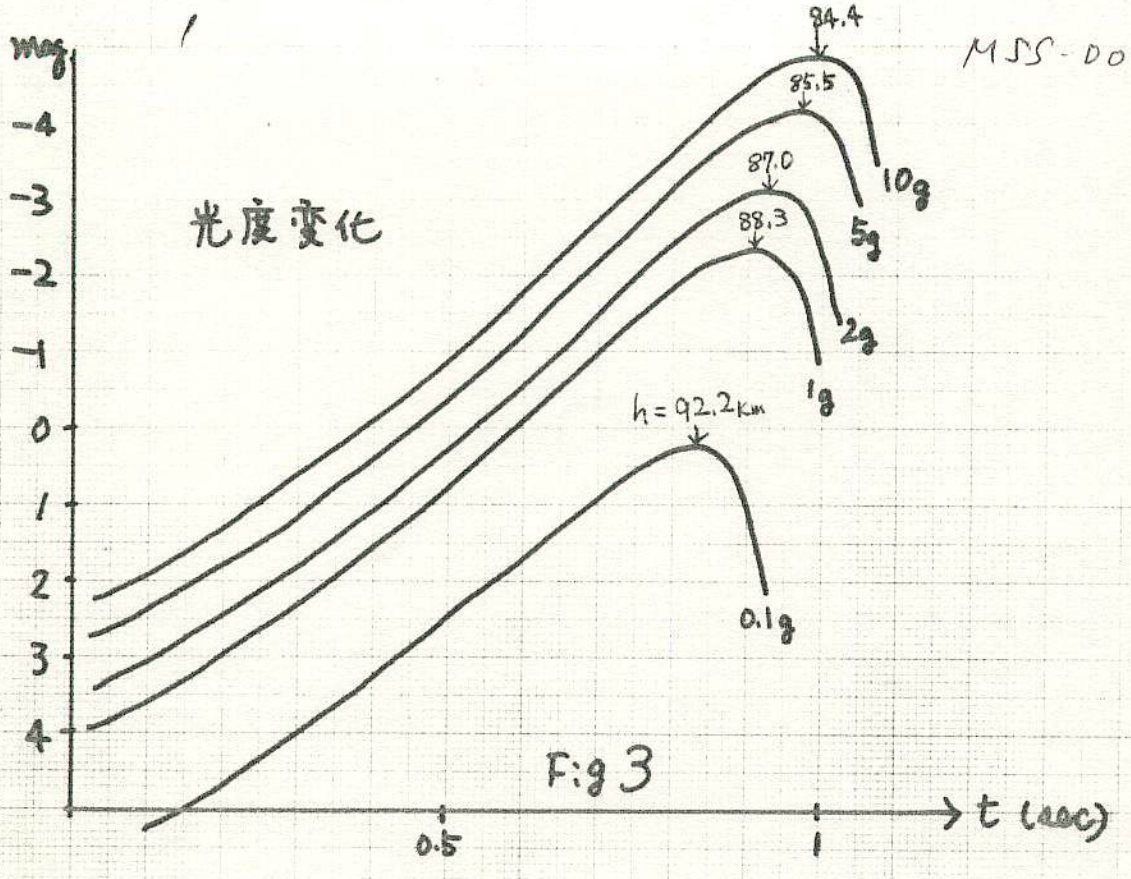

Fig 3

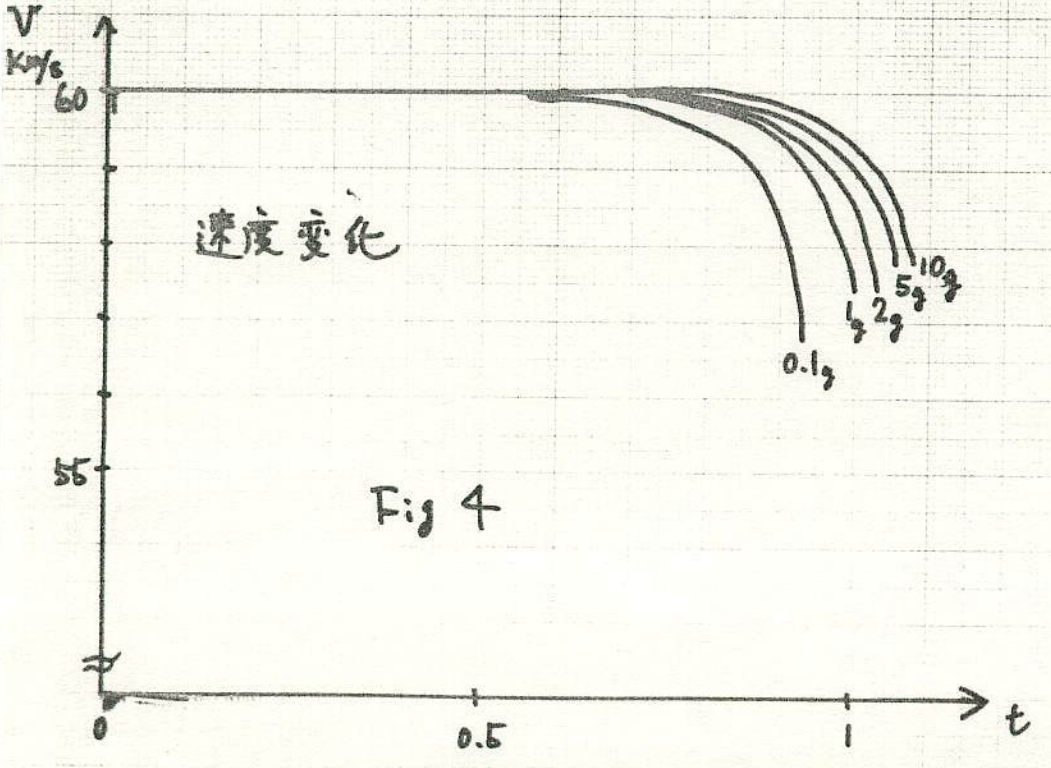

Fig 4

微分方程式の数値解法についてのメモ

流星物理セミナー資料 (S55, May. 18) MSS-004
長沢 工

9th MSS

[1] ルンゲ・クッタ法

$y' = f(x, y)$ の微分方程式を数値的に解く。

この解のある点の値 (x, y) がわかっているとき、x が h だけ増加した $x+h$ に対する y の値を求める

$$\left.\begin{aligned} k_1 &= f(x, y) \\ k_2 &= f\left(x+\frac{h}{2},\ y+\frac{1}{2}hk_1\right) \\ k_3 &= f\left(x+\frac{h}{2},\ y+\frac{1}{2}hk_2\right) \\ k_4 &= f(x+h,\ y+hk_3) \end{aligned}\right\} \text{を計算し、} \quad x+h \text{に対する値は} \quad y + \frac{h}{6}(k_1+2k_2+2k_3+k_4)$$

例 $y' = y$, $x=0$, $y=1$, $h=0.1$

$$\left.\begin{aligned} k_1 &= f(x, y) = y = 1 \\ k_2 &= y+\frac{1}{2}hk_1 = 1+\frac{1}{2}\times(0.1)\times 1 = 1.05 \\ k_3 &= y+\frac{1}{2}hk_2 = 1+\frac{1}{2}\times(0.1)\times 1.05 = 1.0525 \\ k_4 &= y+hk_3 = 1+(0.1)\times 1.0525 = 1.10525 \end{aligned}\right\} \quad \begin{aligned} &\frac{h}{6}(k_1+2k_2+2k_3+k_4) \\ &= \frac{1}{6}\times 0.1 \times 6.310025 \\ &= 0.1051708333 \end{aligned}$$

したがって $x=0.1$ に対し $y = 1.1051708333$ となる (真の値は 1.1051709180)

これをくり返して $x=1$ に対し $y = 2.7182\,79737$ (真の値は 2.7182 81828)

1ステップに対する打切り誤差は大略 h^5 のオーダーである (オイラー法では h^2 のオーダー)

[2] 誤差原因

a) 打切り誤差

1ステップ先の y の値を計算するのに実際は $y', y'', y''', \cdots$ をすべて必要とする。

$$\left(\Delta y = hy' + \frac{1}{2}h^2y'' + \frac{h^3}{3!}y''' + \cdots\right)$$

しかし上記の近似式ですませてしまうために、真実の値との差を生ずる。これが打切り誤差である。

打切り誤差を小さくするためには きざみ巾 h を小さくしなければならない。倍精度の計算をしても この誤差は小さくならない。

b) 丸め誤差

計算機は有限の桁数で計算をするから その末尾で一般に4捨5入 (計算機内部では 七カ捨てあるいは0捨1入) がおこなわれる。これで丸め誤差が生じる。計算過程で 丸め誤差が集積して大きな誤差となることは、コンピューターの計算では決して無視できない。たとえば、0.01を100回加えても 1にならない計算機はたくさんある。(0.1や0.01は2進法では無限小数である)

丸め誤差を小さくするには、次のようにする

- きざみ巾を大きくして演算回数を減らす。
- きざみ巾を誤差のでないように2のべき乗にする (0.1より 0.125がよい)。
- 倍精度の計算をする

[3] きざみ巾

上記のことから、打切り誤差を小さくするには、きざみ巾 h が小さい方がよく 丸め誤差を小さくするには きざみ巾 h は大きい方がよい。(きざみ巾を小さくすれば 誤差はいくらでも小さくなると考えてはいけない) 両方の誤差を合わせてもっとも小さくする最適のきざみ巾があるわけであるが、はじめに このきざみ巾を推定するのはむずかしい。

現実の対策としては (結果の有効数字が 5~6 桁でよい場合を念頭におく) まず打切り誤差を押える。

◎ 倍精度計算にて 丸め誤差を小さくおさえ 適宜なきざみ巾で一応計算をし これに同じところを きざみ巾を半分にて 計算し 打切り誤差を見積る; 両者の差が小さければ 次のステップへ進む という計算が必要である。

◎ 計算の進行につれて、きざみ巾を適当に変更するようなプログラムにすることが必要。

◎ $y' = f(x,y)$ の形では $h \cdot \frac{\partial f}{\partial y}$ が大きいと とんでもない結果が出やすい。この値をめやすにしてきざみ巾 h を定める 方法もある

[4] 変数変換

変数を変換して方程式を書き直すと、解きやすい形になる場合がある。2元以上の連立方程式では特にその効果が大きいようである。

たとえば $\begin{cases} \frac{dx}{dt} = -y \\ \frac{dy}{dt} = x \end{cases}$ という連立微分方程式を初期条件 $t=0,\ x=1,\ y=0$ で

解き $t=1$ に対する x, y の値を求めることを考える。もちろん このままでルンゲ・クッタ法を適用しても計算はできる。しかしここで 変数を $(x,y) \to (r,\theta)$ に変換してみる

$$\begin{cases} x = r\cos\theta \\ y = r\sin\theta \end{cases}$$

これによって方程式は $\begin{cases} \frac{dr}{dt}\cos\theta - r\sin\theta\frac{d\theta}{dt} = -r\sin\theta \\ \frac{dr}{dt}\sin\theta + r\cos\theta\frac{d\theta}{dt} = r\cos\theta \end{cases}$

と変換され、結局 $\begin{cases} \frac{dr}{dt} = 0 \\ \frac{d\theta}{dt} = 1 \end{cases}$ という形になる 初期条件は $t=0$ で $r=1$ $\theta=0$ である

ここから $r=1$, $\theta=t$ が得られて それ以上計算の必要はほとんどない。$t=1$ に対する値は $r=1$, $\theta=1$ で、つまり $\begin{cases} x = \cos 1 = 0.54030 \\ y = \sin 1 = 0.84147 \end{cases}$ となる。はじめの式にそのままルンゲクッタ法を適用して この値が得られるかどうかやってみるとよい。

ただし、一般に、どのような変数変換をすれば、計算に便利な形になるかを発見するのはそうやさしくない。それについては非常に高度な理論があるがここでは省略する。

[5] 計算プログラムの工夫

誤差の重なりを防ぐようにプログラムに工夫をすることは一般に有益である。たとえば 前述のように 0.1のきざみ巾をとって次つぎに加えていくやり方はよくない。ルンゲクッタ法に限らず一般に次のような注意が必要である。

- 同じ程度の大きさの2数の差をとらない。(桁落ち防止)
- 大きさの極端に異る2数の和や差をとらない。

その他 別に説明する。

隕石落下シミュレーション MSS-009

月面惑星研究会 長谷川均

2次元における隕石落下の方程式は.

$$\begin{cases} \dfrac{d^2x}{dt^2} = -\dfrac{x}{r^3}GM - \dfrac{C_D}{2m}S\rho V u & (1) \\ \dfrac{d^2y}{dt^2} = -\dfrac{y}{r^3}GM - \dfrac{C_D}{2m}S\rho V v & (2) \\ \dfrac{dm}{dt} = -\dfrac{1}{2}\sigma C_D A m^{\frac{2}{3}} \rho_m^{-\frac{2}{3}} \rho V^3 & (3) \end{cases}$$

で表わされる。この連立微分方程式を数値的に解くことによって. 時々刻々の位置, 速度, 質量等がわかる。(1)~(2)の方程式は. 2階になっているので 1階にの方程式に分解する。

$$\begin{cases} \dfrac{du}{dt} = -\dfrac{x}{r^3}GM - \dfrac{C_D}{2m}S\rho V u & (4) \\ \dfrac{dv}{dt} = -\dfrac{y}{r^3}GM - \dfrac{C_D}{2m}S\rho V v & (5) \\ \dfrac{dx}{dt} = u & (6) \\ \dfrac{dy}{dt} = v & (7) \end{cases}$$

ここで $r=\sqrt{x^2+y^2}$, $V=\sqrt{u^2+v^2}$, であり. ρ は. x, y の関数であり. S は.

$$S = A m^{\frac{2}{3}} \rho_m^{-\frac{2}{3}} \quad (8)$$

で計算できるので. (2), (3), (4), (5), (6), (7) の微分方程式は.

$$\frac{du}{dt} = f(x, y, u, v, m) \quad (9)$$

$$\frac{dv}{dt} = g(x, y, u, v, m) \quad (10)$$

$$\frac{dx}{dt} = h(u) \quad (11)$$

$$\frac{dy}{dt} = i(v) \quad (12)$$

MSS-009

$$\frac{dm}{dt} = j(x, y, u, v, m) \qquad (13)$$

と書ける。これをルンゲ・クッタ法（4次）により解く。

$$\begin{cases} u_{t+1} = u_t + \frac{1}{6}(k_0 + 2k_1 + 2k_2 + k_3) \\ v_{t+1} = v_t + \frac{1}{6}(l_0 + 2l_1 + 2l_2 + l_3) \\ x_{t+1} = x_t + \frac{1}{6}(m_0 + 2m_1 + 2m_2 + m_3) \\ y_{t+1} = y_t + \frac{1}{6}(n_0 + 2n_1 + 2n_2 + n_3) \\ m_{t+1} = m_t + \frac{1}{6}(o_0 + 2o_1 + 2o_2 + o_3) \end{cases}$$

ここで

$$\begin{cases} k_0 = f(x_t, y_t, u_t, v_t, m_t) \times \Delta t \\ k_1 = f\left(x_t + \frac{m_0}{2}, y_t + \frac{n_0}{2}, u_t + \frac{k_0}{2}, v_t + \frac{l_0}{2}, m_t + \frac{o_0}{2}\right) \times \Delta t \\ k_2 = f\left(x_t + \frac{m_1}{2}, y_t + \frac{n_1}{2}, u_t + \frac{k_1}{2}, v_t + \frac{l_1}{2}, m_t + \frac{o_1}{2}\right) \times \Delta t \\ k_3 = f(x_t + m_2, y_t + n_2, u_t + k_2, v_t + l_2, m_t + o_2) \times \Delta t \end{cases}$$

l, m, n, o についても同様である。もとの方程式をベクトル形式で書くと、

$$\frac{d\mathbf{u}}{dt} = \mathbf{f}(\mathbf{u}), \quad \mathbf{u} = \begin{bmatrix} x \\ y \\ u \\ v \\ m \end{bmatrix}, \quad \mathbf{f} = \begin{bmatrix} f(\,) \\ g(\,) \\ h(\,) \\ i(\,) \\ j(\,) \end{bmatrix}$$

$$\mathbf{u}_{t+1} = \mathbf{u}_t + \frac{1}{6}(\mathbf{k}_0 + 2\mathbf{k}_1 + 2\mathbf{k}_2 + \mathbf{k}_3)$$

ここで

$$\begin{cases} k_0 = ff(u_t) \times \Delta t \\ k_1 = ff\left(u_t + \frac{k_0}{2}\right) \times \Delta t \\ k_2 = ff\left(u_t + \frac{k_1}{2}\right) \times \Delta t \\ k_3 = ff(u_t + k_2) \times \Delta t \end{cases}$$

$t=0$ における u の値を 初期値として、くり返し 計算することによって、解が得られる。

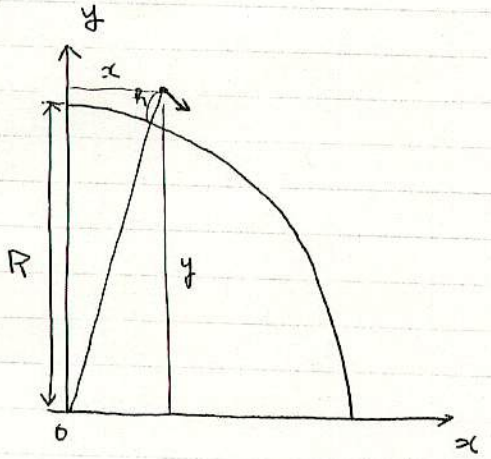

x, y : 隕石の座標.
u, v : 隕石の速度.

GM : 地心重力定数.
$= 3.986005 \times 10^{14} m^3 s^{-2}$

r : 隕石の地心距離.
C_D : 抵抗係数. 0.5～1.
S : 隕石の断面積
ρ : 大気の密度
ρ_m : 隕石の密度.
m : 隕石の質量.
σ : 摩耗係数.
A : 形状因数. 1～2.
Δt : 時間ステップ.

ρについては、US 標準大気を 近似して 使う。

最近のマイクロコンピューターは、グラフィック機能が付いているので隕石の経路、質量変化などのグラフが見られるので便利である。

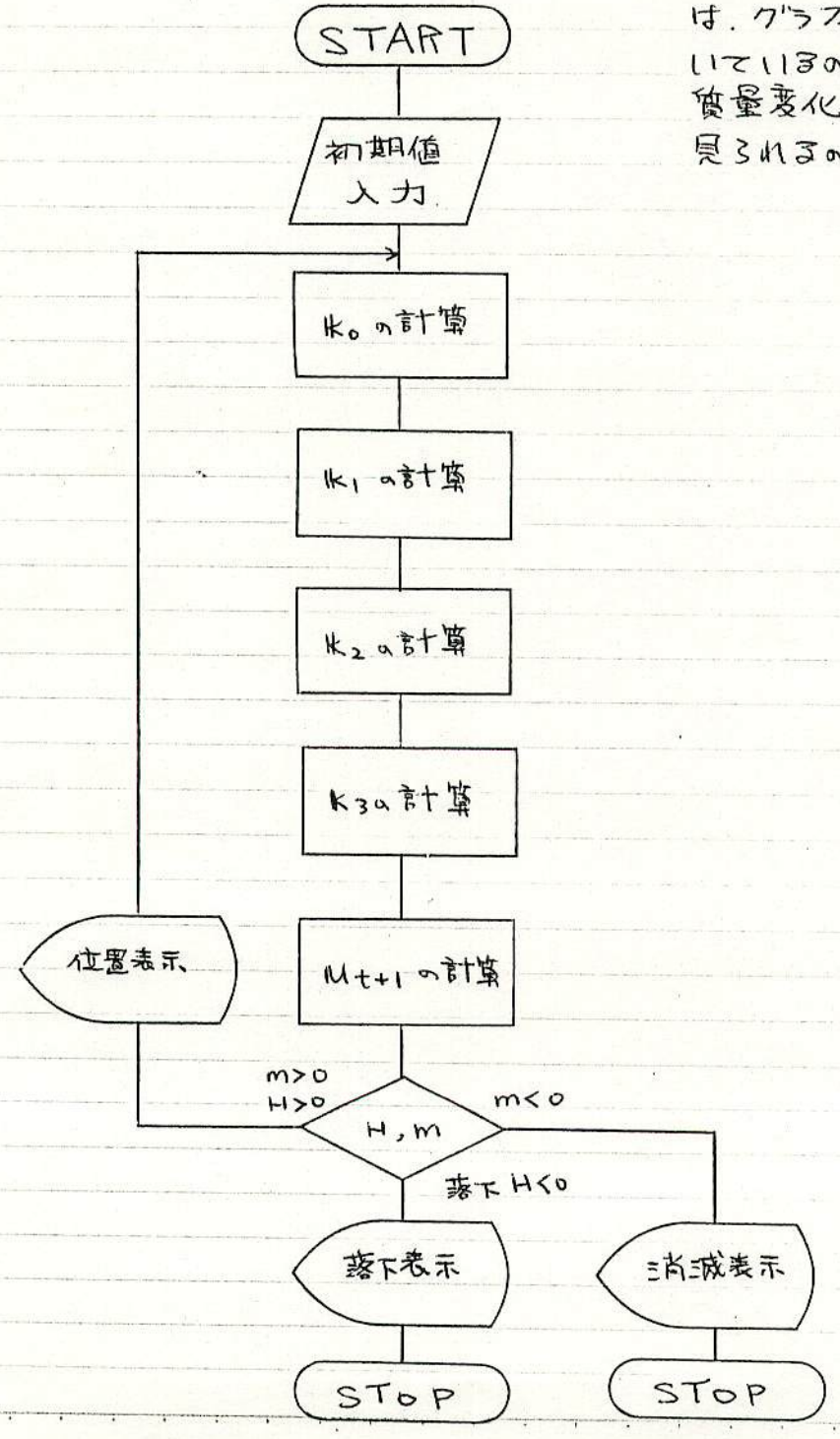

12th MSS 入7

隕石落下シミュレーション

Computer Simulation on the Meteorite Fall

流星物理セミナー　小笠原雅弘

Masahiro Ogasahara

1980 Aug 29 - 31

MSS-12

Yabu Object 1979 Dec.15 02h20m55sJST

V_∞ 21 km/s
Zr 74°
ρ_m 3.7 g/cm³
M_∞ 100 kg

	sec	Height km	Mass kg	Velocity m/s	Mag
	1.0	0.942E+05	1.000E+02	0.210E+05	-4.2
	2.0	0.885E+05	0.999E+02	0.210E+05	-5.3
	3.0	0.829E+05	0.996E+02	0.210E+05	-5.9
	4.0	0.773E+05	0.991E+02	0.210E+05	-6.7
	5.0	0.717E+05	0.981E+02	0.210E+05	-7.6
	6.0	0.663E+05	0.957E+02	0.210E+05	-8.4
	7.0	0.608E+05	0.907E+02	0.209E+05	-9.2
	8.0	0.555E+05	0.807E+02	0.207E+05	-9.6
max	9.0	0.503E+05	0.626E+02	0.204E+05	-10.1
	10.0	0.453E+05	0.361E+02	0.196E+05	-9.7
	11.0	0.407E+05	0.112E+02	0.177E+05	-8.1
	12.0	0.369E+05	0.133E+01	0.136E+05	-4.4
	13.5	0.337E+05	0.141E+00	0.635E+04	2.1
	16.0	0.318E+05	0.929E-01	0.195E+04	
	18.5	0.309E+05	0.896E-01	0.103E+04	
	30.7	0.288E+05	0.883E-01	0.314E+03	
	50.7	0.260E+05	0.881E-01	0.166E+03	
	70.7	0.231E+05	0.880E-01	0.137E+03	
	90.7	0.207E+05	0.880E-01	0.113E+03	
	116.7	0.181E+05	0.879E-01	0.942E+02	
	166.7	0.142E+05	0.878E-01	0.695E+02	
	216.7	0.111E+05	0.877E-01	0.553E+02	
	266.7	0.866E+04	0.876E-01	0.460E+02	
	316.7	0.657E+04	0.876E-01	0.394E+02	
	366.7	0.475E+04	0.875E-01	0.345E+02	
	416.7	0.314E+04	0.875E-01	0.307E+02	
	466.7	0.163E+04	0.874E-01	0.289E+02	
	516.7	0.224E+03	0.874E-01	0.268E+02	

Yabu Object

M_∞~500 kg

	ec	Height km	Mass kg	Mag
	0.1	0.994E+05	0.500E+03	
	1.1	0.937E+05	0.500E+03	
	2.1	0.880E+05	0.500E+03	
	3.1	0.823E+05	0.500E+03	
	4.1	0.767E+05	0.499E+03	
	5.1	0.712E+05	0.499E+03	-6.7
	6.1	0.657E+05	0.497E+03	-7.4
	7.1	0.603E+05	0.494E+03	-7.9
	8.1	0.549E+05	0.486E+03	-8.9
	9.1	0.496E+05	0.470E+03	-9.7
	1 .1	0.444E+05	0.438E+03	-10.4
	. .1	0.392E+05	0.377E+03	-11.1
max	1 .1	0.343E+05	0.275E+03	-11.5
	1 1	0.295E+05	0.145E+03	-11.8
	1 1	0.253E+05	0.429E+02	-11.5
	15 1	0.220E+05	0.799E+01	
	17.	0.187E+05	0.184E+01	
	19.	0.170E+05	0.150E+01	
	22.	0.161E+05	0.146E+01	
	29.	0.145E+05	0.144E+01	
	49.	0.115E+05	0.144E+01	
	69.8	0.841E+04	0.143E+01	
	89.8	0.572E+04	0.143E+01	
	109.8	0.348E+04	0.143E+01	
	150.8	0.177E+03	0.143E+01	

Table 1, 2

方程式系として、長沢工氏（星の手帖 Vol.7 p98-103）の式を、2次元に簡単化したものを用い、落下する隕石に働く力は、地球の重力と大気の抵抗のみと考える。

地球大気は、US標準大気（1962）をもとにした等温大気の近似式

$$\rho = 1.4925\ EXP\left[h \times (-1.4366 \times 10^{-4})\right]\ (kg/m^3) \quad -(1)$$

を用いた。連立微分方程式をハンゲ・クッタ法という数値解法で解く。計算にはPC-8001（32kバイト拡張）マイクロコンピューターを用いた。0.1sec.の時間ステップで10～30分の計算時間を要する。

実際に隕石落下が写真観測されたロスト・シティ隕石のデータと、コンピューターによるシュミレーションの結果とを比較し、この計算がほぼ妥当なものであることを確かめた。流星の明るさ（絶対等級）Mは、$\dot{m}p$を1秒あたりの質量減少として

$$M = -2.5 \log\left(\frac{\tau}{2} \dot{m}p V^2\right) \quad -(2)$$

であらわされ、τは光力係数と呼ばれ、CgS系では

$$\tau = 10^{-19} V \quad -(3)$$

1979年12月15日のYabu-Objectを密度3.7g/cm³の普通コンドライト状物体と考え、大気外での質量をパラメーターとしていろいろ計算を行なったところ、（Table 1, 2）質量を200～300kgとするのが観測と良く一致することがわかった。地上40km位で最大等級は-11等となる。残存量は数百gと計算されるが、発見の可能性は小さいだろう。速度が20km/sをこえると隕石として落下する割合が極端に小さくなる。

計算には、長谷川均氏（木星研究グループ）の協力をいただいた。なお詳しくは「星の手帖.秋号」に掲載予定。

17th MSS　流星会議資料

22th Meteor Conference
at Utsunomiya

流星のコンピュータシミュレーション
Computer Simulation on the Meteors

流星物理セミナー　小笠原・雅弘
MSS　M. Ogasahara

コンピュータによる数値積分を用いて Perseids と Geminids の流星現象をシミュレーションした.

Per.	Gem.
$V \sim 60$ km/sec.	$V \sim 35$ km/sec.
$Z_r \sim 45°$	$Z_r \sim 90°$
$\rho_m \sim 0.3$ g/cm^3	$\rho_m \sim 1.0$ g/cm^3

積分のステップ幅 Δt は 0.0/0.01 sec. ごとで 0.05 sec. ごとに高度. 質量. 速度. 等級をプリントアウトしてまとめたのが Fig-1 である. 質量範囲は $10^{-3} \sim 10^{1}$ g であり. それぞれの最大等級を示した. 同じ 1g の質量でも. Perseids では −3.6 mag Geminids では −1.6 mag と最大等級が異なってくる.

Fig-2 ではシミュレーション(Cal.)と. 実際の観測(Obs.)とを比べた. 観測は KPM ネットワークによってとらえられた2例の流星の測光データである.

Geminids では光度変化のパターンが大きく異なっている. Perseids a KPM 7505 などは末端の爆発がみられる. シミュレーションの方は単純な Single body theory で計算を行なっているので流星体が複雑にこわれる Fragmentation (破砕化. この時に爆発的に光度が明るくなる.) などの現象を再現することができない.

コンピュータによる数値計算は. 長谷川 均氏(日・惑星研究会)の協力を得て. 日電の PC-8001 にて行なった. 同氏に感謝いたします.

1981 Aug 21-23

MSS-017

Fig-1

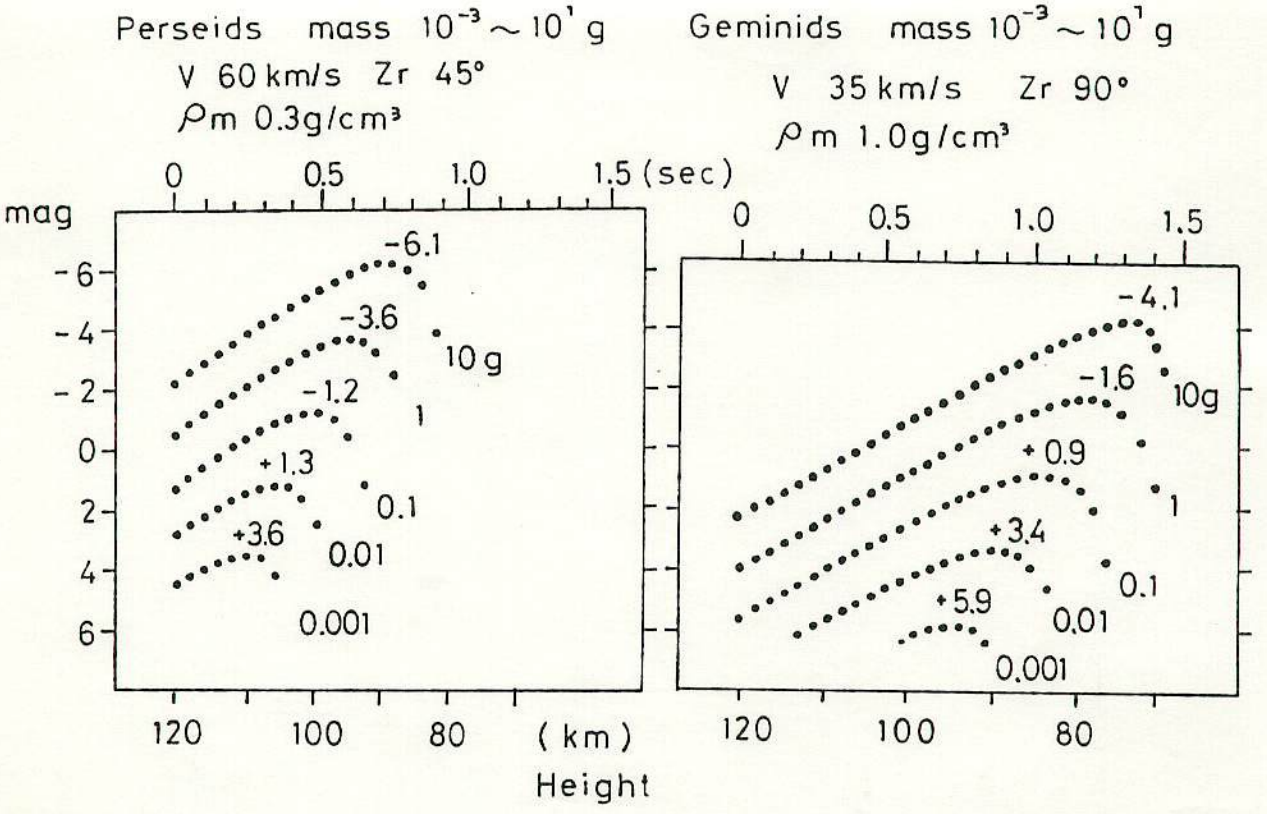

Fig-2

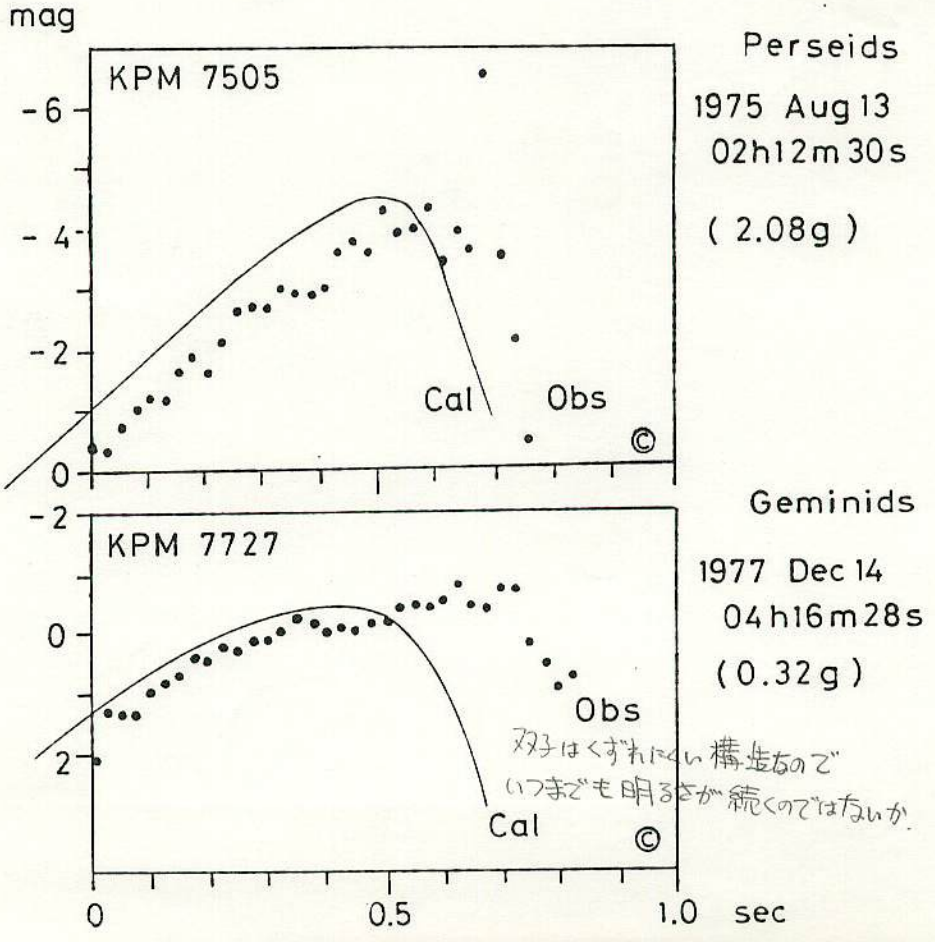

双子はくずれにくい構造なので
いつまでも明るさが続くのではないか

NO. 37名会抄
DATE

19th HSS 1982 Jan. 15

Cumulative flux of the Prairie Data

小笠原雅弘
Masahiro Ogasahara

$10^3 \sim 10^7$(g) の mass range では. McCrosky (1968) が Prairie Network により求めた. Cumulative flux は. Hawkins, Harrison and Brown が meteorites から求めたものよりかなり大きい. Dohnanyi はこの原因を流星体の大気中での ablation (摩耗) と考えている. (Dohnanyi 1973)

隕石の残存率 η を求め. McCrosky データの修正を試みた.

Ceplecha and McCrosky (1976) より Prairie Network 224例を分類すると

			mean velocity
Type I (O-chondrite)	94例	42.0%	23.8 ± 8.0 km/s
Type II (C-chondrite)	90例	40.2%	23.8 ± 13.8 km/s
Type III A, B (Cometary)	40例	17.9%	28.0 ± 12.7 km/s

mass range が $10^3 \sim 10^7$(g) では $\eta_{II}(23.8) \sim 0$, $\eta_{III}(28.0) \sim 0$ で Type II, III の隕石落下は期待できない. (Ogasahara and Hasegawa 1981)

したがって Type I の残存率を $\eta_I(v)$ とすると. McCrosky (1968) の Cumulative flux Φ_0 は以下の修正をしなければならない.

$$\Phi_1 = \Phi_0 \sum_{v=13}^{24} a(v)\,\eta_I(v)$$

modified Cumulative flux

$\log N(m) = -19.35 - \log m$
(m : kg)

MSS-019

NO.

DATE

Table - 1

Velocity (Km)		Sample	$a(v)$	$\xi_I(v)$ (落下質量/大気外質量 残存率)
13.0 ~ 14.9	mean 14	11	0.049	0.0529
15.0 ~ 16.9	16	10	0.045	0.0215
17.0 ~ 18.9	18	13	0.058	0.00775
19.0 ~ 20.9	20	5	0.022	0.00248
21.0 ~ 22.9	22	13	0.058	0.000703
23.0 ~ 24.9	24	6	0.027	0.000177
25.0 ~		36	——	——

$\Phi_1 = \Phi_0 \sum_{v=14}^{24} a(v)\,\xi_I(v)$ Total $\Phi_1 = 0.00410\ \Phi_0$

Fig. に ablation の補正をしたグラフを加えた.

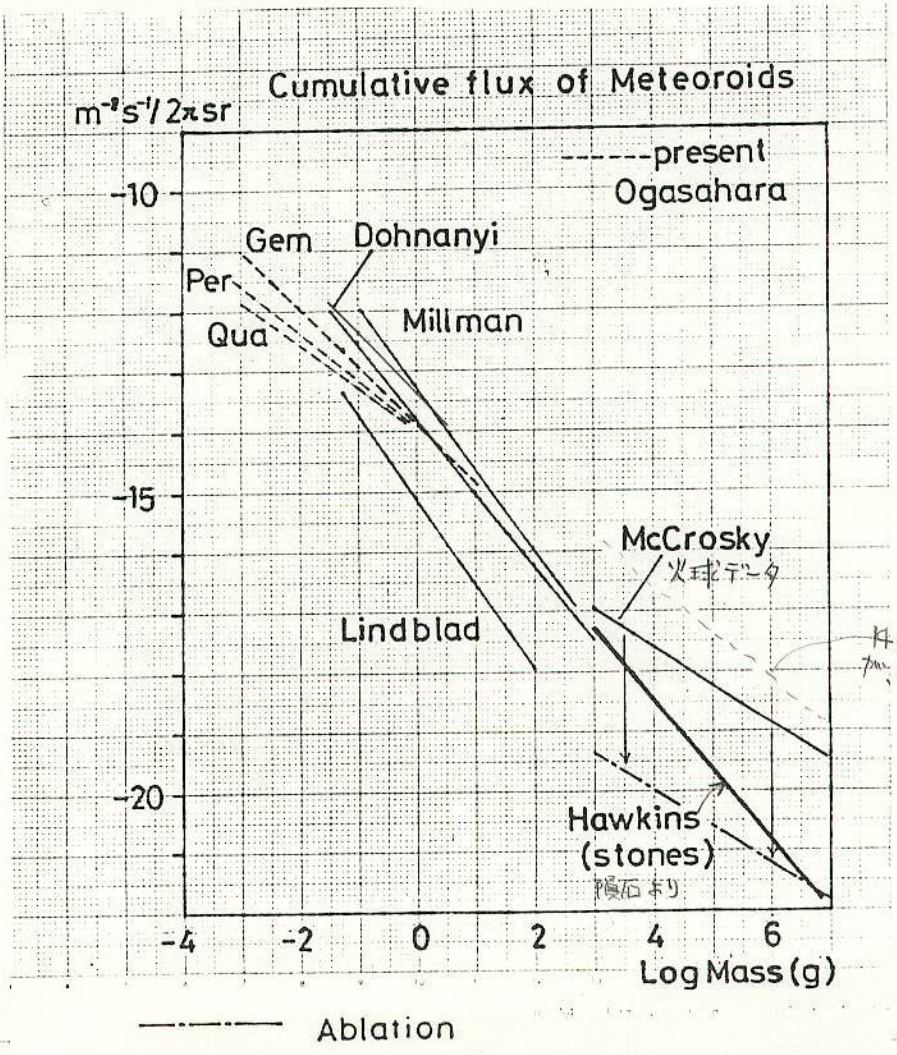

私のMSSではこだわったが、それはマチガイ

19th MSS

JOURNAL OF GEOPHYSICAL RESEARCH, VOL. 86, NO. A10, PAGES 8815-8817, SEPTEMBER 30, 1981

A Fireball in Jupiter's Atmosphere

A. F. COOK

Harvard-Smithsonian Center for Astrophysics, Cambridge, Massachusetts 02138

T. C. DUXBURY

Jet Propulsion Laboratory, California Institute of Technology, Pasadena, California 91103

One fireball was photographed during two encounters with Jupiter. Its total luminosity was 1.2×10^5 0 mag s (at standard range 100 km). If we employ the luminous efficiency proposed by Cook et al. (1981) for slip flow of a meteoroid in its own vapors we obtain an estimated mass of 11 kg. A rough absolute magnitude is −12.5. If we note that we searched for a total of 223 s during two exposures, we estimate a number density near Jupiter of 7×10^{-28} cm^{-3} for masses of meteoroids of 3 kg and greater. This value is about a factor of 6 smaller than a rough upper limit reached from an extrapolation from terrestrial observations of meteors and comets.

During Voyager 1's encounter with Jupiter, two images were obtained on small portions of Jupiter's dark side. These were recorded through the narrow angle camera without a filter, partly to search for fireballs. The corresponding images during Voyager 2 were taken with filters at considerably longer range so that they need not be considered as part of the search, especially as the first two images turned up only one fireball. A brief description of the cameras is given by *Smith et al.* [1979], with a reference quoted for greater detail.

The image on which the fireball appeared consisted of three exposures of 35, 35, and 83 s separated by two slews of 13 s each for a total of 153 s of exposure and 179 s of elapsed time. This schedule of events began at March 5, 1979, 1745:24 UT at the spacecraft. No filter was employed. The range to Jupiter was 555,000 km, resolution of the camera was about 20 km, and the projected path length was 75 km, which is subject to distortion by drift of the imaging platform between limit switches. The minimum duration corresponding to this projected length and a velocity of 64 km s^{-1} is 1.17 s. The total luminosity observed was 1.2×10^5 0 mag s uncertain by about ±25% (estimated). These numbers lead to a rough absolute magnitude of −12.5. These magnitudes are crudely photographic magnitudes. The velocity far from Jupiter was taken to be small compared to the escape velocity. The longitude and latitude on Jupiter were 32°W and 50°N, respectively.

Figure 1 exhibits the image, and Figure 2 the light curve. The latter shows the flickering exhibited by the original image and not well reproduced in Figure 1. Figure 1 does exhibit the expanded halo around the upper-right (western) end of the track which strongly suggests that the fireball penetrated below the top of Jupiter's haze layer (at or higher than the 3.5 mbar level [*Cook et al.*, 1979]). The appearance is much more striking on the original image. We conclude that the fireball came into the atmosphere from the east.

The only available luminous efficiency to be employed with these observations is that proposed for a meteoroid in slip flow in its own vapors by *Cook et al.* [1980]. Their equation (4) takes the form

$$m_\infty = \frac{2}{\tau V^2} \int I_{pg}\, dt \tag{1}$$

where m_∞ is the mass outside the atmosphere, τ is the luminous efficiency, V is the velocity of the meteor, I_{pg} is luminosity, and t is time. The integral is taken over the visible path of the meteor. For application to our fireball we have for the integral 1.2×10^5 0 mag s, as already stated, for the velocity 6.4×10^6 cm s^{-1} where we neglect its variations along the trajectory as is done in (1), and for the luminous efficiency we use 5.4×10^{-13} 0 mag gm^{-1} cm^{-2} s^3 to find a mass of 11 kg. Use of this luminous efficiency can be justified in slip flow in a meteoroid's own vapors, because most exciting collisions occur between meteoric atoms, and the radiation produced is to a first approximation independent of the composition of the planetary atmosphere. This is the compact coma model of *Öpik* [1958].

There are two available tests of the flow regime for our fireball. The first employs the equation for the rate of loss of mass [*Millman and McKinley*, 1963]

$$\frac{dm}{dt} = -\frac{\Lambda A}{2\zeta \rho_m^{2/3}} m^{2/3} \rho_a V^3 \tag{2}$$

where m is the mass of the meteoroid, Λ is the heat transfer coefficient, A is a dimensionless shape factor, ζ is the heat of ablation, ρ_m is the density of the meteoroid, ρ_a is the atmospheric density, V is the velocity of the meteor, and t is time. We note that the rate of change of atmospheric pressure, p, with time may be written down from the barometric equation as

$$\frac{dp}{dt} = g\rho_a V \cos Z_R \tag{3}$$

where Z_R is the zenith distance of the radiant, and g is the acceleration of gravity. The ratio of these two equations is

$$\frac{dm}{dp} = -\frac{\Lambda A}{2\zeta \rho_m^{2/3} g} m^{2/3} V^2 \cos Z_R \tag{4}$$

If we make the approximations of neglecting change in velocity, gravity, and shape, we may integrate to find,

$$p = \frac{6\zeta \rho_m^{2/3} g \cos Z_R}{\Lambda A V^2} (m_\infty^{1/3} - m^{1/3})$$

where m_∞ is the mass outside the atmosphere. The pressure, p_e, at the end point corresponds to exhaustion of mass ($m^{1/3} =$

Paper number 80C1832.
0148-0227/81/000C-1832$01.00

MSS-19

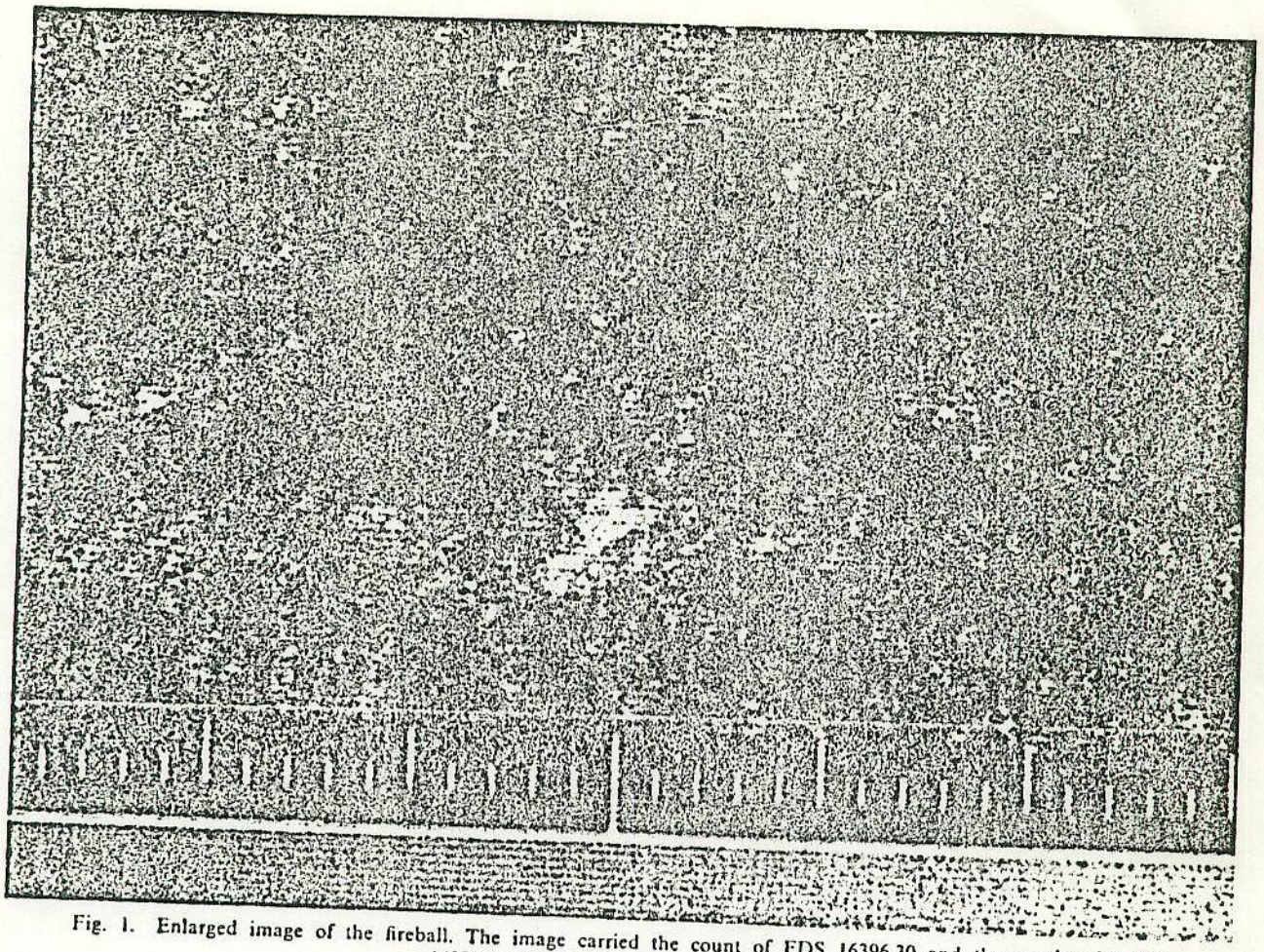

Fig. 1. Enlarged image of the fireball. The image carried the count of FDS 16396.30 and the number PICNO 1427J1+000. Details are given in the text.

0) so that

$$p_e = \frac{6\zeta\rho_m^{2/3} g \cos Z_R}{\Lambda A V^2} m_\infty^{1/3} \quad (5)$$

We choose representative values of $\Lambda/(2\zeta) = 10^{-12}$ cm^{-2} s^2 [*Jacchia*, 1949], $\rho_m = 1$ gm cm^{-3} and $A = 1.5$ to estimate

$$p_e = 3.1 \cos Z_R \text{ mbar} \quad (6)$$

The other available test is that the end point appears to be below the top of the haze layer, as already discussed above. These two tests appear to be mutually consistent.

At a density of 1 gm cm^{-3} the radius of the meteoroid comes to 14 cm, far larger than a mean free path in Jupiter's atmosphere at 3 mbar pressure. We conclude that the fireball was in continuum flow. If most of its radiation is from the bow shock, the luminous efficiency employed here is fictitious. If it were from the wake, it would be lower than for slip flow in a meteoroid's own vapors. In that case, the mass would be greater than estimated here.

A further and final check for consistency may be had by estimating a number density of objects of the above mass near Jupiter, using this observation and also by using studies of meteors at the earth [*Cook et al.*, 1980; *Southworth and Sekanina*, 1973; *McCrosky*, 1968; *McCrosky et al.*, 1971] and of the distribution of comets [*Shoemaker and Wolfe*, 1981]. *Cook et al.* [1980] to estimate a cumulative number density near the earth of

$$\log N_{mG} = -23.8 - 1.335 \log m_\infty \pm 8 \pm 10$$

where N_{mG} is the number density (per cm^3) of meteoroids of mass m_∞ (gm) or greater near the earth's orbit. This relation is valid in the range

$$-4.7 \le \log m_\infty \le +1.0$$

with an uncertainty in mass scale of about ±0.5. *McCrosky*

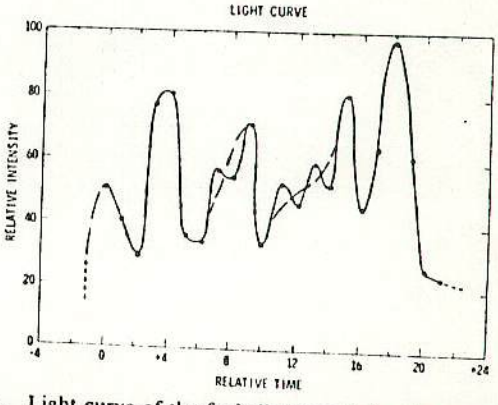

Fig. 2. Light curve of the fireball. Long dashes denote extension back to threshold or alternative fits. Short dashes schematically indicate extensions below threshold.

[1968] as revised by *McCrosky et al.* [1971] find a relation for large masses of meteoroids which may be converted from cumulative flux upon the earth's atmosphere to cumulative number density near the earth's orbit by addition of 6.0 to the logarithm [*Cook et al.*, 1980]:

$$\log N_{mG} = -24.8 - 0.62 \log m_\infty \qquad +3.0 \le \log m_\infty \le +6.0$$

This expression is valid over the indicated range. We employ the larger of the two expressions over the intermediate range $+1.0 \le \log m_\infty \le +3.0$. They cross at $\log m_\infty = +1.4$. *Southworth and Sekanina* [1973] estimate that the density at Jupiter's orbit is about the same as at the earth. This is extrapolated from the statistics of meteors encountered by the earth and is very uncertain.

If we assume that the distribution of meteoroids follows that of comets, we may employ the treatment of *Shoemaker and Wolfe* [1981] to estimate that, if Liouville's Theorem (conservation of density in phase space) applies from the orbit of the earth to that of Jupiter, then the stated estimates in their Table 2 imply a reduction in number density at Jupiter's orbit by a factor

$$\left(\frac{2}{a_J} - \frac{\overline{1}}{a}\right) \Big/ \left(\frac{2}{a_E} - \frac{\overline{1}}{a}\right)$$

vis-à-vis that at the Earth's orbit. For the semi-axis-major of the orbit of Jupiter, $a_J = 5.203$ AU, of the earth, $a_E = 1$ AU, and the harmonic mean semi-axis-major of the comets (assumed for meteoroids), $1/(\overline{1/a}) = 7.153$ AU, this factor is 1/7.605. To the extent that comets with perihelia near Jupiter's orbit have exhaustion lifetimes longer than their dynamical lifetimes, this factor will yield too large a density near Jupiter's orbit. A further reduction is introduced by the presence of meteoroidal orbits near the earth's orbit with aphelia well inside Jupiter's orbit. We adopt this factor to establish an upper limit. Next, *Shoemaker and Wolfe* [1981] find that concentration of nodes with respect to the plane of Jupiter's orbit near that orbit introduces a further factor 2.09. These two results combine to predict an upper limit near Jupiter's orbit at 1/3.64 the cumulative number density near the earth's orbit:

$$\log N_{mJ} \le -24.24 - 0.62 \log m_\infty \qquad +1.4 \le \log m_\infty \le +6.0$$

Here N_{mJ} is the number density of meteoroids near Jupiter's orbit. The last digit is retained for computation and has no significance; indeed the next to last digit barely has significance!

Use of our total coverage of about 2.8×10^7 km^2 and exposure of 223 s yields a rate of 1.6×10^{-10} km^{-2} s^{-1} for objects of approximately 2.8 kg mass and larger. The flux far from Jupiter is to be scaled down [*Cook et al.*, 1980] by a factor $(V_J/V_\infty)^2$ where V_J is the random velocity of approach of meteoroids far from Jupiter (estimated at 4.4 km s^{-1} according to Table 1 of *Shoemaker and Wolfe* [1981]), and V_∞ is the estimated velocity of meteoroids (64 km s^{-1}) at entry into Jupiter's atmosphere. This is further rescaled for anisotropy by fitting the enhancement factors at the distances of the individual Galilean satellites given by *Shoemaker and Wolfe* [1981] in their Table 1. The flux far from Jupiter is 7.7×10^{-13} km^{-2} s^{-1}. Multiplication by 4 (omnidirectional approach relative to circular orbit) and division by V_J yields a volume density of $N_{mJ} = 7 \times 10^{-13}$ cm^{-3}, $\log N_{mG} = -27.16$. Our prediction above yields $\log N_{mJ} \le -26.38$. The predicted upper limit is a comfortable factor of 6 above the rate estimated from observation. We must regard these results as being in agreement.

For completeness, especially if more extensive observations are made by a future mission, some calculations should be made of emissions from bow shocks around meteoroids traveling through Jupiter's atmosphere at 64 km s^{-1} and at 1–10 mbar atmospheric pressure.

Acknowledgment. We thank G. Garneau of the Image Processing Laboratory at JPL for assistance in this analysis. This paper reports one phase of research supported by NASA and JPL under contract NAS-1-100 and of research supported by JPL at the Smithsonian Astrophysical Observatory under that NASA contract.

REFERENCES

Cook, A. F., T. C. Duxbury, and G. E. Hunt, A lower limit on the top of Jupiter's haze layer, *Nature, 280*, 780–781, 1979.

Cook, A. F., T. C. Weekes, E. O'Mongain, and J. T. Williams, Flux of optical meteors down to Mpg = +12, *Mon. Notic. R. Astron. Soc., 193*, 646–666, 1980.

Jacchia, L. G., Photographic meteor phenomena and theory: Meteor photometry, fundamental equations and constants, durations and flares, *Tech. Rep. 3*, Harvard Coll. Obs., Cambridge, 1949.

McCrosky, R. E., Distribution of large meteoric bodies, *Spec. Rep. 280*, Smithsonian Astrophys. Obs., Cambridge, Mass., 1968.

McCrosky, R. E., A. Posen, G. Schwartz, and C.-Y. Shao, Lost City Meteorite—Its recovery and comparison with other fireballs, *J. Geophys. Res., 76*, 4090–4108, 1971.

Millman, P. M., and D. W. R. McKinley, Meteors, in *The Moon, Meteorites and Comets*, edited by B. M. Middlehurst and G. P. Kuiper, pp. 674–773, University of Chicago, 1963.

Öpik, E. J., *Physics of Meteor Flight in the Atmosphere*, Interscience, New York, 1958.

Shoemaker, E. M., and R. F. Wolfe, Cratering time scales for the Galilean satellites, in *The Satellites of Jupiter*, edited by D. Morrison, University of Arizona Press, Tucson, 1981.

Smith, B. A., L. A. Soderblom, T. V. Johnson, A. P. Ingersoll, S. A. Collins, E. M. Shemaker, G. E. Hunt, M. Masursky, M. H. Carr, M. E. Davies, A. F. Cook, J. Boyce, G. E. Danielson, T. Owen, C. Sagan, R. F. Beebe, J. Veverka, R. G. Strom, J. F. McCauley, D. Morrison, G. A. Briggs, and V. E. Suomi, The Jupiter system through the eyes of Voyager 1, *Science, 204*, 951–972, 1979.

Southworth, R. B., and Z. Sekanina, Physical and dynamical studies of meteors, *CR-2316*, NASA, 1973.

(Received June 9, 1980;
revised December 22, 1980;
accepted December 23, 1980.)

1982 - Jan - 15

A Fireball in Jupiter's Atmosphere

19th MSS

A. F. Cook and T. C. Duxbury

(J. G. R. Vol 86 No. A. 10 8815-8817) 1981

日惑星研究会 長谷川 均

Voyager 1 の narrow angle camera により、木星大気中の火球が撮影された。撮影されたのは、1979年3月5日 17:45:24 UT で、木星までの 555000 km の距離にいた時だった。火球の像は 35, 35, 83 sec の3つの露出からなり、total で 153 sec であり、撮影間隔を含めて、179 sec であった。また、no-filter で行なわれた。

camera の分解能は、撮影時において、20 km であり、木星面上に投影すると 75 km になる。速度を 64 km s^{-1} とすると、1.17 s の時間変化に一致する。

火球の total luminosity は 1.2×10^{5} 0mag (±25%) であった。これを等級(被)になおすと 約 −12.5 mag となる。木星から遠い所での速度は、脱出速度と比べて小さいと思われる。火球は、32°W 50°N に出現した。写真の火球の経路の上(西側)で halo が見られる。これは、火球が、木星大気上層の haze layer に侵入したことを示すのだろう。この高さは、Cook et al. (1979) が恒星の occul. より 3.5 mb と得た。以上のことから火球は、東→西へと大気中に入ったと考える。

地球上の流星と同じように、質量をおめる。(測光質量)

$$m_\infty = \frac{2}{\tau V^2}\int I_{pg}\, dt$$

m_∞: 大気外質量, τ: luminous efficiency, V: 速度, I_{pg}: luminosity, t: time

を用いると、積分は、すでに 1.2×10^{5} 0mag と得ていて、$V = 6.4\times10^{6}$ cm s^{-1}, $\tau = 5.4\times10^{-13}$ 0mag gm^{-1} cm^{-2} s^{3}

とすると、質量は、11 kg となる

火球の落下能力について、

mass の方程式を用いる。

$$\frac{dm}{dt} = -\frac{\Lambda A}{2\xi \rho_m^{2/3}} m^{2/3} \rho_a V^3$$

m : mass
Λ : heat transfer coefficient
A : shape facter
ξ : heat of ablation
ρ_m : density of meteroid
ρ_a : atmospheric density
V : velocity
t : time

静力学方程式

$$\frac{dp}{dt} = g\rho_a V \cos z_R$$

z_R : zenith distance
g : acceleration of gravity

を用いると.

$$\frac{dm}{dt} = -\frac{\Lambda A}{2\xi \rho_m^{2/3} g} m^{2/3} V^2 / \cos z_R$$

↑ その論文ではxだった

となり. 速度変化, 重力, 形の変化を無視すると. 簡単に積分できて.

$$P = \frac{6\xi \rho_m^{2/3} g \cos z_R}{\Lambda A V^2} (m_\infty^{1/3} - m^{1/3})$$

火球消滅点では $m = 0$ であり, $\Lambda/(2\xi) = 10^{-12}\ cm^{-2} s^2$, $\rho_m = 1\ g\ cm^{-3}$, $A = 1.5$

とすると.

$$P_e = 3.1 \cos z \text{ mbar}$$

となる. これは. 先に上げた. haze layer の top より下まで 火球が侵入したということと一致する.

次に 木星付近での cumulative number について 調べる.

地球付近での number density N_{MG} は.

$$\log N_{MG} = -23.8 \pm 8 - 1.335 \log m_\infty \quad (-4.7 \le \log m_\infty \le +1.0)$$

もう少し 大きい もの 対して (火球)

$$\log N_{MG} = -24.8 - 0.62 \log m_\infty \quad (+3.0 \le \log m_\infty \le +6.0)$$

である. これを用いて. Shoemaker and Wolfe (1981) に従って おくてみる. 流星物質の分布は Comet のそれに. 従うとすると. 次のような比になる. ガリレオ衛星の観測から Cumulative flux が求められている.

$$\left(\frac{2}{a_J} - \frac{1}{a}\right) \Big/ \left(\frac{2}{a_E} - \frac{1}{a}\right)$$

Jupiter Earth

$a_J = 5.203$, $a_E = 1\ AU$ $1/(1/a) = 7.153\ AU$ とすると. factor は 木星での flux の減少 $1/7.605$ となる. 一方. 木星軌道面への node が 集中することから. factor $= 2.09$. 両者を合わせると $1/3.64$ になる. よって.

$$\log N_{MJ} \le -24.24 - 0.62 \log m_\infty \quad (+1.4 \le \log m_\infty \le +6.0)$$

camera の 視野が $2.8 \times 10^7 km^2$ で 露出が 2233 s total であったことから. 2.8 kg 以上の object の rate は. $2.6 \times 10^{-10}\ km^{-2} s^{-1}$ となる. また. 木星から 遠い距離では flux は $(V_J/V_\infty)^2$ で 小さくなる. よって. flux は. $7.7 \times 10^{-13}\ km^{-2} s^{-1}$ となる. これより.

$$N_{MJ} = 7 \times 10^{-13}\ km^{-3}, \quad \log N_{MJ} = -27.16$$

元の論文では cm^{-3}

予想した. upper limit は. $\log N_{MJ} \le -26.38$ であり. 6倍, 観測値より 大きかった.

隕石落下のシュミレーション

高増（東大地震研）

(1) 隕石落下の基礎方程式

流星体に働く力

1) 大気抵抗
2) 重力
3) コリオリ力
4) 遠心力

1) 大気抵抗

$$F_a = -\frac{C_D}{2} S \rho v v$$

C_D ; 抵抗係数　　ρ ; 大気密度
S ; 進行断面積　　v ; 流星体の速度

2) 重力

$$F_g = -\mu \frac{m}{R^3} R \quad (|R|)$$

μ ; 地心重力定数　　m ; 流星体の質量
R ; 流星体の地心距離

3), 4)

コリオリ力　　$2 m v \times \omega$
遠心力　　$m \omega \times (R \times \omega)$
ω ; 地球の自転角速度

1), 2) に比べて 3), 4) は、実際には小さいので 1), 2) だけ考慮して 運動方程式をたてる。

$$m \dot{v} = -\frac{C_D}{2} S \rho v v - \mu \frac{m}{R^3} R$$

ここで S は、m の関数で

$$S = A \left(\frac{m}{\rho_m}\right)^{\frac{2}{3}}$$

A ; 形状因数

と表わされるので、地心座標で前式を表わせば、

$$m\ddot{\boldsymbol{r}} = -\frac{C_D}{2}A\left(\frac{m}{\rho_m}\right)^{\frac{2}{3}}\rho\,\dot{\boldsymbol{r}}\dot{\boldsymbol{r}} - \mu\frac{m}{r^3}\boldsymbol{r} \qquad \cdots\cdots(1)$$

質量減少の基礎方程式

$$\zeta\dot{m} = -\frac{1}{2}S\rho v^3$$

ζ：流星体単位体積当りの気化熱 ……(2)

(2) 微分方程式の数値解法

$\vec{v}(t_0+\Delta t) \fallingdotseq \vec{v}(t_0) + \dot{\vec{v}}(t_0)\cdot\Delta t$ ……オイラー法

$y(x_0+\Delta x) \fallingdotseq y_0 + \frac{dy}{dx}\Delta x$

$= y_0 + \Delta x\frac{dy}{dx} + \frac{(\Delta x)^2}{2}\left\{\frac{\partial f}{\partial x} + \frac{\partial f}{\partial y}\frac{dy}{dx}\right\} + \cdots$

ルンゲ・クッタ法

$$\begin{cases} \dfrac{dy}{dx} = f(x,y) \\ \text{初期値} \qquad x = x_0 \text{ で } y_0 = y(x_0) \end{cases}$$

に対して $x = x_0 + h$ の時の $y(x_0+h)$ を求める。

$$\begin{cases} k_1 = h\cdot f(x_0, y_0) \\ k_2 = h\cdot f(x_0+h,\ y_0+k_1) \\ y(x_0+h) = y(x_0) + \frac{1}{2}(k_1+k_2) \end{cases}$$

h が十分小さければ上式は $y(x_0+h)$ のテイラー展開の2次の項までと一致する。 $\Longrightarrow$ 2次のルンゲ・クッタ法

〈4次のルンゲ・クッタ法〉

$$\begin{cases} k_1 = h\cdot f(x_0, y_0) \\ k_2 = h\cdot f\left(x_0+\frac{h}{2},\ y_0+\frac{k_1}{2}\right) \\ k_3 = h\cdot f\left(x_0+\frac{h}{2},\ y_0+\frac{k_2}{2}\right) \\ k_4 = h\cdot f(x_0+h,\ y_0+k_3) \\ y(x_0+h) = y(x_0) + \frac{1}{6}(k_1+2k_2+2k_3+k_4) \end{cases}$$

高階方程式のルンゲ・クッタ法

高階方程式を解くには、まず方程式を1階方程式にすることが必要で 例えば

$$\frac{d^2x}{dt^2} = ax$$

は、 $\frac{dx}{dt} = y$

とおいて、

$$\frac{d^2x}{dt^2} = \frac{dy}{dt} = ax$$

と書くことができるから、連立一階方程式

$$\begin{cases} \frac{dx}{dt} = y \\ \frac{dy}{dt} = ax \end{cases}$$

に帰着させることができる。連立一階方程式に対しては、

$$\begin{cases} \frac{dy_i}{dx} = f_i(x; y_1, y_2, \cdots\cdots, y_n) \\ \text{初期値} \quad x = x_0 \quad y_i = y_{i,0} \end{cases}$$

$$k_{i,1} = h f_i(x_0; y_{1,0}, y_{2,0}, \cdots\cdots, y_{n,0})$$
$$k_{i,2} = h f_i(x_0 + \tfrac{h}{2}; y_{1,0} + \tfrac{k_{1,1}}{2}, \cdots\cdots, y_{n,0} + \tfrac{k_{n,1}}{2})$$
$$k_{i,3} = h f_i(x_0 + \tfrac{h}{2}; y_{1,0} + \tfrac{k_{1,2}}{2}, \cdots\cdots, y_{n,0} + \tfrac{k_{n,2}}{2})$$
$$k_{i,4} = h f_i(x_0 + h; y_{1,0} + k_{1,3}, \cdots\cdots, y_{n,0} + k_{n,3})$$

$$y_{i,1} = y_{i,0} + \frac{1}{6}(k_{i,1} + 2k_{i,2} + 2k_{i,3} + k_{i,4})$$
$$(y_{i,1} = y_i(x_0 + h))$$

と書ける。

(3) 計算

(1)に従って、(2)のルンゲクッタ法を用いて計算する。基礎方程式中の定数は、参考1)にならって

$C_D = 1.2$
$A = 2.0$
$\sigma = 3.0 \times 10^{-2} \quad s^2 km^{-2}$
$\rho_m = 3.75 \quad g \cdot cm^{-3}$
$\mu = 3.98600 \times 10^{14} \quad m^3 s^{-2}$

とした。

$\begin{cases} m\ddot{x} & g\,m\,s^{-2} \\ m\dot{x} & g\,s^{-1}\,m\,s^{-1} \end{cases}$

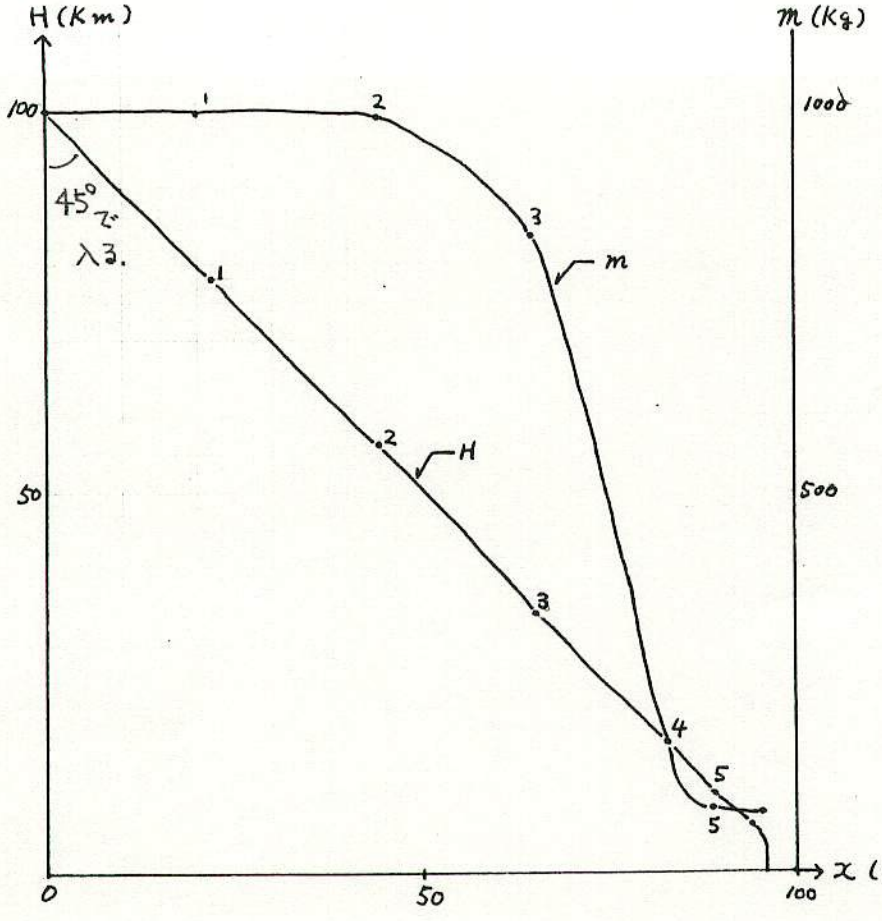

突入速度 { x = 20 km/s
y = 20 〃

大型計算機 FORTRAN
Δt: 0.1 sec.

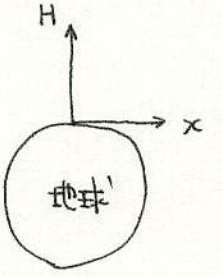

(4) 隕石落下シュミレーションによってわかること

i) 質量減少の様子
ii) 落下経路
iii) 観測との比較による係数の測定

(5) 問題点

基礎方程式で、(1)式の左辺は、本来 $\frac{d}{dt}(m\dot{r}) = m\ddot{r} + \dot{m}\dot{r}$ でなければならず、これを用いると(1)式は、 この式と(2)式を使って

$$m\ddot{r} = -\frac{C_D}{2} A \left(\frac{m}{\rho_m}\right)^{\frac{2}{3}} \dot{r}\dot{r}(1-\sigma\dot{r}^2) - M\frac{m}{r^3} r$$

と書ける。現在 $\sigma \fallingdotseq 3\times10^{-2}\ s^2 km^{-2}$ (普通コンドライト)であるが、この値では、1桁以上大きすぎる。

参考 1) 流星観測の立場からみた隕石落下　長沢 工 (月刊地球 '81 9月)
2) 計算物理(I)　藪下 信 (培人書館)

MSS-026

26-MSS用

ICARUS 48, 308–328 (1981)

Which Fireballs are Meteorites? A Study of the Prairie Network Photographic Meteor Data

G. W. WETHERILL

Department of Terrestrial Magnetism, Carnegie Institution of Washington, Washington, D.C.

プレーリーネットの写真から隕石のものをさがし出す

AND

D. O. REVELLE

Department of Physics, Northern Arizona University, Flagstaff, Arizona 86011

Received May 14, 1981; revised September 21, 1981

しかし(東海大)

Plausible meteorite mass distributions imply that in the Prairie Network data there must be many fainter fireballs produced by meteorites with physical properties that, except for mass, are very similar to the recovered ordinary chondrite (*H5*) Lost City. Four criteria are proposed for identifying these other meteorites among the fireballs. These are: deceleration to final velocity ≤8 km/sec; a photometric mass/dynamic mass ratio within a factor of 2 of that of Lost City, agreement of the observed and theoretical single-body end heights (calculated using dynamic mass), and a lightcurve no more irregular than those of the three recovered fireballs. These criteria can be related to the PE criterion of Ceplecha and McCrosky, but include a wider range of observational data, and also differ from the PE criterion in avoiding inclusion of data not helpful to the particular problem of identifying ordinary chondrite fireballs. By use of our criteria, 27 Prairie Network fireballs are identified as being meteorites comparable to or greater in strength and density to Lost City, most of these should be ordinary chondrites. The orbital element distributions of these objects span a wide range, include those of recovered fireballs, and show that the 4.0-AU aphelion of the Pribram meteorite is not unusually large. Perihelia are concentrated near 1.0 AU, in agreement with previous inferences from time-of-fall and radiant distributions, demonstrating the usefulness of these data based on visual observations.

光度変化が多い

遠日点距離

三原(理大野田)

↓

片田

I. INTRODUCTION

Most of our knowledge concerning the primitive solar system is obtained from chemical, isotopic, and petrographic studies of meteorites. With the exception of the three recovered meteorites with photographic fireball data (Pribram, Lost City, Innisfree) however, we have little information regarding the location of meteorites in the solar system prior to their impact on the Earth.

In the present study, fireball (bright meteor) data from the Prairie Network (McCrosky *et al.*, 1978, 1979; Ceplecha and McCrosky, 1976) are used to identify those fireballs that in all likelihood are ordinary chondritic meteorites. With the exception of Lost City (McCrosky *et al.*, 1971), fragments of these objects were not recovered from the ground, presumably because their small terminal mass either ruled out the feasibility of a search or resulted in the search being unsuccessful. If some of these unrecovered fireballs can be identified as belonging to recognized meteorite classes, e.g., ordinary chondrites, our knowledge of the preatmospheric orbits of these meteorites would be greatly increased.

The starting point of the present work is a strong belief that many small ordinary chondrites must be present among the photographed bright fireballs. The basis for this belief is the fact that the three recovered fireballs, all ordinary chondrites, were among the more luminous fireballs photo-

0019-1035/81/110308-21$02.00/0

graphed by the photographic networks. Of the 322 Prairie Network fireballs for which lightcurves have been published (McCrosky *et al.*, 1979) only 5 have photometric masses greater than that of Lost City, when calculated from the integral of the luminosity over their flight path. The Pribram fireball (magnitude −19) was as bright as any of the Prairie Network fireballs and was the second brightest of those reported by Ceplecha (1977) for the European Network. Similar data have not been published for the Canadian Network, from which Innisfree (Halliday *et al.*, 1981) was collected. However its brightness was very similar to that of Lost City. Estimates of the masses of these objects, together with photometric data, are given in Table I. Masses obtained by various methods vary widely. Although not central to the conclusions of this paper, readers may find it useful to consider an estimate of the "true mass" as being within a factor of about 2 of that given in the last column.

If the size of chondrites is distributed any way similar to that usually found in comminution products, the number of small bodies greatly exceeds the number of large bodies, even when most of the mass is concentrated in a few largest objects (Dohnanyi, 1969; Hartmann and Hartmann, 1968; Hughes, 1981). For a differential power-law mass (m) distribution

$$dN/dm \propto m^{-a}, \qquad (1)$$

and with an exponent in the usual range from 1.7 to 1.85, there should be about 25 to 60 bodies of mass between 100 g and 10 kg for each meteorite in the 10- to 100-kg mass range of Lost City and Innisfree. These smaller meteorites must be well-represented among the fireballs, and the problem is simply to identify which ones they are. Although the available Prairie Network data were not reduced in a way to form a statistically reliable sample, there should be no marked bias against including these fainter ordinary chondrites among the many fainter fireballs. In fact, the association of accurate data with lower entry velocities, and the motivation to recover meteorites, probably worked in the direction of preferentially including faint survivable meteorites relative to weaker objects of the same brightness, rather than excluding them. Based on the rate of occurrence of larger fireballs such as Lost City, Innisfree, and Pribram, and the difficulty of recover-

TABLE I

MASS ESTIMATES (kg) AND PHOTOMETRIC DATA FOR FIREBALLS RECOVERED AS METEORITES

Meteorite	Recovered mass	Initial mass from entry model[a]	Initial mass from cosmic ray effects[b]	Initial photometric mass	Max mag (M_p)	Initial mean dynamic mass[c]	Est. of initial corrected photometric mass[d]
Pribram	5.8	1,300	320	21,500[e]	−18.7	—	1700
Lost City	17.1	52	65	490[f]	−11.6	21.0	38
Innisfree	4.6	18	?	318[g]	−12.1	14.6	25

[a] ReVelle and Rajan (1979), Innisfree value slightly revised in accordance with revision of v_∞.
[b] Bhandari *et al.* (1981).
[c] This paper. Innisfree sum of dynamic mass for all photographed trails (see Table II).
[d] Estimated by assuming integral luminous efficiency too high by a factor of 13, calculated from average ratio of (photometric mass)/(mass from entry model) for Lost City and Innisfree.
[e] Ceplecha (1977).
[f] McCrosky *et al.* (1978).
[g] ReVelle (1980).

ing meteorites with entry velocity greater than 23 km/sec because of severe atmospheric ablation at high velocities, it is estimated that within a factor of 2 or so, 25% of the 176 fireballs entering at <23 km/sec and for which usable deceleration data are given are small ordinary chondrites.

This approach differs from that usually taken in meteor studies. The more common procedure is to attempt to combine the observational data with physical theory and thereby calculate from first principles both the mass and the density of the meteoroid. Calcualtions made in this way lead to densities ~1 g/cm³ or less, even for the recovered meteorites with measured densities of about 3.7 g/cm³. Acceptance of these low densities has led to the common belief that almost all fireballs are fluffy, low-density objects, or "dustballs," and hence have little relevance to the meteorites studied in the laboratory. A break with this traditional interpretation was made by Ceplecha and McCrosky (1976) and Bronshtén (1976), who inferred that a large fraction of the Prairie Network fireballs represented higher-density objects, probably similar to those of recovered meteorites. The present work supports the conclusion of these investigators, even though the conclusion was reached by a different route.

This discrepancy regarding density illustrates a fundamental difficulty in the usual direct approach to the interpretation of meteor data that is well-recognized. In our view this discrepancy is not primarily caused by density differences, but results from the mass determined from the photometric data being higher than the true mass by a factor of about 10 (ReVelle and Rajan, 1979; ReVelle, 1980), and the effective cross-sectional area of the meteoroid being about a factor of 2 higher than that of a single spherical body, probably as a result of fragmentation during passage through the atmosphere. If so, the photometric masses would be too high by a factor of ~10, and the masses calculated dynamically would be low by a factor of ~2. Alternatively, this difference of a factor of 20 between dynamic and photometric mass could be interpreted as the consequence of the actual density of the meteoroid being a factor of $20^{1/2}$ lower than the chondritic density of 3.7 (i.e., 0.8 g.cm³) assumed in calculating dynamic masses (cf. Eq. (9), Appendix). The true cause of the discrepancy is not of major importance to this discussion, however. In order to avoid confusing these two important questions, discussion in the present paper has been formulated in a way that is independent of the absolute mass scale.

In this work, no attempt is made to calculate densities directly from the observational data. Instead, observations of the recovered fireballs will be used to identify characteristics of their dynamics while passing through the atmosphere that are relevant to their having been recovered. In this way criteria are established for identifying those fireballs with similar dynamical characteristics. The individual fireballs are then tested one by one to learn if they satisfy these criteria. This permits dividing the fireballs into two groups: those that resemble demonstrably recoverable meteorites so closely that they cannot be distinguished from them, and those that at least appear to be different. Finally, *given* that a large population of faint ordinary chondrites must be present among the fireballs, it is much more plausible to associate this population with those fireballs that resemble ordinary chondrites, rather than choosing those that do not. To be sure, other recoverable meteorites such as achondrites, enstatite chondrites, as well as Ornans-type (CO) and Vigorano-type (CV) carbonaceous chondrites are likely to be indistinguishable from ordinary chondrites by observation of physical phenomena. This will cause the resulting catalog of ordinary chondrite orbits to be "contaminated" with these bodies roughly in proportion to their fall frequency of about 16% Wasson (1974). In addition, some ordinary chondrites that are more friable than the recovered fireballs will proba-

bly be rejected from the catalog. However, this will not jeopardize the validity of those that remain.

II. SELECTION CRITERIA

The four selection criteria employed are described in this section.

(1) Successful deceleration to low velocity (8 km/sec)

The fundamental property of a meteoroid which permits its recovery is the capability of surviving as a ponderable body as it is decelerated from its entry velocity of 11–23 km/sec down to its free fall terminal velocity of about 100 m/sec. The residual mass M remaining after ablation of a meteoroid as it is decelerated to zero velocity is given by

$$M = M_\infty e^{-\sigma v_\infty^2/2}, \qquad (2)$$

where M_∞ is the mass at velocity v_∞, and σ is the average ablation coefficient (see references in ReVelle, 1979). Dynamical studies of the three recovered fireballs show that a value $\sigma = 2.0 \times 10^{-12}$ sec^2/cm^2 is appropriate for ordinary chondrites. (ReVelle, 1979). With this value of σ, less than 50% of the remaining mass will be ablated after the velocity falls below 8 km/sec.

In addition to mass loss by ablation, the meteoroid can be destroyed by aerodynamic pressure P_d:

$$P_d = (C_D/2)\,\rho v^2, \qquad (3)$$

where v is the velocity, ρ is the atmospheric density at the altitude for which the velocity is v, and C_D is the drag coefficient. The value appropriate for a sphere in continuum flow, $C_D = 0.92$, is used. By use of either the observed atmospheric trajectories (McCrosky *et al.*, 1979) or theoretical expressions for the variation of pressure with velocity, it is found that peak pressures are reached after deceleration to 16 km/sec for entry velocities of 23 km/sec and at 8 km/sec for entry velocities of 12 km/sec. These peak pressures are $\gtrsim 10^7$ dynes/cm^2 for large recovered fireballs of the mass of Lost City (~60 kg) and will be less for smaller chondritic fireballs that are completely decelerated at the lower atmospheric density of higher altitudes.

These pressures are much less than the crushing strengths of $\sim 10^9$ dynes/cm^2 found in laboratory measurements of meteorites (Buddhue, 1942). Nevertheless, the recovered fireballs were observed to fragment in the atmosphere at P_d values more than 100 times smaller than their crushing strengths. The reasons for this are not really known. It is possible that these otherwise strong chondrites have been cracked by interplanetary collisions and fragment into their constituent pieces at these low pressures. In any case, the principal difference between the recoverable chondrites and bodies of comparable entry velocity that fail to survive passage through the atmosphere is not whether or not they fragment, but rather whether or not following fragmentation strong constituent pieces remain that continue their flight deeper into the atmosphere. The 53 Prairie Network fireballs (out of 322) that continue their deceleration below 8 km/sec are judged to be those most resembling the recovered meteorites in this regard, and were retained on the list of candidate ordinary chondrites, pending their satisfying the remaining criteria.

(2) Photometric Mass Not More Than Twice the Mean Dynamic Mass, Calculated from Deceleration Data

By use of meteor theory it is possible to estimate the mass of a fireball by integration of its luminosity over its flight path. On an absolute basis, this is difficult because of uncertainty in the value of the "luminous efficiency," the fraction of the energy loss that is radiated as a visible light. Meteor theory also permits measurement of a "dynamic mass" from the deceleration data as described in the Appendix. This is also difficult to establish absolutely because of uncertainties in the "shape factor," the

density of the meteoroid, and particularly fragmentation during flight. Regardless of the absolute calibration of these mass scales, however, physically similar objects should exhibit a similar ratio of photometric mass to dynamic mass. Comparison of the physical properties of the other Prairie Network fireballs with the recovered fireballs can then be made by comparison of this ratio with that found for a recovered chondrite, chosen here to be Lost City, the ratio for which is taken to be 1.0 (by definition).

In the present work, the photometric masses given by McCrosky *et al.* (1978) are used. These values are then divided by 23.3, the ratio of the photometric mass of Lost City (490 kg) to its dynamic mass (21.0 kg) in order to "normalize" the data to Lost City. Dynamic masses were calculated by us from the data of McCrosky *et al.* (1979). The velocity and photometric data for Innisfree were obtained from prepublication data now reported in Halliday (1981). A photometric mass of 318 kg, based on the principal photographed trail of this meteorite, was calculated using the method described by Ceplecha and McCrosky (1976), and thus is directly comparable with the photometric masses given by McCrosky *et al.* (1978). When normalized to Lost City, the ratio of photometric mass to the dynamic mass (9.6 kg) of the principal Innisfree trail is found to be 1.4.

The equivalent ratio found for other fireballs varies from similarly small values up to values $\approx 10^3$. The very high values are clearly inconsistent with ordinary chondrites, and the question at hand is how high can the ratio be and still be considered indistinguishable from ordinary chondrites. In the absence of an observationally established range of values, the experimental uncertainty of a factor of about 2 in this ratio is used to define this criterion. Fireballs with ratios less than 2.0 that of Lost City, are retained on the candidate list, those with ratios greater than 2.0 are dropped. Comparison of ratios of dynamic mass to best estimates of the actual mass at atmospheric entry (Table I) suggests that for the recovered meteorites the dynamic mass is too low by a factor of about 2, probably as a consequence of the fragmentation observed even for these strong objects. In order not to exclude small objects less likely to fragment, fireballs with scaled ratios as low as 0.25 are retained rather than rejected as being "too strong to be chondrites." After eliminating bodies failing to meet this criteria, the list of candidates is reduced from 53 to 32. If the fireballs with ratios in the range 0.25 to 0.50 had been excluded, this number would be reduced to 28.

(3) End Height Agrees with the Single-Body Theoretical Value, Calculated Using Dynamic Mass, as Well as with That of Lost City to within ±1.5 km, When Scaled for Mass, Velocity, and Entry Angle in Accordance with Classical Meteor Theory

The dynamic mass calculated from the deceleration data can be used to calculate a theoretical end height by use of meteor theory, as discussed in more detail in the Appendix. When this theoretical end height is calculated for Lost City and Innisfree, the values agree within experimental error, with the observed end heights. This can be considered an empirical characteristic of the atmospheric trajectory of these recovered meteorites.

Fundamentally, the observed agreement between theoretical and observational end heights is a consequence of the fact that if the initial dynamic mass is correctly measured from deceleration data, and decreases over the entire trajectory in accordance with the standard ablation law (Eq. 2), then use of the deceleration data and measurement of the end height represent equivalent methods of measuring the initial dynamic mass. However, in practice the techniques are not equivalent. The dynamic masses are calculated from the decelerations given by McCrosky *et al.* (1979) and primarily sample the dynamic mass early in

MSS-026

the trajectory, whereas the end height is sensitive to effects occurring late in the flight in the vicinity of the maximum dynamic pressure. For this reason the agreement of the calculated and observed end heights is an indication that the atmospheric flight of these recovered meteorites is "well-behaved." That is to say, the fireball decelerates all the way to the end of its visible trajectory in accordance with the same shape factor-drag coefficient product and average ablation coefficient applicable to the earlier portion of its trajectory, in spite of observed phenomena, particularly fragmentation, that occur along the flight path.

In order to facilitate comparison between the recovered and unrecovered fireballs over a wide range of dynamic masses, velocities, and entry angle, the data for all of the fireballs were standardized by scaling to a "nominal" chondritic fireball with characteristics similar to Lost City, and using classical meteor theory. These nominal values are given in Table II, where they are compared with those found for Lost City and Innisfree. This procedure is equivalent to comparing a theoretical value for each fireball with its own observed end height. These "scaled end heights" for Lost City and Innisfree are seen to range from 23.0 km down to 21.2 km, and are comparable to the nominal value of 21.1 km. Scaled heights calculated at somewhat higher velocity (~6 km/sec) for the recovered meteorites are slightly different, but all fall within ±1 km of the nominal value. The ~6-km/sec values could be considered more appropriate for comparison with the fainter fireballs that were not observed down to as low velocities as Lost City and Innisfree. A criterion is adopted that fireballs will be considered ordinary chondrite candidates if their scaled end height agrees with that of Lost City within ±1.5 km, i.e., if it falls between 19.7 and 22.7 km. This criterion corresponds to the factor-of-2 uncertainty in dynamic mass discussed earlier and includes all but one of the Innisfree and Lost City values. This criterion is equivalent to the criterion "ΔZ" used by Wetherill and ReVelle (1981), where ΔZ is the difference (in km) between the observed end height and the nominal value of 21.1 km. Application of this criterion removes an additional 8 fireballs from the list, leaving 24. Of these eight objects eliminated, seven had scaled end heights that were too high, ranging up to 30.7 km, whereas one had a value only slightly too low (19.5 km) and it is doubtful that the latter should actually be excluded.

TABLE II

SCALED HEIGHTS OF RECOVERED FIREBALLS CORRESPONDING TO MEASURED VELOCITIES NEAR END OF TRAIL

Meteorite	v_E (km/sec)	v_∞ (km/sec)	Z_R (°)	Height (km)	Scaled height (km)	$m_{d\infty}$ (kg)
Lost City	3.4	14.2	52	19.5	21.2	21.0
	6.1	14.2	52	22.6	21.6	21.0
Innisfree:						
Trail A (main)	3.7	14.5	23	20.9	23.0	5.3
	6.9	14.5	23	22.2	21.2	5.3
Trail B (largest fragment)	2.1	14.5	23	19.8	22.5	4.1
	6.1	14.5	23	21.9	20.6	4.1
Standard	6.0	15.0	45	21.1 (calculated)	≡ 21.1	21

The importance of end heights as a diagnostic criterion for identifying fireballs with recovered ordinary chondrites was emphasized in the earlier work of Ceplecha and McCrosky (1976). The present discussion differs from their use of end heights in that our work emphasizes dynamic mass rather than photometric mass in the theoretical treatment of end heights. We also make use of classical meteor theory in our scaling laws, in contrast to the empirical expression used by Ceplecha and McCrosky. Nevertheless, as discussed later, it will be seen that the set of actual fireballs identified as ordinary chondrites is very similar to that of these earlier workers.

(4) Similarity of the Shape of the Photometric Lightcurves to Those of Recovered Meteorites

The photometric luminosity of the recovered fireballs exhibit certain common features. The visible trail begins as a meteor of of about −2 magnitude at an altitude of 70–100 km. It becomes steadily brighter as it penetrates deeper into the atmosphere, passes through a maximum, and then fades as the velocity decreases as a consequence of atmospheric drag. The meteorite becomes too faint to be observed at an altitude ranging from 13 km in the case of Pribram to 20 km for Lost City and Innisfree. Below these altitudes, the meteorite falls to the ground invisibly at its terminal velocity of about 100 m/sec.

The differences between the lightcurves of the three recovered meteorites can be used to help understand the range of variation in light curves that are possible between different ordinary chondrites. (Fig. 1).

In this comparison no significance should be attached to differences in end height or absolute magnitude. These factors have already been included in previous criteria. The only consideration is the shape. On theoretical grounds, the effect of a meteorite having a higher end height will be to displace the altitude of maximum luminosity upward a distance approximately equal to the differences in end heights. For fireballs with the same entry velocity, the ratio of their intensity will be approximately proportionate to the ratio of their photometric masses. In terms of magnitude, this means that an intensity or mass ratio α corresponds to a difference in the maximum luminosity of about 2.5 log α, i.e., 2.5 magnitudes for each factor of 10 in mass. At the upper end of the lightcurve, at any given altitude a mass ratio α should produce an intensity difference of $\alpha^{2/3}$ corresponding to a difference of $\frac{2}{3}$ log α. The shape of other lightcurves thus can be compared with Lost City by displacing them horizontally to compensate for the ratio of photometric masses. The lightcurves should then approximately match at higher altitudes, the end height and altitude of maximum lumi-

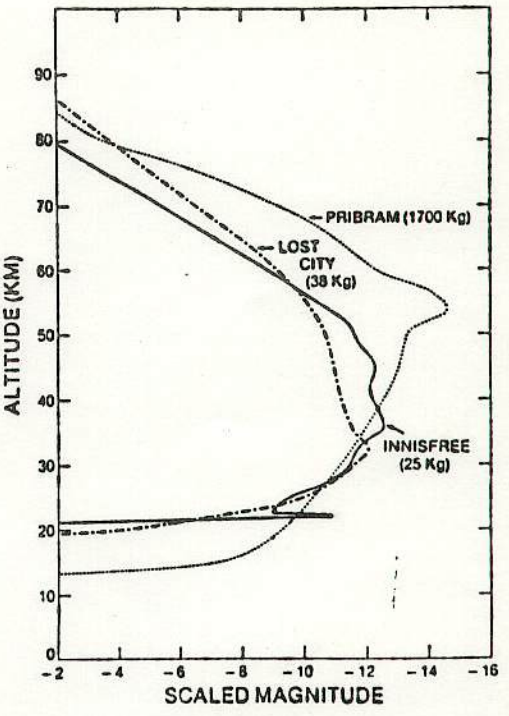

FIG. 1. Lightcurves of the recovered fireballs Pribram, Lost City, Innisfree. Masses are estimated from the photometric mass, divided by the constant factor of 13 (last column, Table I). Absolute magnitude (abscissa) is scaled for mass to facilitate comparison (see text).

nosity should be displaced upward by roughly equal amounts. This horizontal displacement has been made in Fig. 1, and the abscissa is therefore labeled "scaled magnitude."

The lightcurve of Lost City appears "ideal" except for a small flare at 32 km. This flare is not apparent in the tabulation of McCrosky *et al.* (1979), but is presented in the more detailed discussion of McCrosky *et al.* (1971). If this were the only comparative data available, there would be good reason to doubt the recoverability of fireballs with more irregular lightcurves. However, Pribram and Innisfree exhibit considerable irregularities. Pribram reaches maximum luminosity far above its end height and exhibits several flares. Innisfree undergoes fluctuations in brightness, culminating in a bright flare (magnitude ~11) near the end of its visible trajctory. If this ordinary chondrite had been observed at a greater distance and had not been recovered, it might have been concluded that this flare represented its nearly complete disintegration.

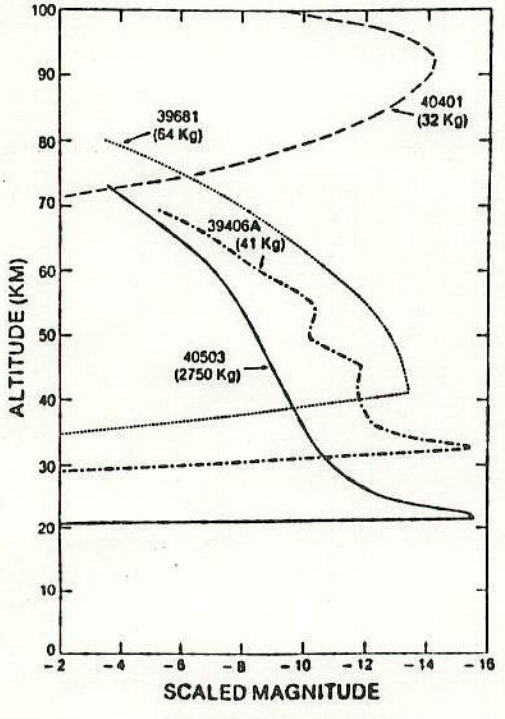

FIG. 2. Lightcurves of four Prairie Network fireball that fail the criteria of this paper.

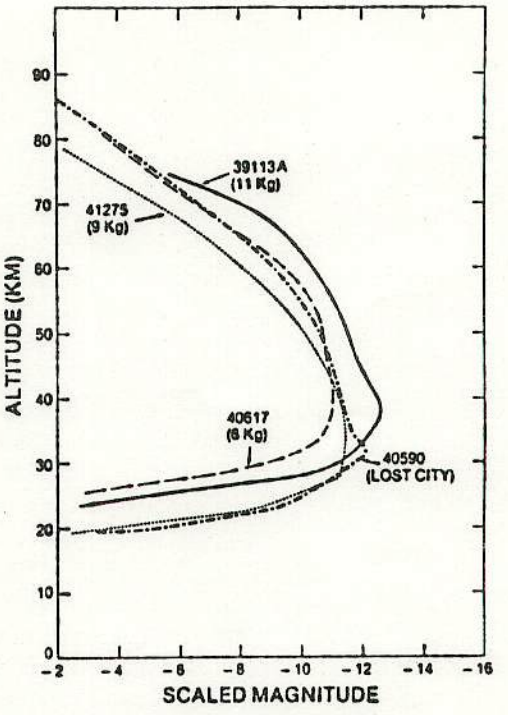

FIG. 3. Lightcurves of the four largest Prairie Network fireballs satisfying the "meteoritic" criteria of this paper. Masses estimated as in Fig. 1.

Not all fireballs exhibit the fairly well-behaved lightcurves measured for the recovered fireballs. Several of these are shown in Fig. 2. On the basis of these lightcurves, as well as their failure to satisfy the preceding three criteria, it is very unlikely that these objects are recoverable meteorites. Characteristics associated with the lightcurves of these fireballs are irregularities (especially sudden flares in brightness), very high luminosities while still at high altitudes, and absence of the final fading portion of the lightcurve.

Most of the fireballs satisfying the first three criteria appear more similar to Lost City than do Innisfree and Pribram. This is illustrated in Fig. 3 where the lightcurves of the four most massive Prairie Network fireballs satisfying criteria (1), (2), and (3),

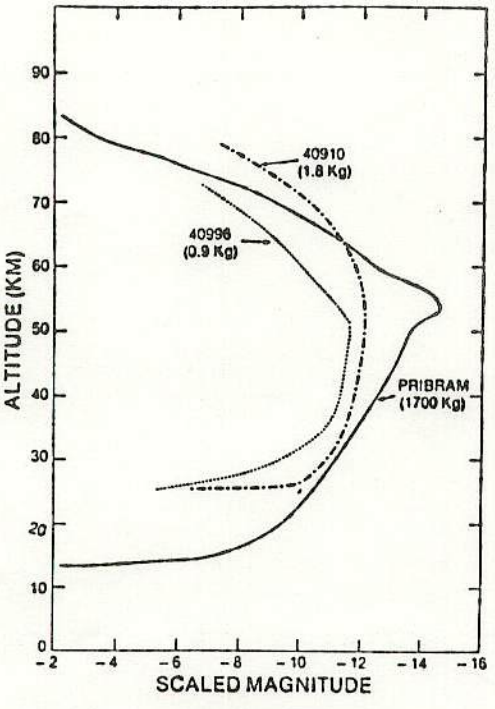

FIG. 4. Comparison of lightcurve of Pribram with those of two meteoritic fireballs exhibiting maximum intensity at high altitude.

40590 (Lost City), 41275, 40617, and 39113A are plotted.

The scaled magnitudes of two fireballs satisfying the first three criteria but with anomalously high altitudes of maximum intensity are shown in Fig. 4. They share this property with Pribram, and this therefore cannot be a criterion for rejecting a fireball as a probably ordinary chondrite.

Figure 5 presents lightcurves for those previously selected fireballs that exhibit flares or a fairly large degree of irregularity in luminosity. Inasmuch as Innisfree and Pribram, and to a lesser extent Lost City, exhibited flares, some flaring is no disqualification.

However, the lightcurve of one object (41327) is considerably more irregular than even Pribram and Innisfree, and on somewhat subjective grounds has been dropped from the list of fireballs with physical properties indistinguishable from recovered ordinary chondrites. The remaining 23 fireballs pass all four criteria. Their physical characteristics are listed in Table III.

In the foregoing selection several meteorites have been eliminated on the grounds that they appeared to be "too strong" (photometric/dynamic mass <0.25) or "too penetrating" (scaled end height <19.7 km). These characteristics should not preclude recovery of the meteorite, and objects with these properties should be present in meteorite collections. In one case (39863A) it is quite possible that an unusually large error in the dynamic mass has caused both the mass ratio to be too high and the scaled end height to be too low. If it is remembered that these bodies may be different from ordinary chondrites it seems worthwhile to include them on the "meteorites" list in some way, and for this reason these objects are listed in Table III, marked with an asterisk.

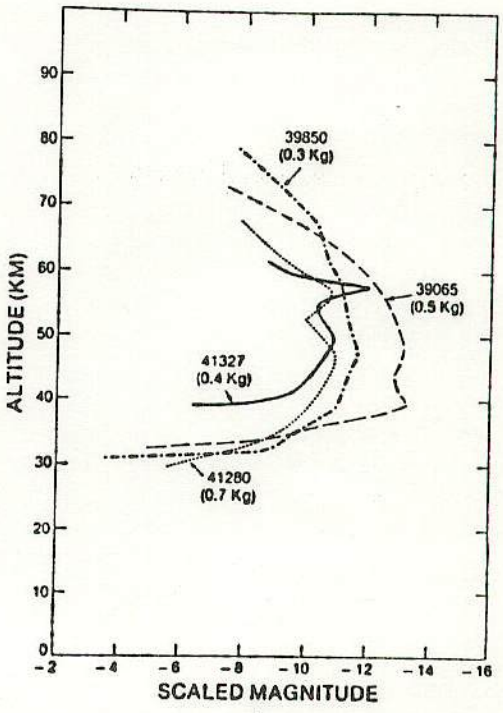

FIG. 5. Lightcurves of Prairie Network fireballs satisfying first three criteria, but exhibiting more than usual irregularities in their lightcurves.

MSS-026

TABLE III

FIREBALLS PROBABLY ASSOCIATED WITH RECOVERABLE METEORITES, USING CRITERIA DISCUSSED IN TEXT

Prairie Network number	Scaled end height (km)	Initial dynamic mass (kg)	$m_{photo}/m_{dynamic}$ (norm. to Lost City)	Entry velocity (km/sec)	Final velocity (km/sec)	Ground search?	Ceplecha–McCrosky type	PE
39057	21.8	0.063	0.9	14.4	6.8	No	I	−4.48
39065	22.7	0.135	1.9	17.2	8.0	No	II	−4.62
30113A	21.8	2.480	0.7	14.9	8.0	No	II	−4.71
39128	22.4	0.170	0.9	13.4	7.7	No	I	−4.50
39182	21.9	1.100	0.3	17.5	7.1	No	I	−4.29
39409	19.8	0.239	2.0	31.7	6.6	No	I	−4.07
39432B	22.6	0.038	1.0	17.0	7.1	No	I	−4.44
39499	22.7	2.080	1.2	12.4	7.0	No	II	−4.62
39812	20.8	0.251	1.2	15.3	7.1	No	I	−4.50
39827A	21.6	0.030	1.7	15.5	8.0	No	II	−4.70
39850	20.8	0.269	1.2	14.4	7.0	No	I	−4.36
39863A[a]	17.1	0.106	3.2	20.3	7.1	No	I	−4.15
39240[a]	19.5	3.140	0.8	17.3	6.1	Yes	I	−4.31
40261	21.0	0.79	0.8	17.8	6.2	Yes	I	−4.19
40318A	21.1	0.036	1.4	11.5	7.0	Yes	II	−4.73
40428B	21.0	0.505	0.5	15.4	6.9	Yes	I	−4.33
40590 (Lost City)	21.2	21.000	≡1.0	14.2	3.4	Yes	I	−4.44
40617	21.9	3.400	1.0	13.2	4.6	Yes	I	−4.56
40660B[a]	19.1	2.130	0.2	26.7	6.1	Yes	I	−3.87
40910	20.0	1.780	0.6	16.4	6.8	Yes	I	−4.25
40996	20.5	1.620	0.3	13.7	4.2	Yes	I	−4.48
41275	20.5	8.900	0.5	13.1	3.8	Yes	I	−4.30
41280	20.6	1.070	0.3	13.3	5.4	Yes	I	−4.55
41432	21.8	0.950	0.3	12.8	7.2	Yes	I	−4.46
41827	19.7	0.010	1.6	14.3	7.5	No	I	−4.46
42149	22.0	0.047	0.8	18.3	5.6	No	I	−4.20
42357A[a]	21.6	0.216	0.2	12.8	7.2	No	I	−4.33
Innisfree (average)	21.8	9.6	1.4	14.5	3.7	Yes	II	−4.65
Pribram	—		—	20.9	7	Yes	I	−4.49

[a] Probably recoverable, but could be "stronger" than recovered chondritic fireballs. See discussion in text.

The physical characteristics of the remaining fireballs with final velocities below 8 km/sec but failing one or more of the other criteria, are given in Table IV.

III. COMPARISON WITH EARLIER WORK

A number of authors have suggested that some of the unrecovered Prairie Network fireballs should be equivalent to ordinary stone meteorites (e.g., Baldwin and Sheaffer, 1971). McCrosky *et al.* (1971) identified 40617 as one such object, but argued that the large photometric mass/dynamic mass discrepancy of Lost City was the result of an unusual shape factor for Lost City, and that low density (~0.8 g/cm³) was a more common cause of the discrepancy between photometric and dynamic mass, including those fireballs subsequently identified by Ceplecha and McCrosky (1976), as probable ordinary chondrites. Bronshtén (1976) made passing use of an end height criterion similar to that of the present work to show that 6 of 29 otherwise unidentified Prairie Network fireballs decelerated more in accordance with meteor theory than fireball 39000, chosen as a standard. Bronshtén did not pursue this point, but instead went on

TABLE IV

PHYSICAL DATA FOR FIREBALLS DECELERATING TO ≤8 km/sec BUT FAILING ONE OR MORE OF THE OTHER CRITERIA

Prairie Network number	Scaled end height (km)	Initial dynamic mass (kg)	$m_{photo}/m_{dynamic}$	Entry velocity (km/sec)	Final velocity (km/sec)	Ground search?	Type	*PE*
A. Fireballs satisfying scaled end height criterion (3) but with $m_{photo}/m_{dynamic} > 2.0$								
39129[a]	21.0	0.060	2.4	12.6	7.3	No	II	−4.61
39169	19.2	0.030	12.4	22.7	7.5	No	I	−4.42
39404[a]	20.0	0.337	5.0	15.3	4.5	No	II	−4.65
39423	21.0	0.023	11.8	34.6	5.7	No	II	−4.72
39476[a]	19.8	0.090	2.2	19.8	7.9	No	I	−4.48
39716B	22.3	0.028	15.4	14.0	7.6	No	II	−5.06
39921C[a]	19.8	1.640	2.9	14.5	7.6	Yes	II	−4.77
40026A	21.3	0.022	81.1	22.9	7.5	No	II	−4.98
40151[a]	20.9	6.331	2.3	13.4	5.2	Yes	II	−4.66
40405	20.2	0.391	7.7	14.8	7.3	Yes	II	−4.77
40433A	21.2	0.172	5.0	13.1	7.8	No	II	−4.84
40806[a]	20.2	0.495	2.1	13.5	5.7	Yes	I	−4.54
41298	20.2	0.257	5.3	15.3	6.9	Yes	II	−4.72
B. Fireballs satisfying $m_{photo}/m_{dynamic} < 2.0$ but with scaled end height >22.7 km								
39055[a]	25.7	0.069	0.42	16.0	4.9	No	I	−4.40
39078[a]	23.5	0.309	0.70	10.8	6.8	No	II	−4.72
39143	30.7	0.656	0.53	20.5	7.8	No	II	−4.71
39815[a]	23.7	2.350	0.73	13.3	4.0	Yes	I	−4.51
39935[a]	24.0	67.300	0.70	17.8	7.4	Yes	I	−4.32
39972	23.5	0.0037	1.90	18.1	6.3	No	I	−4.46
40317A?	29.2	6.280	0.02	19.1	7.9	No	I	−4.32
41014	24.0	0.0139	2.00	17.2	7.2	No	I	−4.47
C. Fireballs that do not satisfy either criterion (2) or (3)								
39425	22.8	0.544	3.7	19.7	8.0	No	II	−4.68
39434	23.1	18.31	10.0	14.5	6.9	Yes	II	−5.19
39667	23.3	0.058	2.7	13.7	8.0	No	II	−4.71
39984B	23.4	0.055	2.4	14.8	6.6	No	II	−4.71
D. Fireball otherwise passing criteria but with very irregular lightcurve								
41327	22.3	0.215	1.0	13.4	7.7	No	I	−4.55

[a] Fireballs would satisfy criteria (1) to (3) if dynamic mass were changed by a factor of 2 or less.

to argue that the 1908 Tunguska meteroid was similar to the remaining fireballs. This is difficult to establish, however, because neither a final velocity nor an accurate mass value is available for Tunguska.

Ceplecha and McCrosky (1976) have classified fireballs by use of a criterion "*PE*" defined by:

$$(PE) = \log \rho + \log (\cos Z_R)^{-1.29} + \log (M_{p\infty})^{-0.42} + \log (v_\infty)^{1.49}, \quad (4)$$

where ρ is the atmospheric density at the end height in grams per cubic centimeter, Z_R is the entry angle (measured from the zenith), $M_{p\infty}$ is the entry mass (photometric) in grams (using the luminous efficiency relationship described in their paper), and v_∞ is the atmospheric entry velocity in kilometers per second.

In addition to *PE*, Ceplecha and McCrosky (1976) defined two other parameters (S_D, S_{DE}) that were found to be of

similar value in the classification of fireballs, but which are not individually tabulated, an average value (SD_R) calculated by three methods being given instead. In response to questions raised regarding the validity of the photometric mass values, Ceplecha (1980) has defined an additional parameter (AL) that differs from PE by use of the more directly observable integral luminosity instead of the photometric mass. As discussed earlier, the value of the luminous efficiency and the absolute value of the photometric masses are not an issue in the discussion of the present paper. For the most part a discussion of the AL criterion would parallel that of PE. Because principal emphasis has been placed on PE, and because values of the other parameters for individual fireballs have not been published, this discussion will be limited to the parameter PE.

This criterion is based on a modification of the classical single-body expression for the end height (see Appendix for more details)

$$\rho = \frac{b\rho_m^{2/3}}{C_D S_F}(\cos Z_R) M_{d\infty}^{1/3} e^{-(\sigma/6)v_\infty^2} \{Ei(\sigma v_\infty^2/6 - Ei(\sigma v_E^2/6)\}, \quad (5)$$

where σ is the ablation coefficient, and $Ei(x)$ is the exponential integral, v_E is the velocity at which the atmospheric density ρ is reached, and the coefficients b, ρ_m, C_D, S_F are defined in the Appendix.

The value of PE in Eq. (4) represents a deviation of the observed end height from a value given by the terms dependent on the parameters Z_R, M_∞, and v_∞. These same parameters appear in Eq. (5), but the dependence of ρ on the parameters is different. If (4) is tranposed so that ρ appears on the left-hand side, Eqs. (4) and (5) can be compared. The entry mass M_∞ occurs raised to the ($\frac{1}{3}$) power in Eq. (5) and to the 0.42 power in (4), cos Z_R to the first power rather than 1.29, and the dependence on v_∞ is simplified to a simple power law in Eq. (4). The exponents in Eq. (4) were determined by statistical least-squares fit of the observed end heights to a sample of 156 Prairie Network fireballs. From the observational data it was found that the value of PE ranged from -3.47 to -7.13. Deeply penetrating fireballs with low end heights (large atmospheric density ρ) have relatively high (small negative) values of PE for the same values of Z_R, M_∞, and v_∞. The exponents in Eq. (4) represent an empirical scaling for entry angle, mass, and velocity in order to compare the "atmospheric penetrating power" of different fireballs. By use of the PE criterion fireballs were classified into four groups:

(I)	$-4.60 < PE$,
(II)	$-5.25 < PE \leq -4.60$,
(IIIA)	$-5.70 < PE \leq -5.25$,
(IIIB)	$PE < -5.70$.

The most penetrating fireballs belong to group I and are identified with ordinary chondrites by these authors. The most numerous group, group II, is less penetrating and is identified with carbonaceous chondrites. Group IIIA is even less penetrating, and is identified with cometary material. IIIB fireballs are the weakest of all and are also presumed to be cometary. One type-IIIB object (39043) is a Draconid meteor: these were already known to be very weak objects from small-meteor data.

Values of PE and Ceplecha–McCrosky type are given for the fireballs that survived to velocities less than 8 km/sec in Tables III and IV. Most (22 out of 27) of the fireballs identified with recoverable meteorites (Table III) are types I, the remainder type II. In contrast most of the objects in Table IV are type II. Thus there is considerable similarity between the fireballs identified by the PE criterion of Ceplecha and McCrosky and the criteria used in the present work.

The relationship between the criteria used in this work and PE can be seen by combining Eqs. (4) and (5). The atmospheric density ρ is the density at the observed end height and will be designated ρ_E. The density ρ in Eq. (5) is the *theoretical*

density at which the velocity is equal to the final velocity v_E. This will be designated ρ_{ET}. These atmospheric densities are related to the observed and theoretical end heights Z_E and Z_T by the relation

$$\rho = \rho_{0e}^{-bz}, \quad (6)$$

where ρ_0 is the density at sea level, and b is the reciprocal scale height of the atmosphere. From (4)

$$\rho_E = 10^{PE} M_{p\infty}^{0.42} (\cos Z_R)^{1.29} v_\infty^{-1.49}. \quad (7)$$

Dividing the expression for ρ_{ET} (Eq. 5) by Eq. (7), expressing density in terms of altitude by Eq. (6) one can solve for PE:

$$\begin{aligned} PE = {} & b(Z_E - Z_T)\log e \\ & + 1/3 \log(M_{d\infty}/M_{p\infty})^{1/3} \\ & + \log\{g(v_\infty, v_E) v_\infty^{1.49} \\ & (\cos Z_R)^{-0.29} M_{p\infty}^{-0.09}\} \\ & + \log(b\rho_m^{2/3}/C_D S_F), \end{aligned} \quad (8)$$

where $g\ (v_\infty, v_E)$ is the velocity-dependent factor in Eq. (5). The first two terms represent criteria used in this article. The first corresponds to the requirement, criterion (3), that the observed and theoretical end heights be in agreement. The second term is a function of the ratio of the dynamic and photometric mass and corresponds to criterion (2). The final term is a constant for bodies with the same physical properties. Except for differences in the third term, it can be seen that two ordinary chondrites with $Z_E \approx Z_T$, and the same ratio of $(M_{d\infty}/M_{p\infty})$ would have the same value of PE. The third term is a fairly slowly varying function of the parameters v_∞, v_E, Z_R, $M_{p\infty}$, and σ. For $v_E = 6$ km/sec and σ's ranging from 0.015 to 0.025 sec^2/km^2, the extreme variation in the contribution of the velocity dependent portion of the third term is 0.42, as v_∞ varies from 13 to 24 km/sec. The contribution of PE from $M_{p\infty}^{-0.09}$ varies by 0.179 from 1 to 100 kg, while that from cos Z_R varies by 0.202 from 30 to 80°. Therefore, although the third term in Eq. (8) is far from dominant it can cause sufficient variation in PE to sometimes shift fireballs satisfying the criteria of this article between types I and II.

The general agreement (for fireballs with final observed velocity ≤8 km/sec) between the present work and that of Ceplecha and McCrosky shows that either of these approaches are capable of identifying meteorites among the fireballs. Nevertheless, there are conceptual and practical differences between the two treatments:

(1) In developing the PE criterion, a single scaling law was fit to fundamentally different types of objects. However, the dependence of the end height is demonstrably different for different types of fireballs. It has already been shown that a large number of fireballs, including those identified as similar to ordinary chondrites have end heights corresponding to atmospheric densities that scale as $M_{d\infty}^{1/3}$. On the other hand, the end heights of some fireballs are essentially independent of their mass. This may be seen in Table V, which shows data for three fireballs belonging to the northern χ-Orionid meteor stream. They have nearly equal entry velocities, and the variation in cos Z_R corresponds to a range of end heights of only 3 km. However, the large mass ratio (~5 × 10^4) would imply end heights differing by 27 km for $M^{1/3}$ scaling and by 33 km for $M^{0.42}$ scaling. The end heights are essentially identical despite the large mass ratio. It is likely that these objects are breaking up by aerodynamic pressures of ~10^6 dynes/cm^2, independent of their mass. For this reason, it does not seem best to permit end heights of bodies of this kind to influence the determination of a scaling law also used for objects with the physical properties of ordinary chondrites.

(2) Final velocity, deceleration, and light-curve shape are certainly relevant to answering the question: Which fireballs resemble ordinary chondrites? In answering this question, it would seem preferable to use all this available data in the best way possible, rather than allow some to remain unused. Ceplecha (1980) discusses the errors inherent in the use of deceleration data

TABLE V

NORTHERN χ ORIONID FIREBALLS, SHOWING LACK OF DEPENDENCE OF END HEIGHT ON MASS

Object	Photometric mass estimates (see note *f* Table I) (g)	Mag.	*a* (AU)	*e*	*i* (°)	ω (°)	Ω (°)	Date	End height (km)
EN041275	$\sim 10^7$	−21	1.98 ± 0.18	0.76	3.5°	174°	252°	12/4/74	56
EN031267	1100	−11	2.20	0.79	3.9	173	250	12/3/67	55
PN42388	160	−9	2.22	0.79	2.8	176	255	12/7/74	59
Small χ Orionids			2.22	0.79	2	179	258	12/4–5	

to calculate dynamic masses. These errors are certainly present, and as discussed in Section II are the ultimate limitations on the resolution of criteria (2) and (3). However, there are also uncertainties in photometry and in the uniformity of the physical processes which determine the lightcurve and hence the photometric mass. The remarkable thing is that in spite of these obstacles, the data for various fireballs do fit together in a consistent manner, and this property is not limited to those parameters used in the *PE* criterion.

(3) The *PE* criterion is described by its authors as semiempirical and of statistical nature. The empirical aspect of the expression leads to the third term of Eq. (8). In addition to the reservations expressed earlier concerning the validity of the exponents in this term, expressing the velocity dependence as a function of v_∞ alone, rather than both v_∞ and v_E, leads to the statistical nature of the *PE* criterion. In some unspecified way v_E is implicitly averaged over the fireballs so that it does not appear in the final expression. The consequence is that only on the average can one expect a fireball assigned to type I to actually be physically indistinguishable from ordinary chondrites. If this were the best one could do, very valuable information could still be obtained, but use of individual values of v_E permit more certain identification of individual fireballs.

(4) In choosing the *PE* criterion from among several alternatives, Ceplecha and McCrosky (1976) emphasized its power to resolve the fireball groups. As will be discussed briefly in Section V it is doubtful that types I and II should be clearly resolvable.

Use of fireball data to infer the physical properties of the meteoroid can be thought of as an inversion problem requiring supplemental data to provide the uniqueness of the solution. In the present work the conviction that there must be many faint ordinary chondrites among the fireballs is given more weight than the assumption that there must be groups with resolvable physical properties.

IV. METEORITE ORBITS

The orbital elements of the fireballs identified as having physical properties very similar to those of the recovered ordinary chondrites are listed in Table VI, based on the data given by McCrosky *et al.* (1978). As pointed out earlier, there are other meteorite classes, such as achondrites, enstatite chondrites, and some carbonaceous chondrites that are physically indistinguishable from ordinary chondrites, and it can be expected that about five of the objects in Table VI are of these other meteorite types.

The mass distribution of the fireballs listed in Table VI is shown in Fig. 6. Although the statistics are insufficient to determine a mass distribution, the data fall in the general range of mass distributions

MSS-027

TABLE VI

ORBITAL ELEMENTS OF FIREBALLS WITH PHYSICAL CHARACTERISTICS OF RECOVERABLE METEORITES

Fireball	a (AU)	e	i	ω	Ω	q (AU)	Q (AU)	v_E (km/sec)	v_∞ (km/sec)	λ (antapex) (°)
39057	4.2	0.76	0.1	6	30	0.99	7.3	6.8	14.4	10
39065	1.12	0.44	0.1	100	38	0.63	1.6	8.0	17.2	96
39113A	1.96	0.54	5.4	218	267	0.91	3.0	8.0	14.9	59
39128	2.00	0.51	5.6	188	282	0.98	3.0	7.7	13.4	32
39182	2.22	0.62	4.4	232	337	0.85	3.6	7.1	17.5	70
39240[a]	2.04	0.53	16.6	210	34	0.96	3.1	6.1	17.3	69
39409	2.44	0.83	13.3	108	17	0.41	4.5	6.6	31.7	99
39432B	2.50	0.66	2.7	227	220	0.87	4.2	7.1	17.0	62
39499	2.00	0.51	0.9	1	108	0.98	3.0	7.0	12.4	6
39812	1.25	0.35	9.4	72	55	0.81	1.7	7.1	15.3	84
39827A	1.01	0.34	1.8	287	250	0.66	1.4	8.0	15.5	110
39850	1.82	0.48	6.4	147	273	0.93	2.7	7.0	14.4	57
39863A[a]	2.56	0.65	21.8	217	287	0.91	4.1	7.1	20.5	77
40261	2.43	0.66	4.5	50	140	0.85	4.1	6.2	17.8	68
40318A	0.93	0.13	1.7	135	197	0.81	1.0	7.0	11.5	112
40428B	1.89	0.46	15.7	170	123	1.01	2.7	6.9	15.4	73
40590 (Lost City)	1.67	0.42	12.0	161	283	0.97	2.4	3.4	14.2	61
40617	2.00	0.52	3.3	194	311	0.98	3.1	4.6	13.2	31
40660B[a]	2.56	0.62	38.1	201	354	0.97	4.2	6.1	26.7	91
40910	1.14	0.43	0.7	98	57	0.64	1.6	6.8	16.9	85
40996	1.82	0.46	9.5	181	325	0.99	2.7	4.2	13.7	47
41275	0.86	0.23	6.9	138	57	0.66	1.1	3.8	13.1	118
41280	2.50	0.60	1.5	179	242	0.99	4.0	5.4	13.3	9
41432	0.74	0.36	1.4	185	215	0.47	1.0	7.2	12.8	171
41827	2.04	0.51	9.5	188	63	1.01	3.1	7.5	14.3	45
42149	1.47	0.32	24.4	195	21	0.99	1.9	5.6	18.3	75
42357A[a]	0.76	0.31	4.7	180	46	0.52	1.0	7.2	12.8	159
Innisfree	1.77	0.44	12	178	317	0.99	2.5	3.7	14.5	57
Pribram	2.40	0.67	10.5	242	17	0.79	4.0	7.	20.9	77

[a] See note on Table IV.

iが20°を越えるのは、3つだけた。

based on recovered meteorites and on other considerations. The assumption that many ordinary chondrite fireballs less massive than Lost City must occur in the Prairie Network data does not lead to the overabundance of small bodies that would result if our criteria were too permissive. On the contrary, the number of bodies smaller than 1 kg is still deficient, and must be explained as resulting from selection of brighter fireballs in the data reduction by McCrosky and his co-workers.

The orbital elements of these bodies cover a wide range. With three exceptions, the inclinations are within 20° of the ecliptic. Aphelia and semimajor axes exhibit the wide spread expected in a general way for bodies whose orbits have evolved as a result of close encounters with the Earth. As shown in Fig. 7, the distribution of perihelia is sharply peaked at the Earth's orbit, leading to the distribution of true geocentric radiants shown in Fig. 8. These results are in agreement with previous studies of the radiant and time of fall distributions of recovered visually observed meteorites. The value of these observations is affirmed, opposing the criticism that such results are

広範囲に渡っている

プレーリーネットワークで得られた火球の軌道要素、質量分布、半長径対近日点距離などの紹介

MSS-027

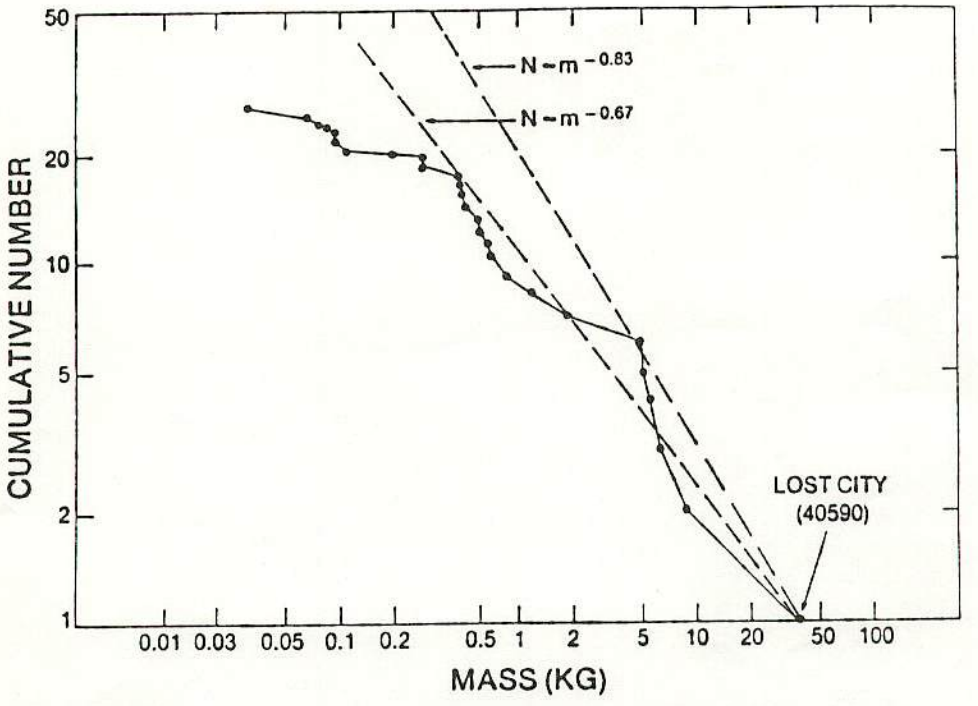

FIG. 6. Cumulative distribution of estimated mass (photometric mass/13) of fireballs selected as meeting all meteoritic criteria. The falloff in number below ~1 kg is attributed to selection related to approaching the sensitivity limit of the cameras near the end of the trajectory.

invalidated by social biases (Fisher and Swanson, 1968, discussed by Wetherill, 1969).

These results extend the data base available for theoretical treatment of meteorite sources, and will be discussed in that context in a subsequent investigation.

V. OTHER OBJECTS

Of the 287 Prairie Network fireballs for which deceleration data exists, 27 have been identified as having physical properties essentially as strong, or even somewhat stronger than the three recovered ordinary chondrite fireballs. What about the rest? These will not be discussed in any detail at this time; the principal goal of the present paper is to provide a catalog of fireballs which have a high probability of being ordinary chondrites or other strong meteorites.

It should be pointed out that the other objects surviving deceleration to 8 km/sec, listed in Table IV, are by no means "dustballs," any or all of them could be recoverable meteorites. Those footnoted in Table IV would satisfy both the end height and mass ratio criteria if the dynamic mass were increased by a factor of 2 or less, possibly resulting from uncertainty in the deceleration data. On the other hand, most of these bodies also exhibited suspicious irregularities in their lightcurves, and there is some basis for suspecting they represent different types of recoverable meteorites.

This is especially true for those objects in Table IVA that decelerated to <8 km/sec in a "well-behaved" way, the observed end height agreeing with the theoretical end height. In these cases, the higher mass ratios could be at least in part the result of lower material density inasmuch as the calculated dynamic mass varies inversely as the square of this density, and the theoretical scaled end height is independent of the

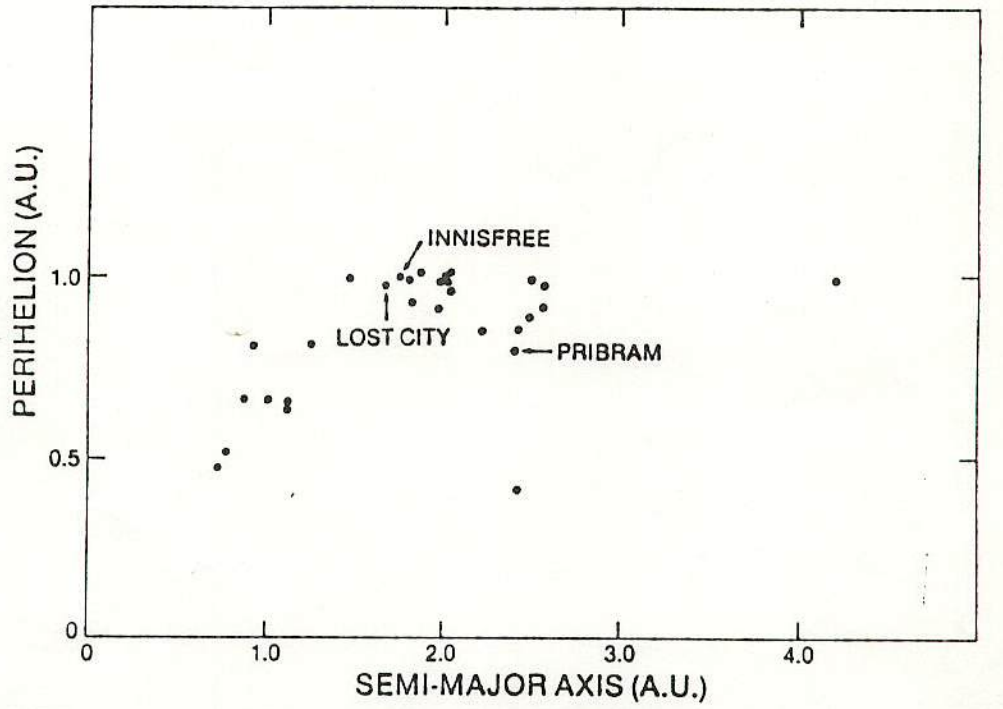

FIG. 7. Distribution of perihelion vs semimajor axis for fireballs satisfying meteoritic criteria. Except for fireballs with very small semimajor axes, perihelia tend to cluster near 1 AU.

material density. Photometric to dynamic mass ratios of 1.1 to 3.1 could correspond to mechanically strong bodies with the range of densities (2.1 to 3.5 g/cm^3) found for carbonaceous chondrites and some achondrites. Mass ratios up to ~6 could be accommodated within the nominal uncertainty of a factor of two in dynamic mass. The ratios >6 difficult to explain in terms of density, and probably are related to extensive fragmentation at a high altitude, possibly combined with density differences.

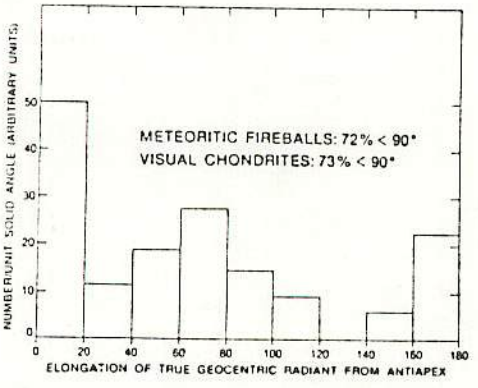

FIG. 8. Distribution of true geocentric radiant of meteoritic fireballs (measured from the antapex of Earth's heliocentric orbit). In agreement with visual observations (Astopovich, 1937; Whipple and Hughes, 1955; Simonenko, 1975) radiants less than 90° predominate. This phenomenon is responsible for the excess number of afternoon chondrite falls (Wetherill, 1968).

Even within the group of ordinary chondrites, the full range of mechanical strength is poorly represented by the three recovered fireballs. For example, thousands of small fragments of the ordinary hypersthene chondrite Holbrook have been recovered, each with individual ablation fusion crusts. The total number of recovered fragments is ~10^4 and the actual number is possibly much greater (Hey 1966). The change in "shape factor" [Eq. (10), Appendix] resulting from fragmentation into n equal size fragments is $n^{1/3}$, and M_d is proportional to n [Eq. (9)]. Therefore use of the shape factor for a single sphere in Eq. (9) when a factor $n^{1/3}$ times as great should

have been used, could result in a large underestimation of M_d. In fact, it is somewhat surprising that the photometric and dynamic masses agree as well as they do in view of the high-altitude fragmentation observed for all three recovered meteorites. This could be a result of a fragmentation law such that most of the mass occurs in the largest fragment. This body will undergo the least deceleration. The measured dynamic mass may then be based on the light from this leading fragment. In the case of Holbrook, adding up the mass of recovered fragments yields a total mass estimated to be about 30 times the mass of the largest fragment. If this fragmentation occurred at high altitude, the measured photometric mass/dynamic mass ratio could have been ~30 for Holbrook. This matter can be resolved only by obtaining "ground truth" by recovery of fireballs exhibiting a greater range of physical properties.

In view of the foregoing discussion, it does not seem likely that there should be a sharp distinction between the physical characteristics of ordinary chondritic and carbonaceous chondritic fireballs, nor that meaningful densities can be calculated by combined use of photometric masses and dynamic masses. In some general way, it is

TABLE VII

ORBITAL ELEMENTS OF FIREBALLS WITH v_E <8 km/sec BUT FAILING ONE OR MORE CRITERIA

Fireball	a (AU)	e	i (°)	ω (°)	Ω (°)	q (AU)	Q (AU)	v_E (km/sec)	v_∞ (km/sec)	λ (°)
A. Fireballs satisfying scaled end height criterion (3) but with $m_{photo}/m_{dynamic}$ >2.0										
39129	2.00	0.51	1.5	15	103	0.97	3.0	7.3	12.6	29
39169	2.32	0.70	13.0	245	324	0.70	3.9	7.5	22.7	86
39404	1.28	0.35	12.0	249	192	0.83	1.7	4.5	15.3	84
39423	2.27	0.89	10.5	307	211	0.24	4.3	5.7	34.6	107
39476	1.89	0.62	7.1	72	85	0.73	3.1	7.9	19.8	82
39716B	1.72	0.45	6.7	214	141	0.96	2.5	7.6	14.0	55
39921C	1.75	0.45	9.4	206	346	0.96	2.6	7.6	14.5	59
40026A	3.03	0.75	15.1	244	88	0.77	5.3	7.5	22.9	80
40151	2.38	0.58	1.0	183	209	0.99	3.8	5.2	13.4	5
40405	2.44	0.60	3.3	208	101	0.97	3.9	7.3	14.8	45
40433A	2.33	0.56	1.5	182	128	1.01	3.6	7.8	13.1	8
40806	0.80	0.29	9.5	19	135	0.57	1.0	5.7	13.5	130
41298	2.27	0.60	3.5	33	80	0.92	3.6	6.9	15.3	52
B. Fireballs satisfying $m_{photo}/m_{dynamic}$ <2.0 but with scaled end height >22.7 km										
39055	2.50	0.61	12.7	200	208	0.97	4.1	4.1	16.0	54
39078	1.01	0.03	0.1	12	51	0.99	1.0	6.8	10.8	44
39143	2.27	0.67	6.4	248	298	0.74	3.8	7.8	20.5	80
39815	2.44	0.59	0.3	183	238	0.99	3.8	4.0	13.3	1
39935	2.33	0.63	5.5	238	359	0.87	3.8	7.4	17.8	68
39972	5.55	0.84	3.3	213	36	0.93	10.4	6.3	18.1	52
40317A	1.69	0.56	3.7	73	196	0.75	2.7	7.9	19.1	82
41014	2.63	0.64	14.8	156	343	0.96	4.3	7.2	17.2	60
C. Fireballs that do not satisfy either criterion (2) or (3)										
39425	2.13	0.54	26.3	168	213	0.99	3.3	8.0	19.7	80
39434	0.71	0.43	3.4	197	42	0.40	1.0	6.9	14.5	143
39667	2.63	0.62	4.7	169	94	1.01	4.3	8.0	13.7	26
39984B	2.13	0.55	4.1	30	227	0.96	3.3	6.6	14.8	57
D. Fireballs otherwise passing criteria but with very irregular lightcurve										
41327	1.82	0.46	6.1	189	290	0.98	2.6	7.7	13.3	49

plausible to associate bodies with the higher scaled end heights and larger photometric/dynamic mass ratios in Table IV with the less dense (*CM*, *CO*, *CI*) carbonaceous chondrites that represent a significant proportion of the recoverable fireballs (~3%) and probably a higher fraction of all the fireballs, in view of the decreased probability of recovery of highly fragmented material.

Orbital data for the fireballs in Table IV are given in Table VII. These are not very different from those in Table VI and no significant difference in conclusions regarding the orbital distribution of ordinary chondrites will result if borderline cases are transferred from Table VII to Table VI or vice versa.

In addition to the 53 fireballs exhibiting deceleration to <8 km/sec there are 269 others with higher final velocities. Many of these are small high-velocity objects that may have simply ablated to negligible mass while still above 8 km/sec. Others (e.g. the fireballs in Table V) appear to have mechanically disintegrated. Discussion of the properties of such bodies is beyond the scope of the present work. It should be pointed out, however, that some of these remaining fireballs did decelerate to their observed final velocities in accordance with the single-body theoretical value (Eq. (12), Appendix) and had photometric/dynamic mass ratios similar to Lost City. The choice of 8 km/sec for the first criterion is not entirely arbitrary. In spite of other differences, most authors agree that at only slightly higher velocities the luminous efficiency is high enough to permit observation of a surviving body of significant mass. Therefore before "certifying" these otherwise well-behaved bodies as ordinary chondrites, some good explanation must be given regarding why they were not observed at lower velocities.

APPENDIX: CALCULATION OF DYNAMIC MASSES AND SCALED END HEIGHTS

The calculations are made by use of single-body meteor theory (Bronshtén, 1964; McIntosh, 1970; ReVelle, 1979). Deceleration measurements (McCrosky *et al.*, 1979) for all 287 Prairie Network fireballs for which data are reasonably self-consistent was used. Data for Innisfree were obtained from I. Halliday.

Dynamic masses were calculated from the deceleration data by use of the expression:

$$M_d(t) = 1/8\,\frac{(C_D S_F \rho)^3 v^6}{\rho_m^2(\dot{v})^3} \qquad (9)$$

where $\dot{v}$ and v are the instantaneous values of deceleration and velocity, respectively.

ρ_m is the material density of ordinary chondrites (3.7 g/cm³);

ρ is the atmospheric density at the height corresponding to $\dot{v}$ and v (NOAA, 1976);

C_D is the dimensionless drag coefficient =0.92;

S_F is the shape factor:

$$S_F = AM^{-2/3}\rho_m^{2/3} = 1.209 \text{ (sphere)}; \qquad (10)$$

A is the cross sectional area (πr^2 for a sphere);

M_d is the mass corresponding to v and $\dot{v}$.

Initial dynamic masses $M_{d\infty}$ were obtained from each of the instantaneous masses from:

$$M_{d\infty} = M_d e^{\sigma/2(v^2\infty - v^2)}, \qquad (11)$$

where v_∞ is the initial atmospheric entry velocity

σ is the effective ablation coefficient $=2 \times 10^{-12}$ sec²cm²

Average values of $M_{d\infty}$ for each fireball were calculated from the unweighted mean of the individual values.

Theoretical final atmospheric densities ρ_{ET} were calculated from the expression:

$$\rho_{ET} = \frac{b\rho_m^{2/3}\cos Z_R \overline{M_{d\infty}}^{1/3}}{C_D S_F} e^{-\sigma v^2\infty/6} [Ei(\sigma v_\infty^2/6) - Ei(\sigma v_E^2/6)], \qquad (12)$$

where b is the reciprocal scale height of the atmosphere (~7 km).

Z_R is the entry angle of the fireball, (measured from the vertical)

$Ei(\eta)$ is the exponential integral;

$$Ei(\eta) = \int_{-\infty}^{\eta} \frac{e^x}{x} dx; \qquad (13)$$

v_E is the final observed velocity.

It should be noted that Eq. (12) is applicable to any point on the observed trajectory and hence v_E and ρ_{ET} need not correspond to the actual "end height" in the event this point is not well determined. Insofar as ρ_{ET} and v_E are near the end of the visible atmospheric flight, the more stringent will be the test of "good behavior" of the fireball's deceleration. In the present work, the final observed velocities of McCrosky *et al.* (1979) were used. In the case of Lost City and Innisfree values of scaled end height at a slightly higher velocity are also given in Table II.

The explicit use of the final velocity v_E in Eq. (12) is the origin of one of the differences between the present work and that of Ceplecha and McCrosky (1976). Our use of v_E is very different from that used in the "*GS*" criterion, defined and rejected by these authors. The *GS* criterion involves introduction of v_E into the theoretical expression for luminosity and therefore requires that v_E be the *actual* end of the luminous trail, not simply some point near the end of trail for which ρ, v, and $\dot{v}$ are available, as is the case with Eq. (12). These authors are correct in stating that the *GS* is of little value because of uncertainties in the actual v_E. However, it seems more likely that the wide range of *GS* values found is at least as much a consequence of the extreme sensitivity of luminosity to velocity at low velocities (ReVelle and Rajan, 1979) as it is to variation in σ, as proposed by Ceplecha and McCrosky.

The comparison of fireballs with differing dynamic mass, entry and final velocities, and entry angle is facilitated by scaling them relative to the atmospheric density at 6 km/sec calculated for a hypothetical standard fireball with nominal parameters similar to those of Lost City. These standard value are $m_{d\infty} = 21$ kg, $v_\infty = 15$ km/sec, $Z_R = 45°$, leading to an atmospheric density corresponding to an altitude of 21.1 km (Table II). The "scaled end heights" tabulated in Tables II, III, and IV were obtained by multiplying the observed atmosphere density at v_E by the ratio of this standard value to the theoretical value found from Eq. (12).

$$(\rho_E)_{\text{scaled}} = \rho_E(\rho_E/\rho_{ET})_{\text{standard}} = 7.5 \times 10^{-5}(\rho_E/\rho_{ET})\text{g/cm}^3. \qquad (14)$$

The scaled end heights are then obtained from (ρ_E) scaled by use of the standard atmosphere (NOAA, 1976). This standardization introduces no assumptions into criterion (3) (Section II) that would not be involved in simple comparison of ρ_E and ρ_{ET} for each fireball, and is done simply to facilitate tabular comparison of the results.

ACKNOWLEDGMENTS

The authors wish to thank I. Halliday for providing unpublished data for Innisfree, as well as B. McIntosh, S. Rajan, and Z. Ceplecha for useful discussions, and M. Coder for assistance in manuscript preparation.

REFERENCES

ASTOPOVICH, I. S. (1939). Some results of the study of 66 orbits of meteorites. *Astron. J. USSR* 16, 15–45.

BALDWIN, B., AND SHEAFFER, Y. (1971). Ablation and breakup of large meteoroids during atmospheric entry. *J. Geophys. Res.* 76, 4653–4668.

BRONSHTÉN, V. A. (1976). The Tunguska meteorite and bolides of the Prairie Network. *Astron. Vest.* 10, 73–80.

BUDDHUE, J. D. (1942). The compressive strength of meteorites. *Contrib. Soc. Res. Meteorites* 3, 39–40.

CEPLECHA, Z. (1977). Fireballs photographed in central Europe. *Bull. Astron. Inst. Czech.* 28, 328–340.

CEPLECHA, Z. (1980). Observational and theoretical aspects of fireballs. In *Solid Particles in the Solar System*, (I. Halliday and B. A. McIntosh, Eds.), pp. 171–183. Reidel, Dordrecht.

CEPLECHA, Z., AND MCCROSKY, R. E. (1976). Fireball end heights: A diagnostic for the structure of meteoric material. *J. Geophys. Res.* 81, 6257–6275.

DOHNANYI, J. W., 1969. Collisional model of asteroids and their debris. *J. Geophys. Res.* 74, 2531–2554.

FISHER, D. E., AND SWANSON, M. F. (1968). The frequency distribution of meteorite–earth collisions. *J. Geophys. Res.* **73**, 6503–6513.

HALLIDAY, I., GRIFFIN, A. A., AND BLACKWELL, A. T. (1981). The Innisfree meteorite fall: A photographic analysis of fragmentation, dynamics, and luminosity. *Meteoritics* **16**, 153–170.

HARTMANN, W. K., AND HARTMANN, A. C. (1968). Asteroid collisions and evolution of asteroidal mass distribution and meteoritic flux. *Icarus* **8**, 361–381.

HEY, M. H. (1966). *Catalogue of Meteorites*. British Museum of Natural History, London.

HUGHES, D. W. (1981). Meteorite falls and finds: Some statistics. *Meteoritics* **16**, 269–281.

MCCROSKY, R. E., POSEN, A., SCHWARTZ, G., AND SHAO, C.-Y. (1971). Lost City meteorite—Its recovery and a comparison with other fireballs. *J. Geophys. Res.* **76**, 4090–4108.

MCCROSKY, R. E., SHAO, C.-Y., AND POSEN, A. (1978). Prairie Network Fireball Data. I. Summary and Orbits. Center for Astrophysics Preprint No. 665. *Meteoritika* **37**, 44–59.

MCCROSKY, R. E., SHAO, C.-Y., AND POSEN, A. (1979). Prairie Network Fireball Data. II. Trajectories and light curves. *Meteoritika* **38**, 106–156.

MCINTOSH, B. A. (1970). On the end point height of fireballs. *Roy. Astron. Soc. Can. J.* **64**, 267–281.

NOAA (National Oceanic and Atmospheric Administration) (1976) *U.S. Standard Atmosphere, 1976*. NOAA-S/T 76-1562 U.S. Govt. Printing Office, Washington, D.C.

REVELLE, D. O. (1979). A quasi-simple ablation model for large meteorite entry: Theory vs. observations. *J. Atmos. Terr. Phys.* **41**, 453–473.

REVELLE, D. O. (1980). A predictive macroscopic integral radiation efficiency model. *J. Geophys. Res.* **85**, 1803–1808.

REVELLE, D. O., AND RAJAN, R. S. (1979). On the luminous efficiency of meteoritic fireballs. *J. Geophys. Res.* **84**, 6255–6262.

SIMONENKO, A. N. (1974). *Orbital Elements of 45 Meteorites*. Atlas. Nauka, Moscow.

WASSON, J. T. (1974). *Meteorites*. Springer-Verlag, Berlin/New York.

WETHERILL, G. W. (1969). Comments on paper by D. E. Fisher and M. F. Swanson, "Frequency distribution of meteorite–earth collisions." *J. Geophys. Res.* **74**, 4402–4405.

WETHERILL, G. W., AND REVELLE, D. O. (1981). Relationship between comets, large meteors, and meteorites. In *Comets* (L. Wilkening, Ed.) Univ. of Arizona Press, in press.

WHIPPLE, F. L., AND HUGHES, R. F. (1955). On the velocities and orbits of meteors, fireballs, and meteorites. In *Meteors* (T. R. Kaiser, Ed.), pp. 145–56. *Spec. Suppl.* **2**, *J. Atmos. Terr. Phys.*

MSS-034

31st M.S.S. 1984・5/13

隕石落下シミュレーションにおける質量欠損の取り扱い

大西 洋

1. 単体モデル

$$\begin{cases} m\dot{v} = -\frac{C_D}{2} S\rho v^2 & \text{---(1)：大気抵抗による減速} \\ \xi \dot{m} = -\frac{\Lambda}{2} S\rho v^3 & \text{---(2)：大気抵抗による質量減少} \end{cases}$$

m：質量　v：速さ　C_D：抵抗係数　S：進行断面積　ρ：大気密度
ξ：気化熱　Λ：熱輸送係数

ただし、$S = A(m/\rho_m)^{2/3}$　A：形状因子　ρ_m：流星体密度

これに地心引力の項を入れて、成分に分けると次式を得る。

$$\begin{cases} \ddot{x} = -\frac{C_D}{2m} S\rho v \dot{x} - \mu \frac{x}{r^3} & \text{---(3)} \\ \dot{m} = -\frac{\Lambda}{2\xi} S\rho v^3 = -\frac{\Lambda}{C_D \xi} \cdot \frac{C_D}{2} S\rho v^3 = -\sigma \cdot \frac{C_D}{2} S\rho v^3 & \text{---(4)} \end{cases}$$

数値積分の一例を下に示す。

① 高度30Kmまで直進し、急減速をうける。
　→ 初速度・空気抵抗支配
② 15Km以下では自由落下。
　→ 引力支配
③ 質量減少は50Km～20Kmで激しい。
④ 残存質量は数%以下。（プリブラム 0.1%，ロストニティ5%，イニスフリー4%）

質量減少を考えるときは、引力の影響を無視できる。

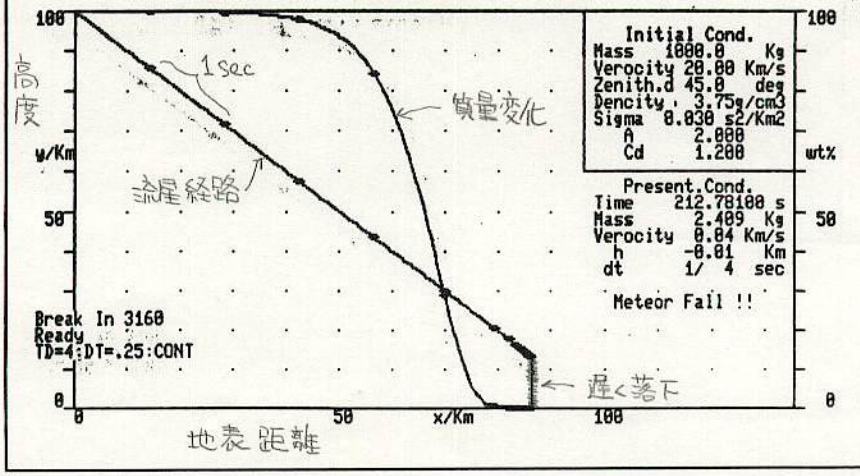

NMS オリエンテーション　6月17日(日)　12h ～ 16h

東大駒場11号館

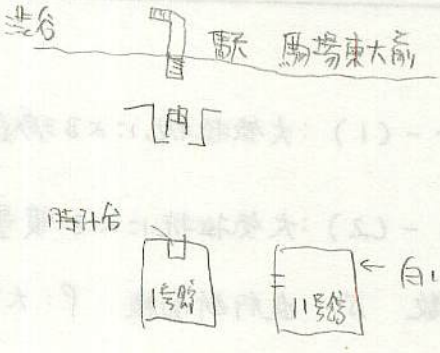

次回　32nd MSS　7月22日(日)

(7)式の変形

$\frac{m}{m_0} = e^{-\frac{\sigma}{2}v_0^2\left(1-\frac{\sigma}{2}v_0^2\right)}$ ---(7)'

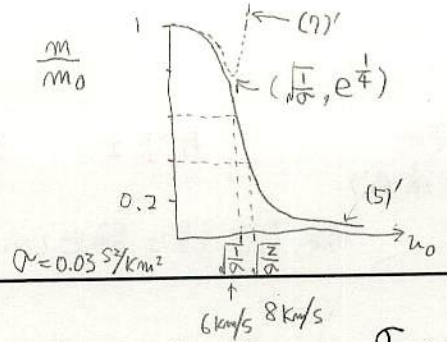

MSS-034

$\frac{m}{m_0} = e^{\frac{\sigma}{2}v_0^2}$ (落下時の質量 m は考えると σ は小さいので省略すると.) ---(5)'

(2) (1)より. $\frac{\dot{m}}{m} = \sigma v \dot{v}$ $\therefore \log m = \frac{\sigma}{2}v^2 + const.$

初速 v_0, 初期質量 m_0 とすれば. $\frac{m}{m_0} = \exp\left(\frac{\sigma}{2}(v^2 - v_0^2)\right)$ ---(6)

2. 質量減少項 (1) のかわりに. $m\dot{v} + \dot{m}v = -\frac{C_D}{2}S\rho v^2$ --- (1)'

$\therefore \dot{v} = -\frac{C_D}{2m}S\rho v^2 - \frac{\dot{m}}{m}v$

$= -\frac{C_D}{2m}S\rho v^2(1-\sigma v^2)$ ← みかけ上. 流体抵抗減少 --- (6)

(5) のかわりに. $\frac{m}{m_0} = \exp\left\{\frac{\sigma}{2}v^2\left(1-\frac{\sigma}{2}v^2\right) - \frac{\sigma}{2}\left(v_0^2\left(1-\frac{\sigma}{2}v_0^2\right)\right)\right\}$ ---(7)

① $v_0 \gg v$ とすると. $1 < \frac{\sigma}{2}v_0^2$ がなりたつと $m/m_0 > 1$ となる。

② σ を十分小さくとっても. m/m_0 に極小ができる。

③ 空気抵抗によって加速されることがある。
∵) 抵抗→質量減少→ (6) で $\dot{v} > 0$

④物理的イメージでは. $(m\dot{v}) = m\dot{v} + \dot{m}v$ とするためには. 蒸発した流星体物質のミクロの熱運動を. マクロの流星体の並進運動に転化するメカニズムが必要となる。

→ 流星体のシミュレーションに質量減少項をとり入れる必要はない。 部分的に取り入れることは可能かもしれないが. それは σ, ρ, C_D, ρ_m などの最適化で吸収されるだろう。

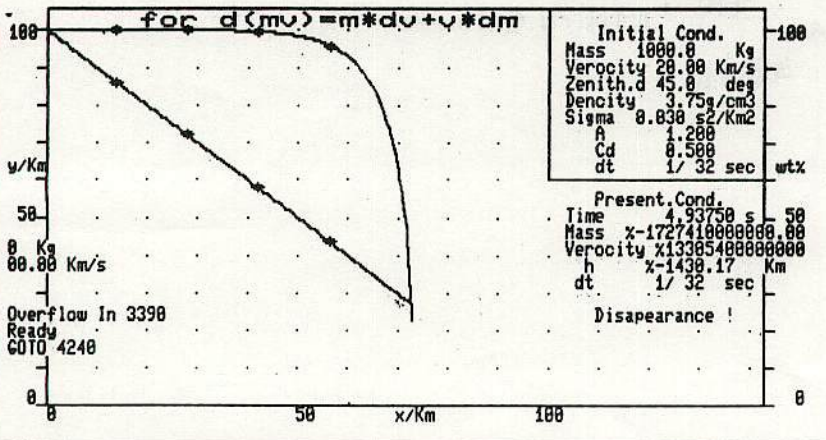

バックグラウンドの流星数変化　　長沢工　　31st-MSS
（散在流星の日周/年周増減）

仮定．散在流星は静止しているものとする．公転していない．

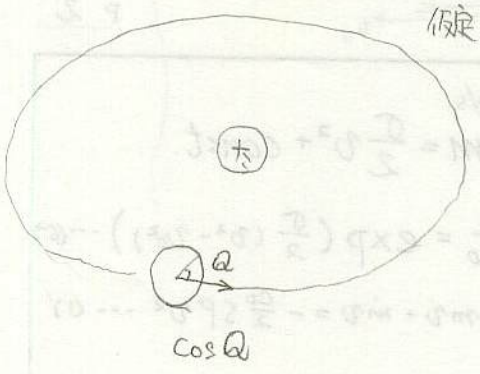

観測地緯度 φ
恒星時　Θ
観測時太陽黄経 λ_s
地球進行方向 $(\lambda_s - 90°, 0)$　黄経，黄緯　　$\varepsilon = 23°27'$

$$\cos Q = \cos\varphi(\sin\lambda_s\cos\Theta - \cos\varepsilon\cos\lambda_s\sin\Theta) - \sin\varphi\sin\varepsilon\cos\lambda_s$$

太陽 $\tan\lambda_s = \frac{\tan\alpha_s}{\cos\varepsilon}$　　α_s（太陽赤経）

地方時 t

$$\Theta = t + \alpha_s - 180°$$

$$\cos Q = \underbrace{\cos\varphi\sin t - \sin\varepsilon\sin\varphi\cos\alpha_s}_{\text{北半球は+　北半球では春分にmax}} + \frac{1}{2}\sin^2\varepsilon \cdots + \frac{1}{8}\sin^4\varepsilon + \cdots$$

6^h にmax
日周変化　　年周変化

The absolute magnitude M_{TV} of each meteor (which is a measure of its intrinsic brightness) was calculated from the apparent magnitude using the correction procedure suggested by Hawkes & Jones (1975b). This correction allows for the variation in the range of the meteors from the cameras and for the decrease in the apparent brightness of meteors due to image motion. Note that we must be careful when comparing these television magnitudes (M_{TV}) with visual meteor magnitudes (M_V), since the colour index (defined as $M_v - M_{TV}$) of television meteors is not well known. To allow for this we made simultaneous visual and television observations of the 1980 Perseid display. For 28 Perseids in the magnitude range from $M_{TV} = +4$ to -2 we found a mean colour index of -0.1 ± 0.3. Thus we can equate television and visual meteor magnitudes.

3 Results

In Figs 2, 3 and 4 we have plotted the characteristic heights of each meteor against the absolute magnitude M. These characteristic heights are (i) the beginning height h_B, which is

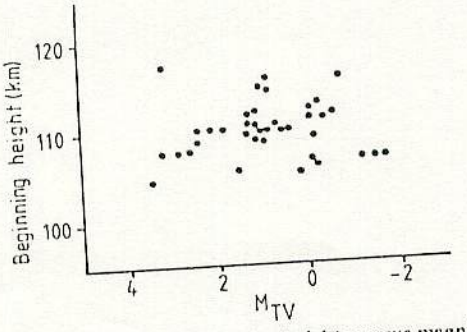

Figure 2. Scatter plot of beginning heights versus magnitude.

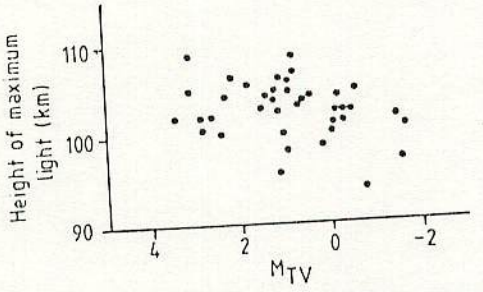

Figure 3. Scatter plot of heights of maximum light versus magnitude.

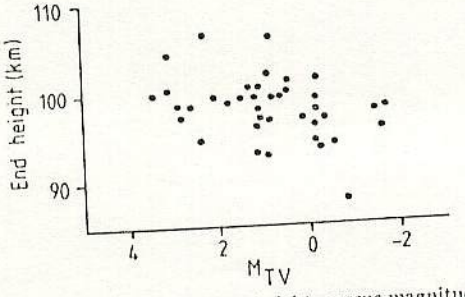

Figure 4. Scatter plot of end heights versus magnitude.

plotted in Fig. 2, (ii) the height of maximum light h_M (plotted in Fig. 3) and (iii) the end height h_E (plotted in Fig. 4). The meteor absolute magnitude is a measure of the meteoroid mass. For Perseids ($v \sim 60\,\mathrm{km\,s^{-1}}$) the mass varies from 1.5×10^{-5} kg for $M = +3$ to 1.5×10^{-3} kg for $M = -2$ (Hughes 1978).

It can be seen from Fig. 2 that there is no significant correlation between beginning height and magnitude. The beginning heights of Perseid meteors are independent of magnitude, with a spread between 105 and 115 km and a mean value of 110 ± 1 km. Figs 3 and 4 show that, despite the large scatter, there are trends in the behaviour of h_M and of h_E, with these heights decreasing with increasing brightness. To quantify these trends we have calculated the correlation coefficient r for each set of data and tested its significance using Student's t-test (Till 1974). We find that $r = 0.35$ for h_M versus magnitude and $r = 0.39$ for the h_E versus TV magnitude. The probabilities of obtaining values of r as great as these by chance are $P = 3$ per cent and $P = 1$ per cent respectively. For comparison a similar analysis of the beginning height versus magnitude gives $r = 0.04$ and $P = 78$ per cent. Thus there is a significant degree of correlation between h_M and magnitude and between h_E and magnitude, so we are justified in fitting at least a straight line through each set of data. To do this we have used the fitting formula proposed by Ross (1980) which takes account of the measuring errors on both axes. This formula is better suited to our purpose than the usual linear regression which allows for errors on one axis only. We find that the best-fitting straight lines are

$$h_M = (3.2 \pm 1.4) M_{TV} + (100 \pm 2), \tag{8}$$

$$h_E = (3.9 \pm 1.5) M_{TV} + (95 \pm 2). \tag{9}$$

However, the dustball theory of Hawkes & Jones (1975a) predicts that a plot of h_M versus M_{TV}, or of h_E versus M_{TV}, should not fit a single straight line but should show a change of slope at a magnitude corresponding to the critical mass m_c. To test this we have arranged the data points in order of decreasing magnitude and divided them into four groups each containing about 10 data points. For each group we have calculated the mean values of h_B, h_M, and h_E and magnitude and have plotted the results in Fig. 5. We have chosen to divide the data in order of decreasing magnitude to maximize the range of magnitudes (~ 3) in Fig. 5. If instead we divide the data in order of decreasing height the final range of

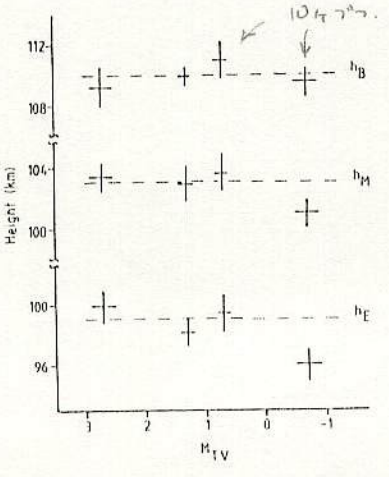

Figure 5. The variation of beginning heights (h_B), heights of maximum light (h_M) and end heights (h_E) with magnitude (M_{TV}) for grouped data. The dashed lines indicate the mean levels referred to in the text.

magnitudes is very much less (~ 1) and so this approach is much less likely to reveal any magnitude-dependent effects such as a change in the slope.

Fig. 5 suggests that h_M and h_E are independent of magnitude for Perseid meteors of magnitude zero or fainter (mass $< 2 \times 10^{-4}$ kg) with mean values of $h_M = 103 \pm 1$ km and $h_E = 99 \pm 1$ km. The two points representing h_M and h_E for the brightest group of meteors fall significantly below these mean levels suggesting that, for meteors brighter than magnitude zero, h_M and h_E decrease with increasing meteor brightness.

As a further test we have recalculated the correlation coefficients r using only the 27 meteors fainter than magnitude zero. We find that $r = 0.07$ for h_M versus magnitude and $r = 0.15$ for h_E versus magnitude. The probabilities of obtaining values of r as great as these by chance are 72 and 46 per cent respectively. Thus, for the meteors fainter than magnitude zero, there is no significant evidence for correlation between h_M and magnitude or between h_E and magnitude. The significant correlations arise only when the 11 meteors brighter than magnitude zero are included.

理大 野田

4 Discussion

The experimental determination of the variation of h_B, h_M and h_E of meteor trails with meteor magnitude shown in Fig. 5 is similar in form to the theoretical curves for the variation of these heights with meteoroid mass shown in Fig. 1. Thus the behaviour of Perseid meteors is consistent with the dustball theory of Hawkes & Jones (1975a). As a further test of this theory we have compared the vertical trail lengths ($\Delta h = h_B - h_E$) of our meteors with the values predicted by dustball theory. For meteors fainter than magnitude zero, Δh is constant with a mean value of 11 ± 2 km, which is close to the predicted value $\Delta h = 9$ km.

The decrease of h_M and of h_E for the group of meteors brighter than magnitude zero suggests that $M_{TV} = 0$ is the critical magnitude at which the h_M and h_E curves change slope. Thus we can estimate that the critical mass for Perseid meteors is $\sim 2 \times 10^{-4}$ kg.

Our result apparently contrasts with the recent results of Hawkes & Jones (1980), who compared the behaviour of sporadic meteors with their dustball theory. These authors made two-station low-light-level television observations of 77 sporadic meteors in the magnitude range $M_v = +1$ to $+5$, which corresponds to the mass range 10^{-4} to 10^{-7} kg. The velocity v and the zenith distance Z of each meteor were determined by triangulation and the mass m was estimated from the total light emission. The variation of h_M with mass, velocity and zenith distance was studied by fitting their data to the formula

$$h_M = c_0 + c_1 \log m + c_2 \log v + c_3 \log \cos Z. \qquad (10)$$

Hawkes & Jones found that the mass term c_1 had a value of -5 ± 2 indicating that, in the magnitude range studied, h_M decreased with increasing mass. If this result is interpreted in terms of dustball theory the critical mass m_c should be less than 10^{-7} kg, which is much lower than the value of 2×10^{-4} kg which we have obtained for Perseid meteors. In our view, however, it is not possible to obtain the critical mass from a simple analysis of sporadic meteor data. We have several reasons for this view.

(i) The formula to which Hawkes & Jones fitted their data assumes *a priori* that there is no change in c_1 within the mass range studied. The dustball theory requires that c_1 is negative for masses greater than the critical mass and that c_1 is zero for masses less the critical mass.

(ii) Selection effects. Optical meteor observations are biased towards small fast meteors since meteor brightness increases rapidly with increasing velocity. In any set of optical

MSS-034

meteor data there will be a correlation between mass and velocity with the mass decreasing as velocity increases. Thus a physical correlation between h_M and v will give rise to an apparent correlation between h_M and m.

(iii) The meteoroid critical mass is strongly dependent on velocity (see equation 7). Any set of sporadic meteor data has a large range of velocities and therefore a large variation in the critical mass.

(iv) Ceplecha (1977) has shown, on the basis of the variation of h_B with velocity, that sporadic meteors can be divided into several distinct groups. Meteors in each group have different densities and compositions. Thus there will be additional variation in the critical mass due to variations in the meteoroid material.

Observations of shower meteors provide a much better test of dustball theory. Meteors from any particular shower have a fixed velocity and a common origin and so they should have a single well-defined critical mass. Moreover, since the meteoroid mass is the major variable, mass-dependent effects can be detected with only a small data sample.

Our result, that a Perseid meteoroid of mass 2×10^{-4} kg should have completely fragmented into fundamental dustball grains when it reaches a height of 110 km, can be used to obtain a value of X, the amount of energy required to fragment unit mass of Perseid material. Taking the mean density of Perseid material as 290 kg m^{-3} (Hughes 1978), a meteoroid of mass 2×10^{-4} kg would have an initial radius $r_0 = 6$ mm. At a height of 110 km the air density is 9.7×10^{-8} kg m^{-3} and the scale height is 8.1 km (COSPAR 1972). From our own observations the mean velocity of the meteors is 63 ± 1 km s^{-1} and the mean value of $\cos Z$ is 0.8 ± 0.1. Using these data in equation (7) we obtain a value of X in the range $3-9 \times 10^5$ J kg^{-1} according to the value of the thermal conductivity factor C. The uncertainty in the value of X is dominated by this uncertainty in C. For comparison the uncertainty in the critical magnitude (~ 0.5) gives an uncertainty in the value of X of about 16 per cent, which can be neglected. Similarly the uncertainty in the scale of meteoroid densities, ~ 50 per cent (Ceplecha 1977), gives an uncertainty in the value of X of about 30 per cent which can also be neglected.

Our estimate of X, the amount of energy required to fragment until mass of Perseid meteoroid material, lies in the range $3-9 \times 10^5$ J kg^{-1}. This is several times lower than the value of X ($1-6 \times 10^6$ J kg^{-1}) adopted by Hawkes & Jones (1975a) in their dustball ablation theory. We conclude that Perseid dustball material is even weaker than the material considered in the theory of dustball ablation. It will be interesting to determine the critical mass in other meteor showers.

Acknowledgments

We thank Dr John Jelley for allowing us to use his observing site at Harwell and Alan Dowdell for providing the observing site at South Wonston and for help with the observations. We gratefully acknowledge the assistance of Jonathan Foyle and Simon Toole in the reduction of the meteor data.

References

Ceplecha, Z., 1977. In *Comets, Asteroids and Meteorites*, p. 143, ed. Delsemme, A. H., University of Toledo Press. Toledo, Ohio. USA.(*Proc. of IAU Colloq. 39*, 1976).

COSPAR, 1972. *COSPAR International Reference Atmosphere (CIRA)*, Akademie-Verlag, Berlin.

Hawkes, R. L. & Jones, J., 1975a. *Mon. Not. R. astr. Soc.*, 173, 339.

Hawkes, R. L. & Jones, J., 1975b. *Mon. Not. R. astr. Soc.*, 170, 363.

層ができるため，C_Dは0.5ぐらいであると考えられ，一定値として扱かうことが多い．また普通コンドライトではρ_mは3.75g cm^{-3}程度である．

以上に述べてきたことからわかるように，流星体の力学質量はC_D, Aなどの仮定のしかたによって，ある範囲で系統誤差が生じる．また，発光初期には加速度($\dot{v}$)がほとんど0であり，精度よく決めるのが困難なので，質量の決定精度が非常に悪い．発光の末端では決定精度が急激によくなってくる．第1表の最終質量は主としてこの方法で決めた発光経路末端の力学質量である．

2 測光質量

流星の光のエネルギーは，流星体の失っていく運動エネルギーに比例する．このように考える積極的な理由があるわけではないが，流星研究者は通常そのように考えている．

この比例係数を光力係数といい，これをτで表わすことにすると，上記の関係は，

$$I=-\frac{\tau}{2}\dot{m}v^2 \tag{3}$$

と書ける．Iは単位時間当りの流星の光のエネルギーである．この関係を書き直すと，

$$dm=-\frac{2I}{\tau v^2}dt$$

$$m=-\int\frac{2I}{\tau v^2}dt+m_E \tag{4}$$

となる．m_Eは発光経路末端での残存質量である．流星写真の測定によって，経路に沿っての流星の明るさ(I)および速度(v)を求めることができるから，τの値さえわかれば，(4)式にしたがって，経路末端から順次に積分していくことで，各点の流星体質量を求めることができる．こうして得られた質量を流星の測光質量という．経路全体にわたって積分すれば大気突入前の初期質量が得られる．残存質量(m_E)は0と考えて計算する場合が多い．第1表の初期質量の値はこうして求めたものである．

ここで問題となるのは光力係数(τ)の値である．この値の決定に関しては多くの話題があり，研究者によって，非常にバラツキのあるさまざまの値が提唱されていた．これは，ロケットから，形，成分のわかっている物体を人工流星として発射し，これを測定するという研究(Ayers 1970)が行なわれて，かなり正確な値が求められ，結着がついた．それによると，τは速度に比例して，

$$\tau=\tau_0 v \tag{5}$$

の形に書ける．明るさの単位に絶対等級0等の明るさをとり，その他の単位SI系で示すと，τ_0は，

$$\tau_0=10^{-10}(0\text{等の明るさ・，}\ \mathrm{kg^{-1}m^{-3}s^4}), \tag{6}$$

ぐらいの値になる．これによると，仮に流星が20kms^{-1}の速さで，絶対等級0等の明るさで，1秒間光り続けたとするなら，その流星体の初期質量は2.5gぐらいになる．現在では，τ_0を定数とせず，多少の速度依存性を考えて，より正確な質量の値を求める努力も行なわれている．

5. 力学，測光質量の比較と流星体密度の推定

前章に述べた方法で，同一流星から，力学質量，測光質量の両方を求めることができる．当然のことながらこれは一致するはずのものである．力学質量の決定精度のよくなる発光経路の後半で，両者の比較をすることができる．

前のところでは詳しく述べなかったが，力学質量の計算には，流星体の密度ρ_mを与えなければならないが，観測の段階ではこれを知ることはできない．そこで，力学質量と測光質量が一致しているかどうかをチェックするのではなく，ρ_mをフリー・パラメータとして，力学，測光質量がなるべく一致するようなρ_mを探し出すという立場で考えてみることにする．経路上のすべての点で完全な一致を期待するのは無理であるが，かなり両者の一致がよいようにρ_mを決めることは可能である．この方法で流星体の密度を求めることができる．こうして決めた密度はそんなに悪いものではなく，ごく普通の流星で0.2～0.3g cm^{-3}ぐらいになる．この値が3～4g cm^{-3}程度であれば，この本体はコンドライト質のものであろうと推定できる．ブレーリー・ネットワークで発見したロスト・シティ隕石でも，C_D, Aの当初の推定値に多少の修正を加えただけで，写真観測から求めた密度と，隕石の実測密度の一致がみられた．

6. 隕石質量減少の理論的見積り

今まで述べたように，流星，火球の観測から，経路に沿ってどのように質量が減少していくかを知ることができる．これをもう少し理論的な形でまとめると，質量減少の基礎方程式はつぎのような形になる．

$$\zeta\dot{m}=-\frac{\Lambda}{2}S\rho v^3 \qquad \text{(基本式Ⅱ)}$$

ここで，

ζ ：流星体単位質量の気化熱

Λ ：熱輸達係数（流星体の失なう運動エネルギーのうち気化に使われる割合）

がある．

この式の右辺は次のように理解すればよい．まず，単位時間内に流星体が掃過する大気質量 m_a は，

$m_a=S\rho v$,

である．流星体はこの大気に v の速度を与える形になるから，大気の得る（したがって流星の失なう）運動エネルギーは，

$$\frac{1}{2}m_a v^2=\frac{1}{2}S\rho v^3$$

となる．そのうち Λ の割合が気化に使われるので，その形が基本式Ⅱの右辺である．

ここで，S に対して，(1) 式を適用して書き直しをすると，

$$\dot{m}=-\frac{\Lambda}{2\zeta}A\left(\frac{m}{\rho_m}\right)^{2/3}\rho v^3 \qquad (7)$$

となる．

ここで適当な地心直交座標系をとって，2次元で，流星の運動方程式を書いてみる．基本式Ⅰは x, y の2方向に分割し，地球引力の項も加える．質量減少の関係式(7)も加えて，これは，

$$\begin{aligned}\ddot{x}&=-Cm^{-1/3}\rho v\dot{x}-\mu\frac{x}{r^3}\\ \ddot{y}&=-Cm^{-1/3}\rho v\dot{y}-\mu\frac{y}{r^3}\\ \dot{m}&=-\sigma Cm^{2/3}\rho v^3,\end{aligned} \qquad (8)$$

と書くことができる．ここで μ は地心引力定数，また

$$\begin{aligned}r^2&=x^2+y^2\\ C&=\frac{C_D}{2}A\rho_m^{-2/3}\\ \sigma&=\frac{\Lambda}{C_D\zeta}\quad \text{：摩耗係数}\end{aligned} \qquad (9)$$

である．μ を含む項は地球引力の影響をあらわすが，隕石の質量減少を考える限り，この項の効果はごく小さい（隕石の落下地点を推定するような場合には，コリオリ力をはじめその他の細かい影響の考慮がさらに必要となる）．第2章で提出した問題のように，与えられた初期条件に対して隕石の質量減少を計算するには，その初期条件によって，微分方程式 (8) を数値的に解いていけばよい．

ここで一番問題になるのは，摩耗係数 (σ) の値をどのようにとるかということである．

σ には，ζ, Λ など決定精度のよくないものが含まれているので，精度のよい値を決定するのが困難であるように思われる．しかし，意外にも，まとめて σ の値を決めるのにはあまり問題がない．4章に述べた方法で，質量減少の様子は観測から求められる．その結果をなるべく忠実に再現することのできる σ を求めてみると，σ は案外によい精度で決まってくる．たとえば，普通コンドライトを考えられる流星体に対して，

$$\sigma\fallingdotseq 3\times10^{-2}\text{s}^2\ \text{km}^{-2} \qquad (10)$$

ぐらいの値が求められる．この値の誤差は，大きめにみても2割以内であろうと思われる．

ここまで説明してきて，やっと第2章で提起した問題に解答をする準備ができた．与えられた初期条件で，微分方程式(8)の数値解を求めればよいのである．

計算結果をひとつ示そう．隕石の発光，摩耗は，ほとんどすべて 100km 以下の大気層で起こるので，計算は高さ 100km からスタートし，地表まで行なった．その他のパラメータの値は，ロスト・シテイ隕石落下の例を参考にして，次のようにとった．

$\sigma=3\times10^{-2}\text{s}^2\ \text{km}^{-2}$

$A=2.0$

$C_D=1.2$

この計算に基づく実経路と，横軸を同じにとって質量減少の様子を示したものが第3図である．この図だけからもいろいろのことがわかるが，これは次のようにまとめられる．